THE UNIVERSITY OF CHICAGO

DENSITY FUNCTIONAL THEORY TRANSFORMED INTO A ONE-ELECTRON REDUCED DENSITY MATRIX FUNCTIONAL THEORY FOR THE DESCRIPTION OF STATIC CORRELATION

A DISSERTATION SUBMITTED TO
THE FACULTY OF THE DIVISION OF THE PHYSICAL SCIENCES
IN CANDIDACY FOR THE DEGREE OF
DOCTOR OF PHILOSOPHY

DEPARTMENT OF CHEMISTRY

BY
DANIEL PATRICK GIBNEY

CHICAGO, ILLINOIS
AUGUST 2024

Dedication Text

To Rachel, Donna, Doug, Matthew, Gus, and Spencer

TABLE OF CONTENTS

LIST OF FIGURES

LIST OF TABLES

ACKNOWLEDGMENTS

First, I would like to thank my wife, Rachel, who has been my rock throughout this PhD process. She has supported me through all the highs and lows of my research, from when it seemed nothing would work and I understood nothing to my first publications—all the while building a home together and adopting two loving cats. I truly cannot thank her enough. I would also like to thank my family, starting with my parents, Donna and Doug, who supported my interests in chemistry and computer science throughout my life, ultimately leading me to where I am today. Lastly, my brother, Matthew, who has always listened to me talk about my research with great interest, encouraging me to keep going.

I would also like to thank my advisor David Mazziotti, who has supported and guided my research throughout my time at UChicago. From starting my work with him by reverse engineering an input file to developing an electronic structure method, it has been a wild and educational ride. Further thanks to his research group: Nik, Scott, Simon, LeeAnn, Ryan, Jordan, Sam, Anna, Irma, Luis, Lily, Serina, and Michael. I'd especially like to thank Nik for assisting me in the early years of my PhD on my research and those in my office, specifically Simon and Sam for always being willing to help with research questions and discussions outside of work.

A big thank you to my friends both at UChicago and outside of it. I'd especially like to thank Melissa whose constant friendship has been invaluable. I will always fondly remember the many random adventures we went on together, and how she pushed me to try activities such as climbing that I probably wouldn't have done by myself. Other Chicago friends I'd like to thank are Julie and Allison for our many Costco and craft fair trips; Miah and the birding club where I learned my favorite bird fact - that the American robin is not actually a robin -, Sam for our many discussions on biking, urban planning, and go, and lastly Josh for our many bike rides and brunch trips. For my friends outside UChicago, I'd like to thank Santiago and Pingel who have always provided a constant source of encouragement

and always been willing to chat. Lastly, I'd like to thank my DnD group Josh, Jessie, Rachel, and Ryan, our biweekly sessions have been a blast.

ABSTRACT

Kohn-Sham Density Functional Theory (KS-DFT or just DFT) has become a go-to method for electronic structure calculations due to its low computational scaling, allowing it to treat large systems, while still being relatively accurate. However, DFT still struggles in strongly correlated systems due to its inability to treat static electron correlation, leading to errors in its prediction of charges, multiradicals, and reaction barriers. This error is primarily driven by the single Slater determinant representation of the Kohn-Sham non-interacting auxiliary wave function, which leads to integer occupations of the electronic orbitals. In this thesis, we address this shortcoming by combining DFT with Semi-Definite Programming (SDP) and a 1-Electron Reduced Density Matrix Functional (RDMF) to capture static electron correlation through fractional orbital occupations. We derive our method termed Reduced Density Matrix Functional Theory (RDMFT) from a unitary decomposition of the 2-electron reduced density matrix's cumulant to obtain a system-specific dependence on the electron repulsion integrals. This methodology retains DFT's $\mathcal{O}(N^3)$ computational scaling while describing static correlation through fractional occupation. We apply this approach to a series of small molecules such as the benzynes and find noticeable improvements over DFT in each system tested. We've also modified the dependence of our method on the 2-electron integrals using the Cauchy-Schwarz inequalities to prevent the RDMF term from decaying to zero with growing system sizes, leading to size extensivity issues. We apply this modification to a series of linear hydrogen chains and find it remedies the size extensive issues of the original derivation. We further apply the modification to the singlet-triplet gaps of the acenes from pentacene to dodecacene and find excellent agreement with variational 2-RDM calculations.

CHAPTER 1

INTRODUCTION

1.1 Quantum Chemistry

Quantum Chemistry involves the prediction of chemical properties using the theoretical foundations afforded by the Schrödinger equation in either its time-dependent

$$i\hbar\frac{\delta}{\delta t}|\Psi(t)\rangle = \hat{H}|\Psi(t)\rangle \tag{1.1}$$

or time-independent forms

$$\hat{H}|\Psi\rangle = E|\Psi\rangle. \tag{1.2}$$

Focusing on the time-independent form; $\hat{H}$ is the Hamiltonian, an operator corresponding to the total energy of our system of interest, Ψ is the associated wave function of the system, and E is the energy of the wave function. To obtain the energy, we can also rewrite Eq. 1.2 by left multiplying each side by $\langle\Psi|$ and dividing by $\langle\Psi|\Psi\rangle$.

$$\frac{\langle\Psi|\hat{H}|\Psi\rangle}{\langle\Psi|\Psi\rangle} = \langle E\rangle. \tag{1.3}$$

This is the expectation value expression of the energy operator, $\hat{H}$, which gives the energy of the wave function. While in general, you cannot divide by your wave function to remove it from one side of the equation, since $\langle\Psi|\Psi\rangle$ is a constant it can be divided. For any general operator $\hat{O}$, its expectation value is calculated similarly as:

$$\frac{\langle\Psi|\hat{O}|\Psi\rangle}{\langle\Psi|\Psi\rangle} = \langle O\rangle. \tag{1.4}$$

Where $\langle O\rangle$ is the expected value of the operator, $\hat{O}$, for the given wave function. As $\langle\Psi|\Psi\rangle$ is proportional to the probability of finding a particle, It is common practice for the wave

function to be normalized such that $\langle\Psi|\Psi\rangle = 1$; assuming normalization allows the above equation can be simplified to:

$$\langle\Psi|\hat{O}|\Psi\rangle = \langle O\rangle. \tag{1.5}$$

Throughout the rest of this work, unless otherwise noted, it will be assumed all wave functions are normalized to one.

1.1.1 Dirac Notation

Before continuing, it would be prudent to explain the notation used above. In 1939 Paul Dirac introduced what is called Bra-Ket or Dirac notation to simplify writing equations in quantum mechanics [1]. The name Bra-Ket comes from the use of the angle brackets as bras $\langle|$ and kets $|\rangle$ to succinctly represent the vectors corresponding to the wave functions. These vectors are normally expressed as:

$$|\psi\rangle = \begin{bmatrix} c_1 \\ c_2 \\ \dots \\ c_m \end{bmatrix} \tag{1.6}$$

and

$$\langle\psi| = \begin{bmatrix} c_1^* & c_2^* & \dots & c_m^* \end{bmatrix} \tag{1.7}$$

where c_i is a complex scalar value and the asterisk denotes the complex conjugate of said value. Common operations in Bra-Ket notation include taking the inner product defined as

$$\langle\psi|\psi\rangle = \begin{bmatrix} c_1^* & c_2^* & \dots & c_m^* \end{bmatrix} \begin{bmatrix} c_1 \\ c_2 \\ \dots \\ c_m \end{bmatrix} = c_1^* c_1 + c_2^* c_2 + \dots + c_m^* c_m = \sum_i^m |c_i|^2 \tag{1.8}$$

where $c_i^* c_i$ can be interpreted as the contribution function $\psi_i^* \psi_i$ has to the total wave function ψ, and the outer product defined as

$$|\psi\rangle\langle\psi| = \begin{bmatrix} c_1 \\ c_2 \\ ... \\ c_m \end{bmatrix} \begin{bmatrix} c_1^* & c_2^* & ... & c_m^* \end{bmatrix} = \begin{bmatrix} c_1 c_1^* & c_1 c_2^* & ... & c_1 c_m^* \\ c_2 c_1^* & c_2 c_2^* & ... & c_2 c_m^* \\ ... & ... & ... & ... \\ c_m c_1^* & c_m c_2^* & ... & c_m c_m^* \end{bmatrix} \tag{1.9}$$

which can be used to obtain density matrices. Bras and kets can be viewed as the conjugate transpose of each other, such that

$$\langle\Psi|^\dagger = |\Psi\rangle \tag{1.10}$$

and

$$|\Psi\rangle^\dagger = \langle\Psi| \tag{1.11}$$

1.1.2 The Born-Oppenheimer Approximation

Returning to the energy operator, $\hat{H}$, it must contain all relevant kinetic and potential energy terms for the system. As the primary types of systems of interest in quantum chemistry are composed of protons and electrons, $\hat{H}$ can be written, in atomic units and neglecting relativity, as:

$$\hat{H} = -\sum_i^N \frac{1}{2}\nabla_i^2 - \sum_A^M \frac{1}{2M_A}\nabla_A^2 - \sum_i^N \sum_A^M \frac{Z_A}{r_{iA}} + \sum_i^N \sum_{j>i}^N \frac{1}{r_{ij}} + \sum_A^M \sum_{A>B}^M \frac{Z_A Z_B}{r_{AB}}. \tag{1.12}$$

Where i and j correspond to the i^{th} and j^{th} electrons in a system composed of N electrons. Likewise, A and B correspond to the A^{th} and B^{th} nuclei in a system composed of M nuclei. The first two terms on the right-hand side of Eq. 1.12 are the electronic and nuclear kinetic energy terms respectively. The third, fourth, and fifth terms are the electron-nuclei attrac-

tion, the electron-electron repulsion, and the nuclei-nuclei repulsion respectively. Therefore, as the wave function exists in the same space as the Hamiltonian it also depends on both the nuclear and electronic coordinates as follows:

$$\Psi = \Psi[r_i, R_a]. \tag{1.13}$$

Solving for the nuclear-electronic wave function as given in Eq. 1.13 is often unnecessary as many molecular properties have minimal dependence on the motion of nuclei. This can be rationalized by recognizing that, since the mass ratio between an electron and a proton is approximately 1:1836, on the timescale of electronic motion, the nuclei are effectively fixed. In nuclei heavier than hydrogen, the mass ratio is even smaller, making this approximation even more justified. Using this idea of decoupling electronic and nuclear motion, the nuclear-electronic wave function can be split into an electronic wave function and a nuclear wave function by fixing the nuclei in space.

$$\Psi = |\Psi[r_i]\rangle|\Psi[R_a]\rangle. \tag{1.14}$$

This is known as the Born-Oppenheimer approximation[2] and allows us to simplify Eq. 1.12 down to the electronic Hamiltonian as:

$$\hat{H}_{elec} = -\sum_{i}^{N} \frac{1}{2}\nabla_i^2 - \sum_{i}^{N}\sum_{A}^{M} \frac{Z_A}{r_{iA}} + \sum_{i}^{N}\sum_{j>i}^{N} \frac{1}{r_{ij}}. \tag{1.15}$$

Where we have dropped the nuclear kinetic energy term as the nuclei's positions are now fixed. Additionally, since the nuclei-nuclei repulsion is now a constant, and thus shifts each energy level of the system equally, it can be removed from the electronic Hamiltonian and

added back in when calculating the total system energy as

$$E_{tot} = E_{elec} + E_{nuc} \tag{1.16}$$

where

$$E_{elec} = \langle \Psi_{elec} | \hat{H}_{elec} | \Psi_{elec} \rangle \tag{1.17}$$

and

$$E_{nuc} = \sum_{A}^{M} \sum_{A>B}^{M} \frac{Z_A Z_B}{r_{AB}}. \tag{1.18}$$

From Eq. 1.17 as the Hamiltonian no longer contains nuclei-dependent terms only the electronic wave function is needed. Eq. 1.15 is the general form of the Hamiltonian used within electronic structure theory.

1.1.3 The Variational Principle

All that remains in solving Eq. 1.17 is finding a wave function for the system of interest. To make the problem computationally tractable we need an objective function that will inform us about how close any arbitrary wave function is to the actual ground state wave function. Where ground state refers to the lowest energy wave function. We can do this by making use of the variational principle which states that any normalized trial wave function gives an energy that is an upper bound of the true ground state energy of the system as:

$$\langle \tilde{\Psi} | \hat{H} | \tilde{\Psi} \rangle \geq \langle \Psi_0 | \hat{H} | \Psi_0 \rangle = E_0 \tag{1.19}$$

with

$$|\tilde{\Psi}\rangle = \sum_{i} c_i |\Psi_i\rangle. \tag{1.20}$$

Here $\tilde{\Psi}$ is our trial wave function and $|\Psi_i\rangle$ are the true wave functions of the ground state ($|\Psi_0\rangle$) and all excited states ($|\Psi_{i\geq 1}\rangle$) of the system which completely span our space and thus any function satisfying the same boundary conditions as the set $\{|\Psi_i\rangle\}$ can be expressed as a linear combination of $\{|\Psi_i\rangle\}$ with coefficients c_i. Here all Ψ's are orthonormalized such that:

$$\langle\Psi_i|\Psi_j\rangle = \delta_{ij} \tag{1.21}$$

where δ_{ij} is the Dirac delta function which is equal to zero for all i $\neq$ j and one when i = j; additionally, the c_i's are constrained such that the trial wave function maintains normalization through:

$$1 = \sum_i |c_i|^2 \tag{1.22}$$

The true wave functions of the system result in ascending energies such that

$$\hat{H}|\Psi_i\rangle = E_i|\Psi_i\rangle \tag{1.23}$$

and

$$E_0 \leq E_1 \leq E_2... \tag{1.24}$$

Where E_0 is the true ground state energy, E_1 is the first excited state energy, and so on. Plugging our trial wave function into Eq. 1.19 gives

$$\sum_{ij} c_i c_j^* \langle\Psi_i|\hat{H}|\Psi_j\rangle \geq \langle\Psi_0|\hat{H}|\Psi_0\rangle. \tag{1.25}$$

Acting with the Hamiltonian to the right using Eq. 1.2 we obtain

$$\sum_{ij} c_i c_j^* \langle\Psi_i|\Psi_j\rangle E_i \geq \langle\Psi_0|\hat{H}|\Psi_0\rangle = E_0. \tag{1.26}$$

Since the wave functions are orthonormalized:

$$\sum_i |c_i|^2 E_i \geq \langle \Psi_0 | \hat{H} | \Psi_0 \rangle = E_0. \tag{1.27}$$

Rearranging:

$$|c_0|^2 E_0 + \sum_{i=1} |c_i|^2 E_i \geq \langle \Psi_0 | \hat{H} | \Psi_0 \rangle = E_0. \tag{1.28}$$

Here it is evident that any trial wave function will be an upper bound to the true ground state energy unless it is equal to the true ground state wave function. This bound can be used as a measure of the quality of any given trial wave function where the lower the energy of the trial wave function the better it should approximate the ground state.

1.1.4 Spin and Spatial Orbitals

To represent an electronic wave function for a single electron we use molecular orbitals (MOs) which are generally taken to be a linear combination of atomic orbitals (LCAOs). Electrons are fermionic particles with two possible spins, denoted as $M_s = \pm 1/2$, where $+1/2$ is an up spin or α electron and -1/2 is a down spin or β electron, they are thus antisymmetric with respect to exchanging a pair of electrons between orbitals. This directly results in the well-known Pauli exclusion principle[3] which states that no two electrons can be in the same orbital with the same spin. As the general form of the Hamiltonian, Eq. 1.15, does not contain information about spin or antisymmetry it is generally incorporated through the orbitals constituting the wave function. This is mathematically representable for a two-electron system with a single alpha and beta electron as:

$$|\Psi\rangle = \Psi(x_1, x_2) = \frac{1}{\sqrt{2}}[\phi_1(x_1)\bar{\phi}_1(x_2) - \phi_1(x_2)\bar{\phi}_1(x_1)] \tag{1.29}$$

Here ϕ_1 and $\bar{\phi}_1$ are alpha and beta spin orbitals respectively. These can be broken down into a spin and spatial component since:

$$\phi_1(x_1) = \chi_1(r)\alpha(\omega) \tag{1.30}$$

and

$$\bar{\phi}_1(x_1) = \chi_1(r)\beta(\omega), \tag{1.31}$$

which while having an identical spatial component are orthogonal as

$$\int \alpha(w)\beta(w)dw = 0. \tag{1.32}$$

From this representation, it is easy to see that interchanging x_1 and x_2 changes the sign of the wave function and that putting two electrons in the same spin-orbital would cause the wave function to be zero and thus invalid. This antisymmetric form of the wave function can be generalized through arbitrary numbers of electrons via a Slater determinant expressible as:

$$|\Psi\rangle = \Psi(x_1, x_2, x_3, ..., x_n) = \frac{1}{\sqrt{N!}} \begin{bmatrix} \phi_{11} & \bar{\phi}_{11} & \phi_{12} & \cdots & \phi_{1d} \\ \phi_{21} & \bar{\phi}_{21} & \phi_{22} & \cdots & \phi_{2d} \\ \vdots & \vdots & \vdots & \ddots & \vdots \\ \phi_{n1} & \bar{\phi}_{n1} & \phi_{n2} & \cdots & \phi_{nd} \end{bmatrix} \tag{1.33}$$

where once again the bar denotes a beta spin-orbital. Assuming a two-electron system and evaluating the determinant of the above matrix, we recover the same antisymmetric wave function from Eq. 1.29.

$$\Psi(x_1, x_2) = \frac{1}{\sqrt{2}} \begin{vmatrix} \phi_{11} & \bar{\phi}_{11} \\ \phi_{21} & \bar{\phi}_{21} \end{vmatrix} = \frac{1}{\sqrt{2}}[\phi_1(x_1)\bar{\phi}_1(x_2) - \phi_1(x_2)\bar{\phi}_1(x_1)]. \tag{1.34}$$

1.1.5 Wedge Products

Another way of expressing an anti-symmetrized wave function is with Grassmann wedge products $\wedge$. Equation 1.34 could be expressed using wedge products as

$$\frac{1}{\sqrt{N}}\phi_1(x_1) \wedge \bar{\phi}_1(x_2) \tag{1.35}$$

where

$$\phi_1(x_1) \wedge \bar{\phi}_1(x_2) = \phi_1(x_1)\bar{\phi}_1(x_2) - \phi_1(x_2)\bar{\phi}_1(x_1). \tag{1.36}$$

In general

$$\phi_i \wedge \phi_j \wedge ...\phi_n = \sum_P sgn(P)\phi_i(P_1)\phi_j(P_2)...\phi_n(P_n) \tag{1.37}$$

where P is a specific permutation of the electrons (x_1, x_2,...,x_n), P_1 and onwards are the indexed terms in the specific permutation (eg. P_1, P_2 are the first and second terms in the permutation) and $sgn(P)$ is the permutation symbol of P which is 1 or -1 if the number of pair permutations needed to recover the original order is even or odd respectively. Wedge product notation, when applied to matrices or tensors, acts as

$$A^i_k \wedge B^j_l = \sum sgn(P^{up})sgn(P^{dn})A^{P_1^{up}}_{P_1^{low}}B^{P_2^{up}}_{P_2^{low}} \tag{1.38}$$

where the upper and lower indices are permuted independently of one another.

1.2 Hartree-Fock

If we assume that the wave function of a system is well represented by a single Slater determinant, then we can obtain the mean field method known as Hartree-Fock[4, 5]. What is meant by mean field here will be discussed in further depth in subsection 1.4.6 on Electron Correlation. Starting from this assumption and acting on the ground state wave function

with the Hamiltonian given in Eq. 1.15 we get

$$[-\sum_{i}^{N}\frac{1}{2}\nabla_i^2-\sum_{i}^{N}\sum_{A}^{M}\frac{Z_A}{r_{iA}}+\sum_{i}^{N}\sum_{j>i}^{N}\frac{1}{r_{ij}}]|\Psi_0\rangle. \tag{1.39}$$

Where we can break the problem into 1 and 2 electron energy terms as

$$\langle\Psi_0|[-\sum_{i}^{N}\frac{1}{2}\nabla_i^2-\sum_{i}^{N}\sum_{A}^{M}\frac{Z_A}{r_{iA}}]|\Psi_0\rangle+\langle\Psi_0|\sum_{i}^{N}\sum_{j>i}^{N}\frac{1}{r_{ij}}|\Psi_0\rangle \tag{1.40}$$

Explicitly evaluating the one body term above using a 2-electron wave function from 1.34 we obtain:

$$\frac{1}{2}\langle\phi_1(x_1)\bar{\phi}_1(x_2)-\phi_1(x_2)\bar{\phi}_1(x_1)|-\sum_{i}^{N}\frac{1}{2}\nabla_i^2-\sum_{i}^{N}\sum_{A}^{M}\frac{Z_A}{r_{iA}}|\phi_1(x_1)\bar{\phi}_1(x_2)-\phi_1(x_2)\bar{\phi}_1(x_1)\rangle \tag{1.41}$$

which can be expanded as:

$$\begin{aligned}
&+\frac{1}{2}\langle\phi_1(x_1)\bar{\phi}_1(x_2)|-\sum_{i}^{N}\frac{1}{2}\nabla_i^2-\sum_{i}^{N}\sum_{A}^{M}\frac{Z_A}{r_{iA}}|\phi_1(x_1)\bar{\phi}_1(x_2)\rangle\\
&-\frac{1}{2}\langle\phi_1(x_1)\bar{\phi}_1(x_2)|-\sum_{i}^{N}\frac{1}{2}\nabla_i^2-\sum_{i}^{N}\sum_{A}^{M}\frac{Z_A}{r_{iA}}|\phi_1(x_2)\bar{\phi}_1(x_1)\rangle\\
&-\frac{1}{2}\langle\phi_1(x_2)\bar{\phi}_1(x_1)|-\sum_{i}^{N}\frac{1}{2}\nabla_i^2-\sum_{i}^{N}\sum_{A}^{M}\frac{Z_A}{r_{iA}}|\phi_1(x_1)\bar{\phi}_1(x_2)\rangle\\
&+\frac{1}{2}\langle\phi_1(x_2)\bar{\phi}_1(x_1)|-\sum_{i}^{N}\frac{1}{2}\nabla_i^2-\sum_{i}^{N}\sum_{A}^{M}\frac{Z_A}{r_{iA}}|\phi_1(x_2)\bar{\phi}_1(x_1)\rangle.
\end{aligned} \tag{1.42}$$

Let's look at two prototypical examples from 1.42, the kinetic energy term in the first and second lines. In the first line, the wave function in the bra and the ket are the same and can

be rewritten into their integral form:

$$\frac{1}{2}\int\int \phi_1^\dagger(x_1)\bar{\phi}_1^\dagger(x_2)[-\frac{1}{2}\nabla_1^2 - \frac{1}{2}\nabla_2^2]\phi_1(x_1)\bar{\phi}_1(x_2)dx_1dx_2 \tag{1.43}$$

which can be further broken down to:

$$\begin{aligned} &-\frac{1}{4}\int\int \phi_1^\dagger(x_1)\nabla_1^2\phi_1(x_1)\bar{\phi}_1^\dagger(x_2)\bar{\phi}_1(x_2)dx_1dx_2 \\ &-\frac{1}{4}\int\int \bar{\phi}_1^\dagger(x_2)\nabla_2^2\bar{\phi}_1(x_2)\phi_1^\dagger(x_1)\phi_1(x_1)dx_1dx_2. \end{aligned} \tag{1.44}$$

Since the orbitals are orthonormalized, when no operator acts on them their integral over all space is either zero or one and can thus be easily integrated out. Using this idea on Eq 1.44 above, it can be further reduced to

$$-\frac{1}{4}\int \phi_1^\dagger(x_1)\nabla_1^2\phi_1(x_1)dx_1 - \frac{1}{4}\int \bar{\phi}_1^\dagger(x_2)\nabla_2^2\bar{\phi}_1(x_2)dx_2. \tag{1.45}$$

If we repeat the above logic with the second line of eq: 1.42 we get

$$\begin{aligned} &+\frac{1}{4}\int\int \phi_1^\dagger(x_1)\nabla_1^2\bar{\phi}_1(x_1)\bar{\phi}_1^\dagger(x_2)\phi_1(x_2)dx_1dx_2 \\ &+\frac{1}{4}\int\int \phi_1^\dagger(x_2)\nabla_2^2\bar{\phi}_1(x_2)\bar{\phi}_1^\dagger(x_1)\phi_1(x_1)dx_1dx_2 \end{aligned} \tag{1.46}$$

Integrating over the electron not acted on by ∇ as we did previously now gives zero due to $\bar{\phi}_1^\dagger$ and ϕ_1's orthogonal spins. This same logic extends to the electronic-nuclear term as well, where it is only non-zero when the electrons are in the same orbitals in both the bra and ket of the wave function. Therefore, for a two-electron system as above, the one-electron

energies can be written as:

$$\begin{aligned}\hat{H}_{core}(1,2) &= \hat{T}(1) + \hat{T}(2) + \hat{V}_{ne}(1) + \hat{V}_{ne}(2) \\ &= -\frac{1}{2}\int \phi_1^\dagger(x_1)\nabla_1^2\phi_1(x_1)dx_1 - \frac{1}{2}\int \bar{\phi}_1^\dagger(x_2)\nabla_2^2\bar{\phi}_1(x_2)dx_2 \\ &- \int \phi_1^\dagger(x_1)\sum_A^M \frac{Z_A}{r_{1A}}\phi_1(x_1)dx_1 - \int \bar{\phi}_1^\dagger(x_2)\sum_A^M \frac{Z_A}{r_{2A}}\bar{\phi}_1(x_2)dx_2\end{aligned} \tag{1.47}$$

Where we introduce $\hat{T}$ and $\hat{V}_{ne}$ for the kinetic and electronic nuclear energies respectively. Doing the same treatment as above but for the electron-electron interactions we obtain the first two terms analogously to 1.44:

$$\begin{aligned}&+\frac{1}{2}\int\int \phi_1^\dagger(x_1)\bar{\phi}_1^\dagger(x_2)\frac{1}{r_{12}}\phi_1(x_1)\bar{\phi}_1(x_2)dx_1dx_2 \\ &-\frac{1}{2}\int\int \phi_1^\dagger(x_1)\bar{\phi}_1^\dagger(x_2)\frac{1}{r_{12}}\phi_1(x_2)\bar{\phi}_1(x_1)dx_1dx_2\end{aligned} \tag{1.48}$$

The first line in eq: 1.48 can be classically interpreted as a coulombic interaction by rewriting it in an equivalent form as

$$\begin{aligned}\hat{J}_{1\bar{1}} = \langle\phi_1\bar{\phi}_1|\phi_1\bar{\phi}_1\rangle =& \frac{1}{2}\int\int \phi_1^\dagger(x_1)\phi_1(x_1)\frac{1}{r_{12}}\bar{\phi}_1^\dagger(x_2)\bar{\phi}_1(x_2)dx_1dx_2 \\ =& \frac{1}{2}\int\int |\phi_1(x_1)|^2\frac{1}{r_{12}}|\bar{\phi}_1(x_2)|^2dx_1dx_2.\end{aligned} \tag{1.49}$$

This is commonly denoted via J or the two-electron integral shorthand $\langle ab|ab\rangle$ as shown above. The second term in eq: 1.48 does not have a nice classical interpretation. If we try to rewrite it as we did for the coulombic term, we obtain

$$\begin{aligned}\hat{K}_{1\bar{1}} = \langle\phi_1\bar{\phi}_1|\bar{\phi}_1\phi_1\rangle =& \frac{1}{2}\int\int \phi_1^\dagger(x_1)\bar{\phi}_1^\dagger(x_2)\frac{1}{r_{12}}\phi_1(x_2)\bar{\phi}_1(x_1)dx_1dx_2 \\ =& \frac{1}{2}\int\int \phi_1^\dagger(x_1)\bar{\phi}_1(x_1)\frac{1}{r_{12}}\phi_1(x_2)\bar{\phi}_1^\dagger(x_2)dx_1dx_2\end{aligned} \tag{1.50}$$

where each electron is split between two different orbitals. This is known as the exchange term, due to the exchange of the electrons' orbitals, and arises from the antisymmetry of the wave function. For a wave function composed of a single Slater determinant, the exchange term is only nonzero for same spin electrons. This term results in a lowering of the energy of the system, hence favoring parallel spins, and is generally denoted via a K or by $\langle ab|ba\rangle$. The two-electron energy terms for this two-electron system can be written as

$$\begin{aligned}\hat{H}_{ee} &= \hat{J}(1,2) - \hat{K}(1,2) \\ &= \langle \phi_1 \bar{\phi_1} | \phi_1 \bar{\phi_1} \rangle - \langle \phi_1 \bar{\phi_1} | \bar{\phi_1} \phi_1 \rangle \\ &= \int\int \phi_1^\dagger(x_1) \bar{\phi}_1^\dagger(x_2) \frac{1}{r_{12}} [\phi_1(x_1)\bar{\phi}_1(x_2) - \phi_1(x_2)\bar{\phi}_1(x_1)] dx_1 dx_2\end{aligned} \tag{1.51}$$

Therefore the electronic ground state for a two-electron system from Hartree-Fock (or a single Slater determinant) is

$$\begin{aligned}E_{elec} &= \hat{H}_{core}(1,2) + \hat{H}_{ee}(1,2) \\ &= \hat{T}(1) + \hat{T}(2) + \hat{V}_{ne}(1) + \hat{V}_{ne}(2) + \hat{J}(1,2) - \hat{K}(1,2)\end{aligned} \tag{1.52}$$

For an N-electron system, the energy is expressed as:

$$E_{elec} = \sum_i^N \hat{T}(i) + \sum_i^N \sum_A^M \hat{V}_{ne}(i,A) + \sum_{i<j}^N \hat{J}(i,j) - \hat{K}(i,j) \tag{1.53}$$

where the sum is over $i < j$ to prevent double counting of the electronic energy due to swapping indices.

1.2.1 Solving for the Ground State

To solve for the ground state in Hartree-Fock we can invoke the variational principle and target the single Slater determinant that gives the lowest energy as the best approximation

to the actual wave function. This can be done by searching for an energetic minima

$$\begin{aligned} E[\psi + \delta\psi] &= \langle \psi + \delta\psi | \hat{H} | \psi + \delta\psi \rangle \\ &= \langle \psi | \hat{H} | \psi \rangle + \langle \delta\psi | \hat{H} | \psi \rangle + \langle \psi | \hat{H} | \delta\psi \rangle + \langle \delta\psi | \hat{H} | \delta\psi \rangle \\ &= E + \delta E + \mathcal{O}(\delta^2 E). \end{aligned} \tag{1.54}$$

Here we will only concern ourselves with first-order solutions where $\delta E = 0$. However, we cannot just directly minimize the energy of the system as the orbitals need to remain orthonormal to each other. Therefore, we can use Lagrange's method of undetermined multipliers to minimize the energy while ensuring the orbitals remain orthonormalized.

$$\mathcal{L} = \langle \psi | \hat{H} | \psi \rangle - \sum_{i}^{N} \sum_{j}^{N} \int \epsilon_{ij} (\phi_i^*(x_1) \phi_j(x_1) dx_1 - \delta_{ij}) \tag{1.55}$$

Where $|\psi\rangle = |\phi_1 \phi_2 ... \phi_N\rangle$ as it is a single Slater determinant and ϵ_{ij} are the Lagrange multipliers. By taking the derivative of eq: 1.55 with respect to the orbitals ϕ and setting the result equal to zero

$$0 = \langle \psi^{'} | \hat{H} | \psi \rangle + \langle \psi | \hat{H} | \psi^{'} \rangle - \sum_{i}^{N} \sum_{j}^{N} \epsilon_{ij} \int [\phi_i^{*'}(x_1) \phi_j(x_1) + \phi_i^*(x_1) \phi_j^{'}(x_1)] dx_1 \tag{1.56}$$

we can obtain a minimum of the energy subject to the orbitals being orthogonal. By choosing a basis such that the Lagrange multipliers ϵ are diagonal and simplifying, we obtain

$$[\hat{H}_{core}(x_i) + \hat{J}(x_i) + \hat{K}(x_i)] \phi_i(x_i) = \hat{F}(x_i) \phi_i = \epsilon_i \phi_i(x_i) \tag{1.57}$$

where $\hat{F}(x_i)$ is the Fock operator. Eq. 1.57 is recognizable as an eigenvalue problem, where the resulting eigenvectors are the molecular orbitals $\phi_i(x_i)$ and the eigenvalues are the orbital energies ϵ_i. However, as $\hat{J}$ and $\hat{K}$ depend on the previous set of molecular orbitals this

procedure needs to be solved "self consistently" giving rise to what is known as the self-consistent field procedure (SCF) used for obtaining Hartree-Fock's ground state. Therefore, to find the ground state Hartree-Fock solution, one takes an initial set of orbitals, constructs $\hat{F}$, and diagonalizes it to obtain a new set of orbitals. This repeats until the change in orbitals between iterations is below a predefined convergence threshold.

1.3 Density Functional Theory

Density Functional Theory (DFT) is one of the most widely used methods for calculating ground state properties of molecular systems due to its relatively high accuracy as well as its computational affordability. This favorable combination arises due to DFT describing electronic interactions as a functional of the electronic density instead of trying to use the full N-electron wave function. The foundations of DFT were theoretically justified by Hohenberg and Kohn[6] in 1964 where they showed using proof by contradiction that the groundstate external potential, denoted V_{ext}, is a unique functional - to within a constant - of the electron density $\rho(\vec{r})$. Here V_{ext} is defined as all potentials the electrons experience besides those generated from other electrons such as the electron-electron interactions, V_{ee}. Therefore, if you know this unique functional of the electron density, a wave function is unnecessary for obtaining ground state properties such as the energy.

Hohenberg and Kohn's proof goes as follows, assume you have two Hamiltonians that differ in only their external potentials, but both give rise to the same density

$$\begin{aligned} \hat{H}^1 &= \hat{T} + \hat{V}_{ee} + \hat{V}^1_{ext} \\ \hat{H}^2 &= \hat{T} + \hat{V}_{ee} + \hat{V}^2_{ext}. \end{aligned} \tag{1.58}$$

Therefore they have two different ground state wave functions

$$\begin{aligned} \hat{H}^1|\Psi^1\rangle = E_0^1|\Psi^1\rangle \Rightarrow \rho(\vec{r}) \\ \hat{H}^2|\Psi^2\rangle = E_0^2|\Psi^2\rangle \Rightarrow \rho(\vec{r}). \end{aligned} \tag{1.59}$$

By the variational principle

$$\begin{aligned} E_0^1 < \langle\Psi^2|\hat{H}^1|\Psi^2\rangle = \langle\Psi^2|\hat{H}^2|\Psi^2\rangle - \langle\Psi^2|\hat{H}^2 - \hat{H}^1|\Psi^2\rangle \\ E_0^2 < \langle\Psi^1|\hat{H}^2|\Psi^1\rangle = \langle\Psi^1|\hat{H}^1|\Psi^1\rangle - \langle\Psi^1|\hat{H}^1 - \hat{H}^2|\Psi^1\rangle. \end{aligned} \tag{1.60}$$

Expanding the two Hamiltonians

$$\begin{aligned} E_0^1 < E_0^2 - \langle\Psi^2|\hat{T} + \hat{V}_{ee} + \hat{V}_{ext}^2 - (\hat{T} + \hat{V}_{ee} + \hat{V}_{ext}^1)|\Psi^2\rangle \\ E_0^2 < E_0^1 - \langle\Psi^1|\hat{T} + \hat{V}_{ee} + \hat{V}_{ext}^1 - (\hat{T} + \hat{V}_{ee} + \hat{V}_{ext}^2)|\Psi^1\rangle \end{aligned} \tag{1.61}$$

and simplifying gives

$$\begin{aligned} E_0^1 < E_0^2 - \langle\Psi^2|\hat{V}_{ext}^2 - \hat{V}_{ext}^1|\Psi^2\rangle \\ E_0^2 < E_0^1 - \langle\Psi^1|\hat{V}_{ext}^1 - \hat{V}_{ext}^2|\Psi^1\rangle. \end{aligned} \tag{1.62}$$

However, since both wave functions yield the same density

$$\begin{aligned} E_0^1 < E_0^2 + \int \rho(\vec{r})[\hat{V}_{ext}^1 - \hat{V}_{ext}^2]d\vec{r} \\ E_0^2 < E_0^1 - \int \rho(\vec{r})[\hat{V}_{ext}^1 - \hat{V}_{ext}^2]d\vec{r} \end{aligned} \tag{1.63}$$

adding them together leads to the contradiction:

$$E_0^1 + E_0^2 < E_0^2 + E_0^1. \tag{1.64}$$

Therefore, the electronic density must be a unique functional of the external potential.

However, how can we be sure that we have the correct density for the ground state? Since each wave function maps to a different electron density as proven above, we can invoke the variation principle to obtain the lowest energy electron density which should be closest to the exact wave function's electron density[6]. To prove this we can write the energy as a functional of the ground state electronic density, as shown above, as

$$E_0[\rho] = T[\rho] + \int \rho(\vec{r})\hat{V}_{ext}d\vec{r} + E_{ee}[\rho] = \langle\Psi|\hat{H}|\Psi\rangle \tag{1.65}$$

If we use a different electronic density

$$E[\tilde{\rho}] = T[\tilde{\rho}] + \int \tilde{\rho}(\vec{r})\hat{V}_{ext}d\vec{r} + E_{ee}[\tilde{\rho}] = \langle\tilde{\Psi}|\hat{H}|\tilde{\Psi}\rangle \tag{1.66}$$

then by the variational principle

$$E_0[\rho] = \langle\Psi|\hat{H}|\Psi\rangle < E[\tilde{\rho}] = \langle\tilde{\Psi}|\hat{H}|\tilde{\Psi}\rangle. \tag{1.67}$$

1.3.1 Kohn-Sham Density Functional Theory

Using the idea that there is a unique functional of the external potential and that the variational principle applies to ground state electronic densities, in 1965 Kohn and Sham[7] introduced a framework for performing ground state calculations in a manner analogous to Hartree-Fock. The difficulty in directly minimizing the electronic density lay in accurately capturing the kinetic energy as a function of the electronic density, as even 60 years later it is still an active area of research. To avoid this issue they introduced a non-interacting auxiliary system such that it gives the same electronic density as the system with interacting particles but can be represented with a Slater determinant. Therefore, the energy can be written as

$$E[\rho] = T_s[\rho] + \int dr v_{ext}(r)\rho(r) + E_H[\rho] + E_{XC}[\rho] \tag{1.68}$$

where

$$\rho(\vec{r}) = \sum_{i}^{N} \phi_i^{\dagger}(\vec{r})\phi_i(\vec{r}) \tag{1.69}$$

$$T_s[\rho] = -\frac{1}{2}\sum_{i}^{N} \int \phi_i^{\dagger}(\vec{r})\nabla_i\phi_i(\vec{r})d\vec{r} \tag{1.70}$$

$$E_H[\rho] = \frac{1}{2}\int\int \frac{\rho(\vec{r})\rho(\vec{r})^{'}}{|\rho - \rho^{'}|} \tag{1.71}$$

$$E_{XC}[\rho] = T[\rho] - T_s[\rho] + \int \rho(\vec{r})\epsilon_{xc}[\rho(\vec{r})]d\vec{r}. \tag{1.72}$$

Here T_s is the non-interacting kinetic energy, E_H is the coulombic term, and E_{XC} is the exchange correlation functional. This functional contains the correction from the non-interacting kinetic energy to the interacting kinetic energy as well as the electronic exchange and correlation effects. Unfortunately, this term is incredibly complicated and likely unknowable in general; therefore it is approximated in practice. Since there is a Slater determinant being used to represent the non-interacting auxiliary system, finding the ground state in Kohn-Sham DFT (KS-DFT) is the same as Hartree-Fock. Obtain the effective Kohn-Sham matrix, which is analogous to the Hartree-Fock's Fock matrix, given as

$$H_{KS}[\rho] = T_s[\rho] + v_{ext}(\rho) + \int \frac{\rho}{|\rho - \rho^{'}|}dr^{'} + v_{xc}(\rho) \tag{1.73}$$

where the third and fourth terms on the right-hand side are the derivatives of Eq. 1.71 and 1.72 respectively. Next, diagonalize the above Kohn-Sham matrix to obtain a new set of orbitals following Eq. 1.69. Use these orbitals to generate an updated electronic density to obtain a new effective Kohn-Sham matrix and repeat until the difference in the densities between iterations is below an acceptable threshold.

1.3.2 Density Functionals

While the exact universal functional, E_{XC}, is not known there have been a plethora of approximations to it constructed over the years. The first being introduced by Kohn and Sham was the Local Spin Density Approximation[7] (LSDA) which is based on the homogeneous electron gas and only depends upon the electronic density at each point in space. Since then many more exchange correlation functionals have been developed leading John Perdew to suggest a Jacob's ladder classification scheme[8], shown in Figure 1.1, based upon the functionals inputs where the higher one ascends the ladder the closer they come to chemical accuracy. The predominantly utilized levels of Jacob's ladder are the lowest 4 consisting of Local Spin Density Approximations (LSDAs), Generalized Gradient Approximations (GGAs), Meta-Generalized Gradient Approximations (mGGAs), and Hartree-Fock exchange (Hybrid). Each step up the ladder introduces a new ingredient for the functionals to utilize, with LDSAs introducing the electron density, GGAs the first derivative of the electron density, mGGAs the second derivative of the electron density, and Hybrid functionals the exchange term from Hartree-Fock. Introducing these new terms also introduces computational overhead, although it tends not to be significant until reaching hybrid functionals. Furthermore, while each level introduces new functional inputs, they do not need to use all the lower-level inputs. An example of this is the PBE0 functional which, while being a hybrid functional, does not use the second derivative of the electron density.

Due to the approximate nature of the exchange correlation functionals in use today, the absolute energies obtained from DFT are not inherently meaningful. Depending on the functional employed, it is easy to produce either a higher or lower energy than FCI - the variationally lowest possible energy in a given basis set - due to the approximate functional erroneously over or under-correlating the electrons. While the absolute energies aren't meaningful, the relative energies still are as they ideally result in a cancellation of errors.

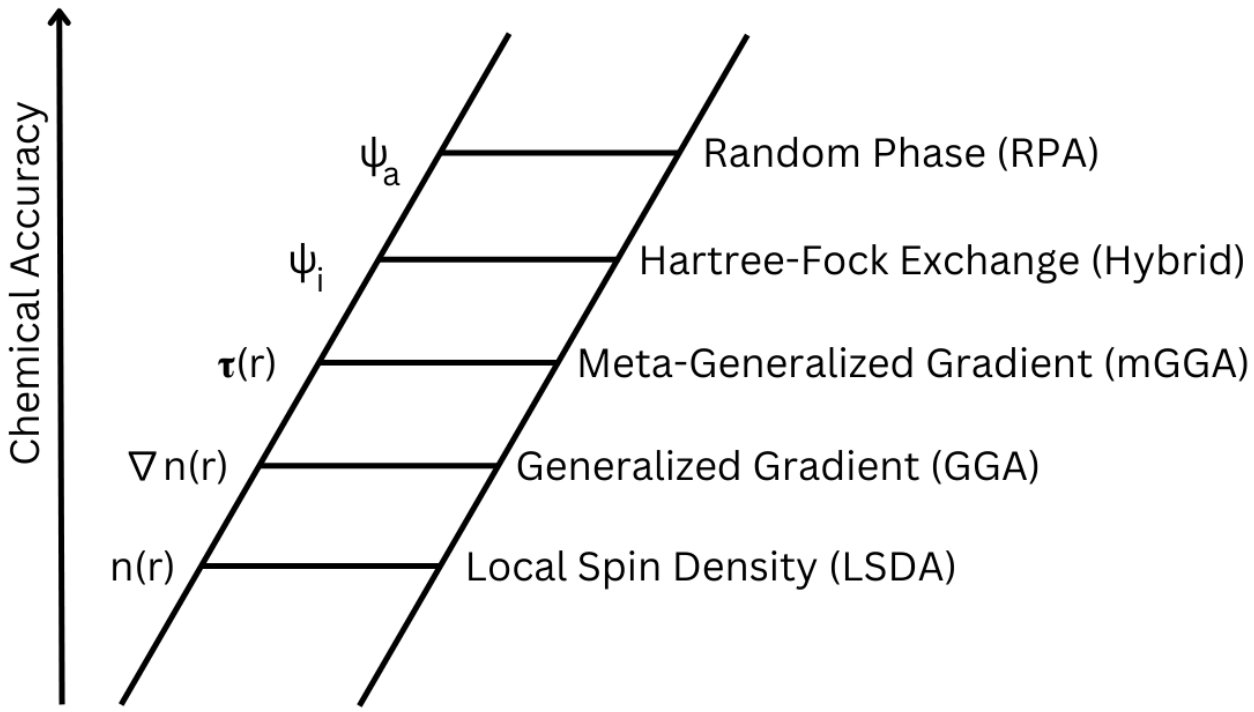

Figure 1.1: Jacob's ladder classification scheme introduced to partition density functionals based upon their functional inputs. n(r), ∇n(r), and τ(r) are electron density, and it's first and second derivative respectively. Ψ_i and Ψ_a are respectively the occupied and virtual orbitals.

1.4 Electron correlation and Post-Hartree-Fock methods

An alternative approach to improving upon Hartree-Fock involves generating a more complicated wave function to represent the system. These are generally taken to be a linear combination of Slater determinants, which themselves can be expressed as excitations from the Hartree-Fock reference.

1.4.1 Second Quantization

To make it easier to write more complex wave functions than a single Slater determinant, it is useful to introduce second quantization. Everything preceding this point utilized first quantization, where the wave function contains the antisymmetry of the system, in contrast, second quantization ensures anti-symmetry via creation/annihilation operators ($a_i^\dagger/a_i$). These op-

erators act to either create or annihilate an electron in orbital i. As an example:

$$a_1|\phi_1\bar{\phi}_1\rangle = |\bar{\phi}_1\rangle => a_1\underline{\downarrow\uparrow} = \underline{\downarrow\ } \tag{1.74}$$

$$a_1^\dagger|\bar{\phi}_1\rangle = |\phi_1\bar{\phi}_1\rangle => a_1^\dagger\underline{\downarrow\ } = \underline{\downarrow\uparrow} \tag{1.75}$$

where

$$|\phi_1\bar{\phi}_1\rangle = \frac{1}{\sqrt{2!}}\begin{vmatrix}\phi_{11} & \bar{\phi}_{11}\\ \phi_{21} & \bar{\phi}_{21}\end{vmatrix} \text{ and } |\phi_1\rangle = \Big|\phi_{11}\Big|. \tag{1.76}$$

We can view the action of the annihilation operator on a Slater determinant using an integral as

$$a_1|\phi_1\bar{\phi}_1\rangle = \int \sqrt{N}\phi_1^*(1)\frac{1}{\sqrt{2!}}[\phi_1(1)\bar{\phi}_1(2) - \bar{\phi}_1(1)\phi_1(2)]d1 \tag{1.77}$$

where N is the number of electrons in the system, which in this case is two. Evaluating the integral results in

$$a_1|\phi_1\bar{\phi}_1\rangle = |\bar{\phi}_1(1)| = |\bar{\phi}_1\rangle \tag{1.78}$$

which is what is expected. It should be noted that $a_1|\bar{\phi}_1\phi_1\rangle$ would evaluate to $-|\bar{\phi}_1\rangle$ as the sign of the Slater determinant has changed. In general, it is common practice to move whichever orbital is being annihilated to the leftmost element of the ket. Doing this causes the sign of the wave function to switch if the orbital has to move an odd number of spaces.

However, it may be easier to manipulate strings of annihilation operators than the corresponding wave function. To understand how annihilation operators can be swapped, we can act on an arbitrary wave function with two different annihilation operators

$$\begin{aligned} a_i a_k|\phi_i\phi_j...\phi_k...\phi_l\rangle &= \\ &= (-1)^n a_i|\phi_i\phi_j...\phi_l\rangle \\ &= (-1)^n|\phi_j...\phi_l\rangle \end{aligned} \qquad \begin{aligned} a_k a_i|\phi_i\phi_j...\phi_k...\phi_l\rangle &= \\ &= a_k|\phi_j...\phi_k...\phi_l\rangle \\ &= (-1)^{n-1}|\phi_j...\phi_l\rangle \end{aligned}$$

Where here n is the number of permutations needed to move the appropriate orbital to the beginning of the ket. As both equations above share the same arbitrary wave function we can add them together to give

$$(a_i a_k + a_k a_i)|\phi_i \phi_j ... \phi_k ... \phi_l\rangle = 0 \tag{1.79}$$

therefore

$$a_i a_k + a_k a_i = 0. \tag{1.80}$$

This is known as an anti-commutation relationship which is also expressible as

$$\{a_i, a_k\} = a_i a_k + a_k a_i = 0. \tag{1.81}$$

Therefore swapping the ordering of adjacent annihilation operators changes the sign of the expression while being more convenient than going through and evaluating the effects upon the wave function.

If the wave function does not contain the orbital which is being annihilated the result is zero

$$a_1|\bar{\phi}_1\rangle = 0 \tag{1.82}$$

and whether the wave function contains the orbital; two adjacent annihilation operators acting on the same orbital is always zero

$$a_1 a_1|\Psi\rangle = 0. \tag{1.83}$$

In contrast to the annihilation operator which removes an electron, the creation operator

adds one, due to the anti-symmetry $a_i^\dagger$ can be viewed as a Grassman wedge product $\wedge$ as

$$a_1^\dagger|\bar{\phi}_1\rangle = \phi_1 \wedge \bar{\phi}_1 = \frac{\sqrt{N!}}{\sqrt{(N+1)!}}(\phi_1\bar{\phi}_1 - \bar{\phi}_1\phi_1) = \frac{1}{2}(\phi_1(1)\bar{\phi}_1(2) - \bar{\phi}_1(1)\phi_1(2)) = |\phi_1\bar{\phi}_1\rangle \quad (1.84)$$

where the N corresponds to the number of electrons in the original wave function and is used to maintain normalization. If we again act on an arbitrary wave function with two different creation operators

$$\begin{aligned} a_i^\dagger a_j^\dagger|\phi_k...\phi_l\rangle &= \\ &= |\phi_j\phi_k...\phi_l\rangle \\ &= |\phi_i\phi_j\phi_k...\phi_l\rangle \\ &= |\phi_i\phi_j\phi_k...\phi_l\rangle \end{aligned} \qquad \begin{aligned} a_j^\dagger a_i^\dagger|\phi_k...\phi_l\rangle &= \\ &= a_j^\dagger|\phi_i\phi_k...\phi_l\rangle \\ &= |\phi_j\phi_i\phi_k...\phi_l\rangle \\ &= -|\phi_i\phi_j\phi_k...\phi_l\rangle \end{aligned}$$

Since they once again share the same wave function we can add them together giving us

$$(a_i^\dagger a_j^\dagger + a_j^\dagger a_i^\dagger)|\phi_i\phi_j\phi_k...\phi_l\rangle = 0 \quad (1.85)$$

revealing the creation operators also obey the anti-commutation relation annihilation operators do

$$\{a_i^\dagger, a_j^\dagger\} = a_i^\dagger a_j^\dagger + a_j^\dagger a_i^\dagger = 0. \quad (1.86)$$

Analogous to annihilation operators, if an electron already exists in the orbital or the same creation operator occurs twice in a row:

$$a_i^\dagger a_i^\dagger|\phi_j...\phi_l\rangle = a_i^\dagger|\phi_i\phi_j...\phi_l\rangle = 0. \quad (1.87)$$

Furthermore, creation and annihilation operators are related to each other through

$$(\langle\Psi|a_i^\dagger)^\dagger = a_i|\Psi\rangle \quad (1.88)$$

therefore a creation (annihilation) operator, $a_i^\dagger$ (a_i), can be thought of as acting to the right to create (annihilate) an electron or through its conjugate transpose as acting to annihilate (create) an electron to the left.

The last situation that needs to be considered is a combination of creation and annihilation operators. There are two cases to look at which are whether they act on the same or different electrons

Same electron

$$(a_i^\dagger a_i + a_i a_i^\dagger)|\phi_j ... \phi_l\rangle = \\ = a_i|\phi_i \phi_j ... \phi_l\rangle \\ = |\phi_j ... \phi_l\rangle$$

$$(a_i^\dagger a_i + a_i a_i^\dagger)|\phi_i \phi_j ... \phi_l\rangle = \\ = a_i^\dagger|\phi_j ... \phi_l\rangle \\ = |\phi_i \phi_j ... \phi_l\rangle$$

In either case - the orbital already existing in the wave function or not - the same wave function is returned, therefore

$$a_i^\dagger a_i = 1 \tag{1.89}$$

Different electrons

$$(a_j^\dagger a_i + a_i a_j^\dagger)|\phi_i \phi_k ... \phi_l\rangle = \\ = a_j^\dagger|\phi_k ... \phi_l\rangle + a_i|\phi_j \phi_i \phi_k ... \phi_l\rangle \\ = a_j^\dagger|\phi_j \phi_k ... \phi_l\rangle - |\phi_j \phi_k ... \phi_l\rangle \\ = 0$$

All other combinations of orbitals i and or j existing in the wave function will be zero due to either creating an electron that already exists or annihilating one that doesn't. Therefore,

$$a_i^\dagger a_j = 0 \tag{1.90}$$

Overall this is expressible as

$$a_i^\dagger a_j = \delta_{ij} \tag{1.91}$$

where δ is a Dirac delta function defined as

$$\delta_{ij} = \begin{cases} 0 & i \neq j \\ 1 & i = j \end{cases}.$$

1.4.2 Second Quantized Operators

Operators can also be written in a second quantized form as

$$\hat{H} = \sum_{ij} h_{ij} a_i^\dagger a_j + \frac{1}{2} \sum_{ijkl} V_{kl}^{ij} a_i^\dagger a_j^\dagger a_l a_k \tag{1.92}$$

where

$$h_{ij} = \int -\frac{1}{2} \phi_i^\dagger(x_1) \nabla^2 \phi_j(x_1) dx_1 - \int \phi_i^\dagger(x_1) \sum_A^M \frac{Z_A}{r_{iA}} \phi_j(x_1) dx_1 \tag{1.93}$$

and

$$V_{kl}^{ij} = \frac{1}{2} \int \int \phi_i^\dagger(x_1) \phi_j^\dagger(x_2) \frac{1}{r_{12}} \phi_k(x_1) \phi_l(x_2) dx_1 dx_2. \tag{1.94}$$

Written in this form the anti-symmetry is contained within the creation annihilation operators instead of the integrals themselves. To obtain the ground state energy in a second quantized form

$$\langle \Psi | \hat{H} | \Psi \rangle = \langle \Psi | \sum_{ij} h_{ij} a_i^\dagger a_j | \Psi \rangle + \langle \Psi | \frac{1}{2} \sum_{ijkl} V_{kl}^{ij} a_i^\dagger a_j^\dagger a_l a_k | \Psi \rangle \tag{1.95}$$

$$= \sum_{ij} h_{ij} \langle \Psi | a_i^\dagger a_j | \Psi \rangle + \frac{1}{2} \sum_{ijkl} V_{kl}^{ij} \langle \Psi | a_i^\dagger a_j^\dagger a_l a_k | \Psi \rangle \tag{1.96}$$

$$= \sum_{ij} h_{ij} {}^1D_j^i + \frac{1}{2} \sum_{ijkl} V_{kl}^{ij} {}^2D_{kl}^{ij} \tag{1.97}$$

where ${}^1D_j^i$ and ${}^2D_{kl}^{ij}$ are the 1- and 2-electron Reduced Density Matrices respectively. These will be discussed in more depth in the Reduced Density Matrix section.

1.4.3 Configuration Interaction

Now that we've built up the second quantization framework, we can use it to go beyond the mean-field Hartree-Fock method for electronic structure theory. Taking $|\Psi_0\rangle$ to be our Hartree-Fock ground state Slater determinant, we can create a more complicated wave func-

tion as a linear combination of excitations (configurations) from this reference. Mathematically,

$$|\Psi\rangle = c_0|\Psi_0\rangle + \sum_{i}^{occ}\sum_{a}^{vir} c_i^a a_a^\dagger a_i|\Psi_0\rangle + \sum_{i<j}^{occ}\sum_{a<b}^{vir} c_{ij}^{ab} a_a^\dagger a_b^\dagger a_i a_j|\Psi_0\rangle... \tag{1.98}$$

where $ij...$ are occupied orbitals and $ab...$ are virtual or unoccupied orbitals and the c_i's are known as the ci coefficients, which represent the contribution to the wave function from each Slater determinant. If we continue this procedure and create a wave function containing every possible excitation (configuration) allowable, then we get Full Configuration Interaction (FCI). The structure of the FCI matrix for this wave function is expressible as

$$\begin{bmatrix} \langle\Psi_0|H|\Psi_0\rangle & 0 & \langle\Psi_0|H|D\rangle & 0 & ... \\ & \langle S|H|S\rangle & \langle S|H|D\rangle & \langle S|H|T\rangle & ... \\ & & \langle D|H|D\rangle & \langle D|H|T\rangle & ... \\ & & & \langle T|H|T\rangle & ... \end{bmatrix}. \tag{1.99}$$

Where $|S\rangle$, $|D\rangle$, $|T\rangle$ are single, double and triplet excitations respectively defined as $a_a^\dagger a_i|\Psi_0\rangle$, $a_a^\dagger a_b^\dagger a_i a_j|\Psi_0\rangle$, and $a_a^\dagger a_b^\dagger a_c^\dagger a_i a_j a_k|\Psi_0\rangle$. Since the Hamiltonian is written in second quantization, as shown in Eq. 1.97, only has up to two body operations it can only connect configurations that differ by at most two electrons. Any pair of configurations differing by three or more electrons, for example, the ground state and a triply excited configuration, will be zero. However, this does not explain why single excitations do not couple with the ground state. The reason for this is Brillouin's theorem, which states that single excitations correspond to an off-diagonal element of the Fock matrix, but since we diagonalized the Fock matrix during the Hartree-Fock procedure these must be zero.

To obtain the wave functions corresponding to the ground and excited states from FCI, the matrix in Eq. 1.99 must be diagonalized. Unfortunately, while FCI is exact within a

$N_{configs}$	K	$N_\alpha = N_\beta$
1	2	2
784	8	2
246016	32	2
66064384	128	2
63504	10	5
165636900	16	8

Table 1.1: Number of configurations required by FCI for varying numbers of orbitals (K) and electrons (N)

given basis set, the number of configurations within the wave function is given by

$$N_{configs} = \binom{K}{N_\alpha}\binom{K}{N_\beta} \tag{1.100}$$

where K is the number of orbitals and N_α and N_β are the numbers of alpha and beta electrons respectively. We can evaluate Eq. 1.100 for different combinations of orbitals and electrons the results of which are given in Table 1.1. From the table, it is evident that the number of configurations required scales factorially with the number of orbitals and electrons. Putting these numbers in context, the largest FCI calculation, as of this writing, was 24 electrons in 24 orbitals which has $\sim$ one trillion configurations, required 8192 CPU cores, and took almost 14 hours to complete[9]. A more commonly listed limit for desktop computers is $\sim$ 18 electrons in 18 orbitals.

1.4.4 Truncated CI

It would not be unreasonable to expect that not all configurations, such as one where all the electrons in a system are excited into higher-level orbitals, would contribute significantly to its ground state character. This is the primary idea behind truncated CI; where the number of electrons excited out of the Hartree-Fock reference is limited in some fashion. If instead of including all excitations one limits themselves to only single and double excitations you'd get a truncated CI which in this case would be known as CISD where the SD refers to single and

double excitations. Due to Brillouin's theorem, which states that single excitations cannot couple directly to the Hartree-Fock reference, any methodology that aims to improve upon Hartree-Fock's ground state energy via excitations must include doubles, and as such CIS would not improve the ground state energy. Although the high order excitations generally contribute less to the ground state wave function than lower order excitations, it turns out truncating excitations results in size consistency issues[10]. This means that as the system size gets larger, a truncated CI's improvement over Hartree-Fock decreases. Mathematically, size consistency is expressed as

$$E(A+B) = E(A) + E(B) \tag{1.101}$$

where for a method to be size consistent the energy of two non-interacting systems - say for example at infinite distance - should be equal to the sum of each system individually. A simple example to show CID's lack of size consistency involves two helium atoms with two spatial orbitals each.

$$\mathrm{He}_1 \left(\begin{matrix} - & \underline{\downarrow\uparrow} \\ \underline{\downarrow\uparrow}\,, & - \end{matrix} \right) + \mathrm{He}_2 \left(\begin{matrix} - & \underline{\downarrow\uparrow} \\ \underline{\downarrow\uparrow}\,, & - \end{matrix} \right) \neq \mathrm{He}_1\mathrm{He}_2 \left(\begin{matrix} - - & \underline{\downarrow\uparrow}\ - & - \ \underline{\downarrow\uparrow} & \underline{\downarrow\uparrow}\,, & - \ \underline{\downarrow\uparrow}\ - & \underline{\downarrow\uparrow}\,, & \underline{\downarrow\uparrow}\ \underline{\downarrow\uparrow} \\ \underline{\downarrow\uparrow}\ - & - & \underline{\downarrow\uparrow} \end{matrix} \right) \tag{1.102}$$

as we can see, there is a quadruply excited configuration when calculating the two Heliums together which cannot be captured by CID but is needed to properly reproduce the energy and make it equivalent to two individual Helium atom energies added together. In practice, due to the issue of size-consistency, truncated CI methods are rarely used as larger system sizes will give increasing small improvements over Hartree-Fock. Instead, a popular technique called Coupled Cluster (CC) which truncates the number of excitations like in truncated CI but does not suffer from size consistency issues is used in its place.

1.4.5 Coupled Cluster

The way coupled cluster theory manages to be size consistent is by writing the wave function through an exponential ansatz as[11]

$$|\Psi\rangle = e^{\hat{T}}|\Phi_0\rangle \tag{1.103}$$

instead of a linear combination of Slater determinants like truncated CI approaches as shown in Eq. 1.98. Since a non-interacting system can be decomposed into a product wave function as follows

$$\Phi(A,B) = \Phi(A)\Phi(B) \tag{1.104}$$

as long as the operator $\hat{T}$ is additive then

$$\begin{aligned} e^{\hat{T}(A,B)}\Phi(A,B) &= e^{\hat{T}(A)+\hat{T}(B)}\Phi(A)\Phi(B) \\ &= e^{\hat{T}(A)}\Phi(A)e^{\hat{T}(B)}\Phi(B) \\ &= \Psi(A)\Psi(B) \end{aligned} \tag{1.105}$$

which ensures size-consistency through

$$\begin{aligned} \hat{H}(A,B)\Psi(A,B) &= \hat{H}(A)\Psi(A) + \hat{H}(B)\Psi(B) \\ &= [E(A)+E(B)]\Psi(A)\Psi(B). \end{aligned} \tag{1.106}$$

Returning to Eq. 1.103 and 1.105 the $\hat{T}$ is known as the cluster operator and is defined as

$$\hat{T} = T_1 + T_2 + T_3 + ... \tag{1.107}$$

where T_n is the corresponding operator for n^{th} level excitations. The single (T_1) and double (T_2) excitation operators are defined as

$$T_1 = \sum_i \sum_a t_a^i a_a^\dagger a_i \tag{1.108}$$

and

$$T_2 = \frac{1}{4} \sum_i \sum_j \sum_a \sum_b t_{ab}^{ij} a_a^\dagger a_b^\dagger a_j a_i \tag{1.109}$$

where the ts are known as the cluster amplitudes. If we assume only T_1 and T_2 make up the cluster operator $\hat{T}$ then we can expand the exponential ansatz using a Taylor series

$$e^{\hat{T}} = 1 + T_1 + T_2 + \frac{1}{2}T_1^2 + \frac{1}{2}T_1T_2 + \frac{1}{2}T_2T_1 + \frac{1}{2}T_2^2 + ... \tag{1.110}$$

where it is evident that coupled cluster theory approximates higher-order excitations through combinations of lower ones. This is made more explicit by observing the relationship between coupled clusters t amplitudes and the corresponding c_i coefficients. Up to triple excitations are given as

$$c_a^i = t_a^i \tag{1.111}$$

$$c_{ab}^{ij} = t_{ab}^{ij} + \frac{1}{2}t_a^i t_b^j \tag{1.112}$$

$$c_{abc}^{ijk} = t_{abc}^{ijk} + t_i^a t_{bc}^{jk} + \frac{1}{6}t_a^i t_b^j t_c t^k \tag{1.113}$$

where even if the explicit T_3 operator is not included in $\hat{T}$ then there is still an approximation to the triply excited state through T_1 and T_2. Unfortunately, while truncated coupled cluster is still size consistent, it is no longer variational. This can be seen by evaluating the energy expression

$$\langle E \rangle = \frac{\langle \Psi_0 | e^{-\hat{T}} H e^{\hat{T}} | \Psi_0 \rangle}{\langle \Psi_0 | \Psi_0 \rangle} \tag{1.114}$$

where if $\hat{T}$ is truncated then

$$\langle E \rangle = \frac{\langle \Theta_B | H | \Theta_A \rangle}{\langle \Psi_0 | \Psi_0 \rangle} \tag{1.115}$$

where $\Theta_A \neq \Theta_B$ as $e^{-\hat{T}} \neq (e^{\hat{T}})^\dagger$. Therefore, when represented as a linear combination of its eigenvectors

$$E = \frac{\sum_{ij} c_i^* d_j \langle \Psi_i | H | \Psi_j \rangle}{\langle \Psi_0 | \Psi_0 \rangle}. \tag{1.116}$$

Since c_i^* does not need to equal d_j there can be a negative contribution to the total energy from a pair of ij which can lead to energies below FCI. In practice, coupled cluster not being variational is not a large issue.

To get accurate properties from coupled cluster theory, it has been noted that triple excitations need to be included. Unfortunately, including them fully in the cluster operator $\hat{T}$ causes the resulting method, known as CCSDT, to scale as $\mathcal{O}(N^8)$ where N is the number of basis functions. This limits CCSDT's applicability to very small systems. There is another approach, however, known as CCSD(T) where instead of the triples being included in the cluster operator they are determined after as CCSD calculation using perturbation theory. This gives a methodology that recovers most of the contributions of the triples while only scaling as $\mathcal{O}(N^7)$. Due to this, CCSD(T) is generally regarded as the gold standard within electronic structure calculations.

1.4.6 Electron Correlation

The reason for wanting to introduce these improvements upon Hartree-Fock is to capture the electron correlation neglected due to the assumption that electrons interact in an averaged or mean field way. Put different, instead of feeling the instantaneous repulsion of an electron's motion, each electron will instead only feel the average of that motion. While this does capture the majority of the electronic interaction, often upwards of 95% of its total energy, that remaining correlated electronic motion can play an important role in describing

properties and reactivity.

This missing electron correlation energy is defined as

$$E_{correlation} = E - E_{HF} \tag{1.117}$$

where E is a higher-level wave function calculation such as FCI. $E_{correlation}$ is used as a measure of the improvement of a correlated calculation over Hartree-Fock where the more correlation energy that is captured, the larger the improvement in the representation of the underlying wave function. Density functional theory is not included in this list as its absolute energy is not reliable as previously discussed.

Electron correlation is generally broken into two domains: Strong or static correlation and weak or dynamic correlation. While these are both fundamentally the same property, electron's correlated motion, they are divided into these two categories for convenience. The simplest way to understand the difference between the two is through the FCI wave function. Strong correlation occurs when there are configurations other than the Hartree-Fock reference that contribute significantly to the character of the wave function. This expresses itself as multiple Slater determinants with large C_i coefficients in the wave function. A prototypical example of strong correlation is breaking the double bond in ethylene as one of the CH_2 groups is rotated 90^o of the other, resulting in a biradical. In contrast, weakly correlated electrons result in small C_i coefficients. In a typical molecular system, there may only be a few strongly correlated electrons, however, all the remaining electrons would still be weakly correlated with one another; thus weak correlation tends to contribute more significantly to the correlation energy.

The reason for dividing electron correlation into a strong and weak category is our algorithms for obtaining electronic properties tend to be able to capture either one of the two well but fail to properly capture or neglect the other entirely. A prime example of this is with density functional theory. Since we do not have the exact functional and are using a

single Slater determinant as our non-interacting reference, DFT fails to accurately describe strong correlation. It is however excellent at describing weak correlation and, since most molecules are only weakly correlated, has led to its rise as one of the main work horse's in quantum chemistry. On the flip side, there are methods such as Complete Active Space SCF where the FCI problem is solved in only a subset of the total orbitals for capturing strongly correlated electrons. As the remaining electrons will still only be described by mean field Hartree-Fock this approach cannot capture the weak electron correlation.

1.4.7 Multi-Configurational Pair Density Functional Theory

Multi-Configurational Pair Density Functional Theory (MC-PDFT) builds upon the idea of using a complete active space SCF calculation but instead of describing the electrons outside the active space with Hartree-Fock, it uses a modification to DFT[12]. The rationale behind this is that the active orbitals will capture the strong correlation and then DFT will describe the remaining dynamical correlation. Along these lines, the energy expression is given as

$$E = \langle \Psi | \hat{T} + \hat{V}_{ne} | \Psi \rangle + V_c[\rho] + E_{ot}[\rho, \Pi] \tag{1.118}$$

where V_c is the coulombic repulsion and E_{ot} is an on-top pair density functional to capture the remaining exchange and correlation.

Unlike density functionals, which use just the electronic density, on-top pair density functionals rely on the on-top pair density, which is the probability of finding two electrons at the same point in space. By using the spin magnetization defined as

$$m(r) = \rho_a(r) - \rho_b(r) \tag{1.119}$$

where a and b correspond to alpha and beta spin electrons, and the electron density $\rho(r)$

one can obtain the on-top pair density $\Pi(r)$ using

$$m(r) = \rho(r)[1 - \frac{4\Pi(r)}{\rho(r)^2}]^{1/2}. \tag{1.120}$$

Functionals previously developed for use in Density Functional Theory have to be "translated" into on-top pair density functionals from traditional density functionals using

$$E_{ot}[\rho(r), \Pi(r)] = E_{xc}\Bigg(\rho(r), \begin{Bmatrix} \rho(r)(1 - \frac{4\Pi(r)}{\rho(r)^2})^{1/2} & \text{if } R \leq 1 \\ 0 & \text{if } R > 1 \end{Bmatrix}, \rho^{'}(r), \begin{Bmatrix} \rho^{'}(r)(1 - \frac{4\Pi(r)}{\rho(r)^2})^{1/2} & \text{if } R \leq 1 \\ 0 & \text{if } R > 1 \end{Bmatrix}\Bigg) \tag{1.121}$$

who's form is motivated by Eq. 1.120. These translated functionals are denoted by a lowercase t in front of the untranslated functional name. For example, the PBE functional when translated is referred to as tPBE.

CHAPTER 2

REDUCED DENSITY MATRIX APPROACHES TO QUANTUM CHEMISTRY

2.1 Reduced Density Matrices and Their Properties

There is another approach to quantum chemistry which, instead of utilizing a wave function or the electron density, uses Reduced Density Matrices (RDM's). The 1- and 2-electron Reduced Density Matrices (1- and 2-RDMs) were introduced previously in Eq. 1.97 when the ground state energy was expressed using second quantization. For ease of reading I've rewritten it here:

$$\langle \Psi | \hat{H} | \Psi \rangle = \sum_{ij} h_{ij} {}^1D^i_j + \frac{1}{2} \sum_{ijkl} V^{ij}_{kl} {}^2D^{ij}_{kl}.$$

where ${}^1D^i_j$ is the 1-RDM defined as:

$${}^1D^i_j = \langle \Psi | a^\dagger_i a_j | \Psi \rangle \tag{2.1}$$

and ${}^2D^{ij}_{kl}$ is the 2-RDM defined as:

$${}^2D^{ij}_{kl} = \langle \Psi | a^\dagger_i a^\dagger_j a_l a_k | \Psi \rangle. \tag{2.2}$$

Diving into properties of RDMs, we'll first start with general properties they all share and then explore properties specific to the 1- and 2- RDMs. All RDMs are hermitian, meaning they equal their conjugate transpose, mathematically expressible as

$${}^pD = {}^pD^\dagger \tag{2.3}$$

where ${}^pD$ is an arbitrary p-electron density matrix. With indices this is

$$ {}^pD^{ij...z}_{ab...h} = {}^p\bar{D}^{ab...h}_{ij...z}. \tag{2.4} $$

Additionally, all RDMs are positive semi-definite denoted

$$ {}^pD \succeq 0 \tag{2.5} $$

meaning their eigenvalues are all greater than or equal to zero. Furthermore, higher-order RDMs contain all lower-order RDMs within themselves and they are accessible by tracing out the additional electrons. Mathematically

$$ {}^{p-1}D(N_e - 1) = \sum_m {}^pD^{ij...m}_{ab...m}. \tag{2.6} $$

The specific density matrices that will be used throughout the remainder of this work are just the 1- and 2-RDMs. Starting with the 1-RDM it's trace needs to be equal to the number of electrons in the system

$$ \mathrm{Tr}({}^1D) = N. \tag{2.7} $$

It is common to diagonalize the 1-RDM

$$ {}^1D = {}^1D_{coeff}\,{}^1D_{occ}\,{}^1D^{\dagger}_{coeff} \tag{2.8} $$

to obtain its eigenvalues, ${}^1D_{occ}$, and eigenvectors ${}^1D_{coeff}$. The eigenvalues, ${}^1D_{occ}$, are known as the orbital occupations and they denote the probability of finding an electron in each orbital. These orbital occupations will lie between 0 and 1 and are often used as an indicator of strong correlation. The stronger the electronic correlation the more the orbitals will deviate from 0 and 1; giving what is often referred to as fractional orbital occupation.

In the limit that the underlying wave function is expressible as a single Slater determinant the result 1-RDM will be idempotent such that

$$ {}^1D^2 = {}^1D. \tag{2.9} $$

The eigenvectors, ${}^1D_{coeff}$, are the one-electron orbitals often referred to as molecular or natural orbitals and denote where the electron is located in space.

Moving on to the 2-RDM, ${}^2D$, as it is a 2-electron probability matrix it's trace equals the number of electrons times the number of electrons minus 1

$$ \mathrm{Tr}({}^2D) = N(N-1). \tag{2.10} $$

Although the 2-RDM has 4 indices and is therefore a rank 4 tensor it is common to flatten it into a matrix so that it can be diagonalized in the same manner as the 1-RDM to obtain its eigenvalues, known as the geminal occupations, and its eigenvectors, known as geminals. These geminal occupations correspond to the simultaneous probability of finding an electron in orbital i and an electron in orbital j.

Additionally, the 2-RDM can be decomposed into a part that depends upon the 1-RDM and a part that cannot as

$$ {}^2D = {}^1D \wedge {}^1D + {}^2\Delta. \tag{2.11} $$

Where ${}^2\Delta$ is the cumulant of the 2-RDM. This cumulant is what contains all the correlation phenomenon beyond what is captured by Hartree-Fock's mean field approach.

2.2 Variational 2-RDM

From Eq. 2.1 is apparent that to obtain the energy using reduced density matrices we don't need to know the wave function of the system, just it's corresponding 1- and 2-RDMs. The

reason higher-order RDMs don't contribute to the energy is that the electronic Hamiltonian only contains one and two body terms. Writing the energy as a function of the RDMs has the benefit of only scaling polynomially with the number of orbitals in the system, instead of factorially as with FCI.

It is tempting from this point to invoke the variational principle and find the RDMs that minimize the electronic energy. Unfortunately, doing so leads to an unboundly negative result. It turns out RDMs need to be minimized subject to N-representability constraints, which enforce that they could be obtained from an N-electron wave function. These constraints are known up through arbitrary p-electron RDMs, but it is most common to only utilize those up to the 2-RDM. Constraining higher-order RDMs becomes unfeasible due to their even increasing memory cost as well as computationally enforcing the constraints. The N-representability constraints up to the 2-RDM are given below:

1-RDM N-Representability Constraints

$$
\begin{aligned}
{}^1D &\succeq 0 \\
{}^1Q &\succeq 0 \\
{}^1D + {}^1Q &= {}^1I \\
N_\alpha &= \mathrm{Tr}({}^1D^\alpha_\alpha) \\
N_\beta &= \mathrm{Tr}({}^1D^\beta_\beta) \\
(N_\alpha - 1){}^1D^{i_\alpha}_{j_\alpha} &= \sum_m {}^2D^{i_\alpha m_\alpha}_{j_\alpha m_\alpha} \\
(N_\alpha){}^1D^{i_\alpha}_{j_\alpha} &= \sum_m {}^2D^{i_\alpha m_\beta}_{j_\alpha m_\beta} \\
(N_\beta - 1){}^1D^{i_\beta}_{j_\beta} &= \sum_m {}^2D^{i_\beta m_\beta}_{j_\beta m_\beta} \\
(N_\beta){}^1D^{i_\beta}_{j_\beta} &= \sum_m {}^2D^{i_\beta m_\alpha}_{j_\beta m_\alpha}
\end{aligned}
$$

2-RDM N-Representability Constraints

$$
\begin{aligned}
{}^2D &\succeq 0 \\
{}^2Q &\succeq 0 \\
{}^2G &\succeq 0 \\
{}^2G^{ij}_{kl} &= \delta_{jl}\,{}^1D^i_k - {}^2D^{ik}_{jl} \\
{}^2Q^{ij}_{kl} &= {}^2D^{kl}_{ij} - {}^1D^k_j\delta_{il} + {}^1D^k_i\delta_{jl} + \\
&\quad {}^1D^l_j\delta_{ik} - \delta_{jl}\delta_{ik} - {}^1D^l_i\delta_{jk} + \delta_{il}\delta_{jk} \\
N_\alpha(N_\alpha - 1) &= \mathrm{Tr}({}^2D^{\alpha\alpha}_{\alpha\alpha}) \\
N_\beta(N_\beta - 1) &= \mathrm{Tr}({}^2D^{\beta\beta}_{\beta\beta}) \\
N_\alpha(N_\beta) &= \mathrm{Tr}({}^2D^{\alpha\beta}_{\alpha\beta})
\end{aligned}
$$

where $\succeq 0$ once again represents positive semi-definiteness, which defines the matrices to have non-negative eigenvalues as it is non-physical to have a negative probability of finding a particle or pair of particles. Additionally, ${}^1Q$ is the 1-Hole matrix, ${}^2Q$ is the 2-Hole matrix, and ${}^2G$ is the particle-hole matrix. These are defined in second quantization as

$$
\begin{aligned}
{}^1Q &= \langle\Psi|a_i a_j^\dagger|\Psi\rangle \\
{}^2Q &= \langle\Psi|a_i a_j a_l^\dagger a_k^\dagger|\Psi\rangle \\
{}^2G &= \langle\Psi|a_i^\dagger a_j a_l^\dagger a_k|\Psi\rangle.
\end{aligned}
$$

When just the 1- and 2-RDM constraints are enforced, known as Variation 2RDM (V2RDM), the obtained RDMs will not, in general, be N-Representable and will result in a variationally lower energy than FCI. Adding additional N-Representability constraints works to raise the energy of the system closer to that of FCI's as the set of allowable RDMs is contracted as shown in Figure 2.1. Concerning the correlation energy of the system, V2RDM will result in more than 100% of FCI's as it overcorrelates the electronic motion.

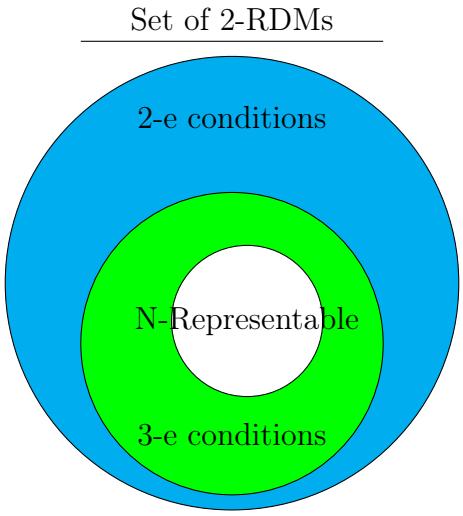

Figure 2.1: Illustration of the set of allowable 2-RDMs as different N-Representability constraints are applied.

However, V2RDM, even with this pitfall, gives energies closely in line with those obtained from CI calculations with the added benefit of being able to solve for the ground state energies of larger systems. It is possible to use V2RDM on systems with up to 60 electrons in 60 orbitals, which far exceeds FCI's limit. This is due to the 2-RDM's memory and computational cost scaling quadratically as a function of system size instead of exponentially like FCI's wave function.

2.2.1 Semi-Definite Programming

To minimize the electronic energy as a function of the 1- and 2-RDMs constrained to be N-Representable, we can use a Semi-Definite Program (SDP). SDPs are a subset of linear programming where the objective function spans the intersection of cones of positive semi-definite matrices which form a convex set. The benefit of using an SDP is that the minimization is guaranteed to converge to the global minima as long as it exists. As Eq. 1.97 is a linear functional of the 1- and 2-RDMs which are constrained to be positive semi-definite and also form a convex set, it maps perfectly to an SDP. To computationally solve

the SDP we can use a boundary point SDP (BPSDP) solver[13] which breaks down the constraints as

$$^2D = R^*R \tag{2.12}$$

$$^2Q = S^*S \tag{2.13}$$

$$^2G = T^*T \tag{2.14}$$

and ensures that the eigenvalues of ^2D, ^2Q, and ^2G are non-negative by construction. The problem is now non-linear and can be solved using an augmented Lagrangian via

$$L(x) = E(x) - \sum_i \lambda_i c_i(x) + \frac{1}{2\mu}\sum_i c_i(x)^2 \tag{2.15}$$

where x is a vector containing the R, S, and T variables, $E(x)$ is the ground state energy, $c_i(x)$ are the equality constraints, $\lambda_i(x)$ are the Lagrange multipliers, and μ is a penalty parameter. This augmented Lagrangian is minimized using a quasi-Newton algorithm and if the solution's constraint's maximal error is below a given threshold the Lagrange multipliers are updated as $\lambda_i^{(n+1)} = \lambda_i^{(n)} - c_i(x)/\mu$ if not the constraints are enforced more tightly by updating the penalty parameter as $\mu^{(n+1)} = 0.1\mu^{(n)}$. Using this BPSDP, the memory cost of solving V2RDM is $\mathcal{O}(N^4)$ with an operations cost of $\mathcal{O}(N^6)$. Therefore, the primary limitation in exploring larger systems with V2RDM is the cost of the minimization procedure, which is a function of the number of constraints on the system. If higher RDM representability constraints are added, the computational complexity increases drastically with it scaling as $\mathcal{O}(N^9)$ when including full 3-RDM conditions.

2.3 Anti-Hermitian Contracted Schrödinger Equation

Instead of directly minimizing the energy as a function of the 2-RDM it is possible to also follow a derivative to arrive at a stationary state of the Schrödinger equation. To show this starting from the Schrödinger equation

$$\hat{H}|\Psi\rangle = E|\Psi\rangle \tag{2.16}$$

we can left multiple both sides by $\langle\Psi|^2\hat{\Gamma}^{ij}_{kl}$ to give

$$\langle\Psi|^2\hat{\Gamma}^{ij}_{kl}\hat{H}|\Psi\rangle = E^2 D^{ij}_{kl} \tag{2.17}$$

where ${}^2\hat{\Gamma}^{ij}_{kl}$ is the reduced density operator

$${}^2\hat{\Gamma}^{ij}_{kl} = a_i^\dagger a_j^\dagger a_l a_k. \tag{2.18}$$

Equation 2.17, also known as the contracted schrödinger equation or CSE, can be expressed as a hermitian and an anti-hermitian part

$$\langle\Psi|\{a_i^\dagger a_j^\dagger a_l a_k, (\hat{H} - E)\}|\Psi\rangle + \langle\Psi|[a_i^\dagger a_j^\dagger a_l a_k, (\hat{H} - E)]|\Psi\rangle = 0. \tag{2.19}$$

Taking just the anti-hermitian part,

$$\langle\Psi|[a_i^\dagger a_j^\dagger a_l a_k, (\hat{H} - E)]|\Psi\rangle = 0 \tag{2.20}$$

expanding the Hamiltonian using 1.92, and evaluating it gives

$$\begin{aligned}\sum_s {}^1K_s^k\ {}^2D_{kl}^{ij} - \sum_s {}^1K_s^l\ {}^2D_{kl}^{ij} + \sum_p {}^1K_j^p\ {}^2D_{kl}^{pi} - \sum_p {}^1K_i^p\ {}^2D_{kl}^{pj} \\ +6\sum_{pst} {}^2V_{st}^{pk}\ {}^3D_{stl}^{ijp} - 6\sum_{pst} {}^2V_{st}^{pl}\ {}^3D_{stk}^{ijp} \\ +6\sum_{pqs} {}^2V_{sj}^{pq}\ {}^3D_{kls}^{pqi} - \sum_{pqs} {}^2V_{si}^{pq}\ {}^3D_{kls}^{pqj} + 2\sum_{st} {}^2V_{st}^{kl}\ {}^2D_{st}^{ij} \\ +2\sum_{pq} {}^2V_{ji}^{pq}\ {}^2D_{kl}^{pq} = 0\end{aligned} \tag{2.21}$$

where the terms that depend on the 4-RDM ended up canceling out due to the anti-commutation operation. This can be further broken down into lower-order RDMs by using the 3-RDM's cumulant expansion

$${}^3D_{qst}^{ijk} = {}^1D_q^i \wedge {}^1D_s^j \wedge {}^1D_t^k + 3^2\Delta_{qs}^{ij} \wedge {}^1D_t^k + {}^3\Delta_{qst}^{ijk} \tag{2.22}$$

where the 2-RDM's cumulant is given as

$${}^2\Delta_{qs}^{ij} = {}^2D_{qs}^{ij} - {}^1D_q^i \wedge {}^1D_s^j. \tag{2.23}$$

By setting ${}^3\Delta_{qst}^{ijk} = 0$ we get a set of equations for the energy that only depends on up to the 2-RDM. It should be noted that this is analogous to coupled cluster theory in that lower-order density matrices can be used to approximate higher-order ones, just as coupled cluster theory approximates higher-order excitations through combinations of lower-order ones.

By minimizing the residual given as Eq. 2.20 the ACSE will optimize towards the nearest stationary state of the Schrödinger equation. This is achieved through a set of differential equations as

$$\frac{d^2D_{kl}^{ij}}{d\lambda} = \langle\Psi(\lambda)|[{}^2\hat{\Gamma}_{kl}^{ij}, \hat{S}(\lambda)]|\Psi(\lambda)\rangle \tag{2.24}$$

where

$$\hat{S}(\lambda) = \sum_{ijkl} {}^2S^{ij}_{kl} a^\dagger_i a^\dagger_j a_l a_k(\lambda) \tag{2.25}$$

and each element of $\hat{S}$ is chosen to minimize the residual through

$${}^2S^{ij}_{kl} = \langle \Psi(\lambda) | [{}^2\hat{\Gamma}^{ij}_{kl}, \hat{H}(\lambda)] | \Psi(\lambda) \rangle \tag{2.26}$$

While this methodology has been shown to recover nearly 100% of the missing correlation energy and can target excited states in addition to the ground state it is still limited to smaller system sizes as storing the 2-RDM scales as $\mathcal{O}(N^4)$ in terms of the memory requirements which prevents the method from going beyond a couple of hundred orbitals.

2.4 Reduced Density Matrix Functional Theory

While we can use either V2RDM or the ACSE to solve for the ground state energy, we're still limited by either the numerical cost of the method or its memory scaling. Both of these limitations can be traced back to the 2-RDM. However, there is an idea to use the 1-RDM as the basic variable for the minimization, which is analogous to the electronic density in DFT. The advantage to this approach over V2RDM is that the 1-RDM has a memory scaling of only $\mathcal{O}(N^2)$ where N is the number of orbitals in your system, which would allow systems with thousands of orbitals to be calculated. To build the foundations of a 1-RDM functional theory Gilbert's theorem shows[14], analogous to the Kohn-Sham theorems, that the ground state electronic energy can also be expressed as a unique functional of the 1-RDM. As the wave function uniquely defines the 1-RDM as shown via Eq. 2.1 all that remains is to show there is a unique mapping from the 1-RDM to the wave function. Using proof by contradiction, Gilbert obtained this as follows: Start with two different external potentials V_{ext} and $V^{'}_{ext}$ that correspond to two different ground states Ψ and $\Psi^{'}$. Via the variational

principle

$$\begin{aligned} E &= \langle \Psi_0 | \hat{H} | \Psi_0 \rangle < \langle \Psi_0^{'} | \hat{H} | \Psi_0^{'} \rangle \\ &= \langle \Psi_0^{'} | \hat{H} | \Psi_0^{'} \rangle + \int [V_{ext}(x, x^{'}) - V_{ext}^{'}(x, x^{'})]^1 D^{'}(x, x^{'}) dx dx^{'} \\ &= E^{'} + \int [V_{ext}(x, x^{'}) - V_{ext}^{'}(x, x^{'})]^1 D(x, x^{'}) dx dx^{'}. \end{aligned}$$

Swapping V_{ext} and $V_{ext}^{'}$

$$E^{'} < E + \int [V_{ext}^{'}(x, x^{'}) - V_{ext}(x, x^{'})]^1 D(x, x^{'}) dx dx^{'}.$$

When added to the above we get

$$\int [V_{ext}^{'}(x, x^{'}) - V_{ext}(x, x^{'})][^1 D^{'}(x, x^{'}) - {}^1 D(x, x^{'})] < 0.$$

From this, if the 1-RDMs are equal, then the left-hand side of the equation would be zero. Which would lead to the contradiction of $0 < 0$. Therefore, the only way for this to be true is for there to be a unique mapping between ground state wave functions and 1-RDMs. This establishes a mapping between V-representable pure state wave functions and the 1-RDM. This was later relaxed to pure-state N-representable 1-RDMs by Levy[15, 16] and then further extended by Valone[17, 18] to ensemble N-representable 1-RDMs.

Extending the foundations of RDMFT to ensemble N-representable 1-RDMs was important as the necessary and sufficient conditions for ensuring a 1-RDM is ensemble N-representable are well known[19] and expressible as

$$^1 D \succeq 0 \tag{2.27}$$

$$^1 Q \succeq 0 \tag{2.28}$$

$$^1D + {}^1Q = {}^1I \tag{2.29}$$

$$\sum_i {}^1D_i^i = N. \tag{2.30}$$

The equivalent set of necessary and sufficient conditions for ensuring pure-state N-representability are not arbitrarily known thus hindering minimizations over the space of pure-state RDMs[20].

2.4.1 RDMFT functionals

Just like DFT, there have been different RDMFT functionals that have been developed over the years, however, while DFT enjoys a plethora of different functionals to choose from, RDMFT has only a handful. This is due to RDMFT generally requiring a two-step minimization approach where the orbitals are optimized under orthogonality constraints and then the orbital occupations are optimized separately. These primarily fall into two different classes, those based upon the two-electron case - for which there is an exact density matrix functional available - and those based upon a reconstruction of the 2-RDM.

2.5 Motivation for this work

The motivating idea throughout this dissertation is to combine the functionals from Density Functional Theory with a Reduced Density Matrix Functional to create a methodology capable of capturing both dynamical correlation with the density functional and static correlation with the reduced density matrix functional. The reason for this combination is that DFT has been widely recognized as giving excellent results for its low computational scaling but tends to fail in systems with strong correlation. RDMFT's functionals have been successful at capturing strong correlation effects but tend to result in over-correlation, artificially lowering the energy. Additionally, RDMFT's current dependence on orbital occupations results in a two-step procedure for minimizing the electronic energy where you alternatively minimize the energy as either a function of the orbital occupations or orbital coefficients. This results

in a minimization with an overall computational scaling of $\mathcal{O}(N^5)$. By combining aspects of these two functional theories, we aim to obtain a methodology that offers the best of both approaches.

The remainder of this thesis is organized around combining these two functional theories presented as copies of the publications we made toward this goal with some minor edits. In the first publication, **Toward a Resolution of the Static Correlation Problem in Density Functional Theory From Semidefinite Programming**, we show that we can substitute the Roothaan-Hall equations for obtaining the Hartree-Fock or Kohn-Sham DFT orbitals at each iteration with a constrained semi-definite program. This directly minimizes the energy of the system using the 1-RDM instead of the standard diagonalization procedure to obtain the MO coefficients. This approach allows us to relax the constraint that the orbitals must be either completely occupied or unoccupied by enabling fractional orbital occupations and creates a framework for future minimization algorithms based on the 1-RDM. Unfortunately, while this work shows the potential promise of directly minimizing the 1-RDM in Hartree-Fock or DFT, through significantly improved singlet-triplet gaps, we could only observe differences from the standard Roothaan-Hall implementations in systems with degenerate frontier orbitals due to the linear nature of our minimization.

We remove this issue in the next publication, **Density Functional Theory Transformed Into a One-Electron Reduced-Density-Matrix Functional Theory for the Capture of Static Correlation**, we postulate a quadratic 1-RDM functional using ${}^1D^2$. This functional is still expressible through the use of semi-definite programming via a slack variable, ${}^1F$, introduced to represent the ${}^1D^2$ term and therefore can be added to our previous minimization. While this slack variable is only bound from below by ${}^1D^2$, in practice it is identical to the exactly obtained ${}^1D^2$ to within the optimization's tolerances. With this quadratic form we're able to obtain fractional occupation in systems without degenerate frontier orbitals modulated through a newly introduced w value. We find this methodol-

ogy improves upon DFT in the tested systems by enabling the capture of static correlation through fractional occupations in line with those obtained from CASSCF calculations. Additionally, we find the w value can be held fixed across a range of systems and still capture static correlation effects. We term this methodology RDMFT.

To proceed with making RDMFT a useful theory in practice we needed to understand how different functionals from DFT affect it and how it relates to similar methodologies. To explore this, in **Comparison of Density-Matrix Corrections to Density Functional Theory** we compare our RDMFT to the information Density Matrix Functional Theory (iDMFT), uncovering a relationship between the Von Neumann Entropy and our quadratic minimization using a Taylor Series expansion. We also explore the effect of changing the density functional on both the w value and the maximal deviations from accurate reference values. We find that the optimal w value scales in an approximately linear manner with respect to the amount of Hartree-Fock exchange in the selected density functional and that the errors tended to increase as more parameterized functionals were used.

In **Universal Generalization of Density Functional Theory for Static Correlation** we find a deeper understanding of our RDMFT by formally deriving it from a unitary decomposition of the 2-RDM's cumulant. This results in the w value being explicitly defined as the trace of the electron repulsion integrals, making RDMFT system specific. This also highlights why previous attempts to use an arbitrary matrix for w instead of a scalar multiple of the identity matrix were unsuccessful. Comparisons to the fixed value of w previously used reveal similar results. Unfortunately, due to the derivation's quadratic scaling on the number of orbitals and linear scaling on the electron repulsion integrals, the RDMFT will asymptotically approach DFT's energy as the system size grows large.

In our last work, **Enhancing Density Functional Theory for Static Correlation in Large Molecules**, we address this size extensivity issue by using the Cauchy-Schwarz inequalities to renormalize each electron repulsion integral. This results in a new w value we

call $\tilde{w}$ that is nearly independent of the system geometry and recovers size extensivity. We show its applicability by applying RDMFT to linear hydrogen chains where the correction fixes the energy per hydrogen and ensures that it is both constant in the non-interacting limit and does not vary with number of atoms. Additionally, we investigate the linear acenes from pentacene to dodecacene and find excellent agreement with reference V2RDM results. With this modification to w RDMFT can be applied to systems of arbitrary size.

CHAPTER 3

TOWARD A RESOLUTION OF THE STATIC CORRELATION PROBLEM IN DENSITY FUNCTIONAL THEORY FROM SEMIDEFINITE PROGRAMMING

3.1 Introduction

Since its conception in the 1960s, Kohn-Sham density functional theory (KS-DFT) has become omnipresent in the calculation of the physical properties of atoms, molecules, liquids, and solids. Its favorable computational scaling compared to wave function-based methods such as coupled cluster or complete active space (CAS) calculations has made it into the foremost tool in computational catalysis and materials science[21, 22]. Nonetheless, current exchange-correlation functionals continue to exhibit a long list of errors, including but not limited to the underestimation of chemical reaction barriers and band gaps of semiconductors, inaccurate description of spin state splittings, and a general failure to describe systems with degenerate or near-degenerate electronic states[23]. These failures can be traced to three fundamental issues: (i) a failure to capture accurately the long-range $1/r^6$ asymptotic behavior of London dispersion forces;[24] (ii) a delocalization error that arises in approximate functionals due to the dominating Coulomb term, leading to ρ being artificially diffuse;[25, 26] (iii) a static correlation error in near-degenerate states due to the single reference nature of KS-DFT.[27, 28]

Over the course of the last five decades great progress has been made in functional development. Nonetheless, it has been shown that while modern functionals are trained to perform well in the calculation of specific chemical and physical properties, the error in

computed electron densities has actually increased, suggesting the results may not reflect physical improvements to the functional but rather good fitting to the energy.[29, 30] Until DFT functionals can correctly account for both fractional spins and charges, a general solution will remain beyond reach and calculations will fail in systems where strong correlation plays a significant role. While multiple approaches relying on optimized effective potentials or modified Hamiltonians[31, 32, 33, 34, 35] have been conceived to account for fractional orbital occupations, recent progress in solving the static correlation error in DFT was presented in a letter by Lee and co-workers in which a new class of charge and spin densities is obtained via the breaking of time-reversal symmetry and the use of complex symmetry in the KS-DFT determinant, which they term "complex polarization".[36]

In this Letter we present a related and yet different approach to the static correlation problem in DFT that implements a semidefinite programming approach instead of the conventional KS self-consistent field (SCF) procedure. The SDP-DFT method variationally minimizes the energy with respect to the 1-electron reduced density matrix (1-RDM).[37, 38, 39, 40, 41, 42, 43, 44, 45] This approach is similar to 1-RDM functional theory (1RDMFT),[46, 19, 47, 48] recent versions of which, such as the PNOF7 functional with MP2 correction,[49] have been shown to describe the O singlet-triplet gap within chemical accuracy. Unlike 1RDMFT however, in SDP-DFT the correlation and exchange parts of the energy are evaluated with one-density exchange-correlation functionals from DFT. Minimizing the energy with SDP allows idempotency breaking in the density matrix subject to the presence of degenerate frontier orbitals, yielding correct fractional-orbital spin densities, similar to those from complex spin-restricted orbitals, without the double-counting issue in wave function-based multiconfigurational DFT approaches.[50, 51, 12, 52] We apply the SDP-DFT algorithm to calculate the singlet-triplet gaps of a set of 11 atoms and molecules surveying a range of commonly used DFT functionals.

3.2 Theory

In contrast to the more complicated wave function-based approaches, DFT uses the electron density as the basic variable of its calculations. The energy is minimized with respect to the electron density; the correct ground-state density of a system is the one that minimizes the total energy through the functional $E[\rho(r)]$. This gives rise to the Kohn-Sham equations and their partitioning of the energy:[7]

$$E[\rho(r)] = T_s[\rho(r)] + E_{Ne}[\rho(r)] + J[\rho(r)] + E_{XC}[\rho(r)] \tag{3.1}$$

where T_s is the kinetic energy functional, E_{Ne} the classical nuclear-electron Coulomb attraction, J the classical Coulomb repulsion, and E_{XC} the exchange-correlation functional. The exact form of $E_{XC}[\rho(r)]$ remains unknown. The electron density $\rho(r)$ may be computed from the 1-RDM ${}^1D$:

$$\rho(r) = 2\sum_{ij} \eta_i(r)\eta_j(r)\,{}^1D^i_j \tag{3.2}$$

where η are the molecular orbitals. In classical KS-DFT the 1-RDM is subject to trace, Hermiticity and idempotency constraints.

Here we modify the traditional KS-DFT SCF approach to minimize the system energy over the convex set of ensemble N-representable 1-RDMs, an approach that has previously been demonstrated to obtain global solutions of restricted Hartree-Fock theory.[53, 54, 55] The ensemble N-representability conditions of the 1-RDM restrict its eigenvalues - the natural occupation numbers - to lie between 0 and 1 in accordance with the Pauli exclusion principle.[19] Although not required here, additional pure-state N-representability conditions of the 1-RDM, known as generalized Pauli constraints, further restrict the eigenvalues of a pure-state 1-RDM for N$\geq$3.[56, 57, 58, 59, 60, 61] The modified theory is formulated in a finite orbital basis set of rank r. The SDP replaces the diagonalization step in the SCF procedure, which in contrast to a traditional KS SCF implementation allows the 1-RDM to

break idempotency and correctly account for orbital degeneracies. In the SDP the degenerate 1-RDM ${}^1D$ is obtained by minimizing the energy expectation value

$$\min \sum_{ij} {}^1H^i_j \, {}^1D^i_j \tag{3.3}$$

where ${}^1H$ is the Kohn-Sham Hamiltonian matrix. All components of the energy in eq 3.3 including the kinetic energy are computed with respect to the nonidempotent 1-RDM. The 1-RDM is subject to ensemble N-representability constraints.[46, 19, 47, 48] Namely, the N-representability constraints require ${}^1D$ and the 1-hole matrix ${}^1Q$ to remain positive semidefinite, meaning their eigenvalues remain nonnegative

$${}^1D \succeq 0 \tag{3.4}$$

$${}^1Q \succeq 0 \tag{3.5}$$

These semidefinite constraints are equivalent to the Pauli exclusion principle.[19, 60] The sum of ${}^1D$ and ${}^1Q$ is also set equal to the one-particle identity matrix

$${}^1D + {}^1Q = {}^1I \tag{3.6}$$

and the trace of ${}^1D$ is set equal to the total number of electrons in the system.

Computationally this procedure is implemented using a semidefinite program, namely, a boundary-point SDP algorithm [62, 13] previously developed for variational 2-electron reduced density matrix (V2RDM) calculations, in which a linear functional of matrices is minimized subject to linear constraints and the restriction that the matrices be positive semidefinite.[63, 64, 65, 66, 67, 68, 69, 70, 71, 72, 73, 74, 75, 76] Computational scaling of $\mathcal{O}(r^3)$, where r is the number of basis functions, compares favorably to a nominal scaling of $\mathcal{O}(r^5)$ in 1RDMFT[49]. As is clear from eqs 3.4 and 3.5, a constraint is not placed on the

idempotency of ${}^1D$, allowing us to obtain the correct nonidempotent 1-RDM with partial occupancies that in the case of electronic degeneracies account for electron correlation.

As shown previously by Ess, Johnson, Hu, and Yang, the ensemble 1-RDM, in which the degenerate orbitals are equally populated, shares the same open-shell singlet density as the exact singlet open-shell wave function and hence produces exact eigenfunctions of the $\langle \hat{S^2} \rangle$ and $\langle \hat{S}_z \rangle$ operators.[77] Computationally, we have shown that for degenerate orbitals the 1-RDMs from SDP-DFT match the 1-RDMs from spin-adapted variational 2-RDM calculations with the explicit singlet constraints $\langle \hat{S^2} \rangle = 0$ and $\langle \hat{S}_z \rangle$=0 [78](see appendix Table A.3). Moreover, SDP-DFT also resolves unphysical symmetry breaking in KS-DFT; in accordance with Unsöld's theorem, the ensemble 1-RDM generates spatially symmetric solutions that are independent of rotations in the manifold of energetically degenerate orbitals (refer to appendix Figure A.1 for C atom densities).[79, 80]

3.3 Results

We apply the SDP-DFT algorithm to a set of 11 atoms and molecules, previously assembled by Head-Gordon and co-workers for the purpose of benchmarking an electronic structure theory's ability to describe multireference character in atoms and small molecules from orbital degeneracies via the calculation of singlet-triplet energy gaps.[36] We remove the charged species NO^-, leaving us a set consisting of C, O, S, Si, NF, NH, O_2, PF, PH, S_2, and SO, all of which have ground triplet states which we compute with $\langle \hat{S}_z \rangle$=1.[81] The excited singlet states are biradicaloids, displaying a form of multi-reference correlation from the degenerate natural orbital occupations.[82] We are using a range of functionals covering the different rungs of Jacob's Ladder,[8] namely, traditional local density approximation (LDA) functionals VWN [6, 7, 83, 84] and SPW92 [85] generalized gradient approximation (GGA) functionals PBE [86, 87] and BLYP,[88, 89] and some of the latest meta-GGA functionals

Table 3.1: Root Mean Squared Deviations (RMSDs) and Mean Signed Deviations (MSDs) of the Singlet-Triplet gaps ($\Delta E_{\mathrm{ST}} = E_{\mathrm{S}} - E_{\mathrm{T}}$) with Respect to the Experimental Reference Values for the Test Set of C, O, S, Si, NF, NH, O_2, PF, PH, S_2, SO. All values in kcal/mol.

	Restricted				Unrestricted			
	SDP-DFT		KS-DFT		SDP-DFT		KS-DFT	
Functional	RMSD	MSD	RMSD	MSD	RMSD	MSD	RMSD	MSD
VWN	5.33	-3.83	17.85	17.56	4.68	-3.03	14.56	-13.86
SPW92	5.46	-4.02	17.73	17.47	4.80	-3.22	14.27	-12.09
PBE	4.46	-1.01	17.46	17.29	4.44	0.07	18.08	-17.08
BLYP	5.00	-2.87	13.76	13.58	4.53	-1.79	19.15	-18.17
TPSS	5.79	2.78	16.81	16.43	6.87	4.26	18.66	-17.78
SCAN	11.91	10.42	19.98	19.73	14.23	12.66	17.53	-16.03
MN15-L	10.11	8.70	9.78	9.17	12.92	11.47	12.34	-11.21
B97M-V	8.54	6.36	11.64	11.43	10.52	8.46	15.10	-14.13

TPSS,[90] SCAN,[91] MN15-L,[92] and B97M-V.[93] The augmented correlation-consistent polarized valence quadruple-ζ (aug-cc-pVQZ) basis set [94, 95] was used for all calculations.

To quantify the performance of DFT functionals within the SDP framework we calculate the singlet-triplet gaps ($\Delta E_{ST} = E_S - E_T$) for the 11 entities in our test set with the chosen functionals and compare those against reference KS-DFT calculations and reported experimental values. Statistical analysis of the performance of the various functionals in spin restricted and spin unrestricted implementations is provided in Table 3.1 in the form of root mean squared deviation (RMSD) and mean signed deviation (MSD) from the experimental reference values.

In traditional unrestricted KS-DFT (UKS-DFT) all functionals significantly underestimate ΔE_{ST}. The newer Minnesota functional MN15-L gives the best performance with an RMSD of 12.34 kcal/mol and an MSD of -11.21 kcal/mol, while BLYP performs worst with an RMSD of 19.15 kcal/mol and an MSD of -18.17 kcal/mol. These are large errors compared to chemical accuracy of 1 kcal/mol, and the improvement of the newest meta-GGA functionals over the 40-year-old VWN is minor at best. Use of the spin unrestricted SDP-DFT (USDP-DFT) algorithm yields greatly improved results over UKS-DFT, with the

largest increases in accuracy observed for the tested LDA and GGA functionals, all of which give RMSDs in the 4-5 kcal/mol range. The popular PBE functional performs best with the RMSD reduced to 4.44 kcal/mol. Of the tested meta-GGA functionals, only TPSS shows a sizable improvement with an RMSD of 6.87 kcal/mol using USDP-DFT, compared to 18.66 kcal/mol in UKS-DFT. MN15-L, the best performing functional in UKS-DFT, is the only functional tested to perform worse in USDP-DFT, with an increase in RMSD of 0.58 kcal/mol.

Applying restricted SDP-DFT (RSDP-DFT) yields results comparable to the unrestricted calculations. While the RMSD is similar for the various functionals across restricted and unrestricted KS-DFT we observe a sign change in the MSD, and ΔE_{ST} is significantly overestimated rather than underestimated in a restricted calculation. Again MN15-L gives the best performance compared to experiment. In contrast to this, the SDP results for restricted calculations mirror those obtained via an unrestricted implementation. Compared to USDP-DFT, the LDA and GGA functionals yield slightly increased RMSDs and MSDs in RSDP-DFT. The meta-GGA functionals show small improvements. MN15-L again performs worse with the SDP algorithm than without it.

Average changes of the total electronic energy between SDP-DFT and KS-DFT for the singlet and triplet spin states of the tested functionals in both spin restricted and unrestricted formalisms are shown in Table 3.2. In both restricted and unrestricted calculations the changes to the electronic energy of the triplet states are minor. LDA functionals VWN and SPW92 show minimal variation in ΔE_{tot} ($\sim$0.4 kcal/mol) upon changing from a KS to a SDP algorithm while all other functionals show a small energy increase. It is worth noting that these changes are entirely driven by changes from the atoms in the data set and both the total energies as well as their individual components remain unchanged upon use of the SDP in the molecules of the data set. This suggests an overestimation of the correlation energy in the triplet state of the atoms in the data set by GGA and meta-GGA functionals

in traditional KS-DFT.

Table 3.2: Mean Energy Differences of Total Electronic Energy between the SDP-DFT and KS-DFT solutions ($\Delta E = (E_{\mathrm{SDP}} - E_{\mathrm{DFT}})/N$) of Singlet and Triplet states in Both Spin Restricted and Unrestricted Frameworks (in kcal/mol)

	Restricted		Unrestricted	
Functional	$\Delta E^{\mathrm{S}}_{\mathrm{tot}}$	$\Delta E^{\mathrm{T}}_{\mathrm{tot}}$	$\Delta E^{\mathrm{S}}_{\mathrm{tot}}$	$\Delta E^{\mathrm{T}}_{\mathrm{tot}}$
VWN	-21.60	-0.21	11.26	0.20
SPW92	-21.62	-0.12	11.02	0.19
PBE	-17.31	0.99	18.75	1.60
BLYP	-15.45	1.00	17.80	1.42
TPSS	-10.97	2.69	25.14	3.10
SCAN	-5.26	4.05	33.34	4.65
MN15-L	4.42	4.89	27.88	5.20
B97M-V	-1.08	3.99	26.77	4.18

Variations are of significantly greater magnitude in the singlet state. In a spin restricted formalism the singlet state is lowered by the SDP optimization in all functionals but MN-15L, with the greatest energetic gains in LDA functionals, ΔE^{S}_{tot} = -21.62 kcal/mol in SPW92, and successive decreases as we progress up Jacob's Ladder to ΔE^{S}_{tot} = 4.42 kcal/mol in MN15-L. In a spin unrestricted formalism singlet states are raised in energy and the functionals follow the opposite trend to the restricted formalism, with the smallest change in LDA functionals and the greatest in meta-GGA functionals, ranging from ΔE^{S}_{tot} = 11.02 kcal/mol in SPW92 to ΔE^{S}_{tot} = 33.34 kcal/mol in SCAN. The lowering in energy upon introduction of the nonidempotent, correlated density via the RSDP-DFT procedure is expected, as the static correlation energy of the open shell singlet is recovered. Conversely, in USDP-DFT, raising of the singlet energy by introducing the correlated density points toward overcorrelation of the open shell singlet by symmetry breaking in the UKS-DFT. The lack of energetic gain in USDP-DFT of meta-GGA functionals and their strong overcompensation in RKS-DFT suggests that the increasingly parametrized nature of these functionals seems to have resulted in a nonphysical relationship between density and correlation energy.

Across all calculations the use of the nonidempotent SDP 1-RDM to evaluate the system

energy leads to uniform changes in the individual components: a decrease in E_{kin} and E_{XC} counteracted to a varying degree by increases in E_C and E_{nuc}. Additional details can be found in the appendix Table A.1. Furthermore, appendix section A.2 considers the projection of the SDP-DFT nonidempotent density matrix onto the nearest idempotent density matrix by Euclidean distance, and the changes in the functional's energy components are given upon relaxation of the idempotent density matrix to the nonidempotent density matrix (Table A.2). The components E_C and E_{XC} decrease and increase, respectively, while E_{kin} and E_{nuc} remain the same. The total energies for functionals VWN through SCAN decrease with $|E_C|>|E_{XC}|$, while those for functionals MN-15L and B97M-V increase unphysically with $|E_C|<|E_{XC}|$.

To further analyze the performance of the SDP algorithm, we consider the errors of the singlet-triplet gaps ΔE_{ST} of the best performing functional, the GGA functional PBE, and the nonimproving MN15-L meta-GGA functional. For each species in our test set the errors are shown in Figure 3.1 for both spin restricted and unrestricted implementations. PBE shows a systematic improvement from a massive underestimation or overestimation of the singlet-triplet gap in UKS-DFT and RKS-DFT, respectively. The oxygen and sulfur atoms are the only species that, while still showing significant improvements over the KS-DFT, display a ΔE_{ST} from SDP-DFT that is significantly lower than the experimental value. Inspection of the changes in the individual energy components of the PBE functional from a KS to SDP implementation shows particularly large stabilization of the singlets for O and S (ΔE'sof -27.78 kcal/mol and -25.41 kcal/mol, respectively, compared to an average change of -17.31 kcal/mol) and disproportionate destabilization of the triplet (ΔE's of 5.76 and 1.80 kcal/mol, respectively, compared to an average change of 0.99 kcal/mol) leading to an underestimation of the singlet-triplet gap. In contrast to PBE, MN15-L in USDP-DFT, which again consistently underestimates the gap in UKS-DFT and overestimates the gap in RKS-DFT for every species, uniformly overestimates ΔE_{ST} with large magnitudes and no

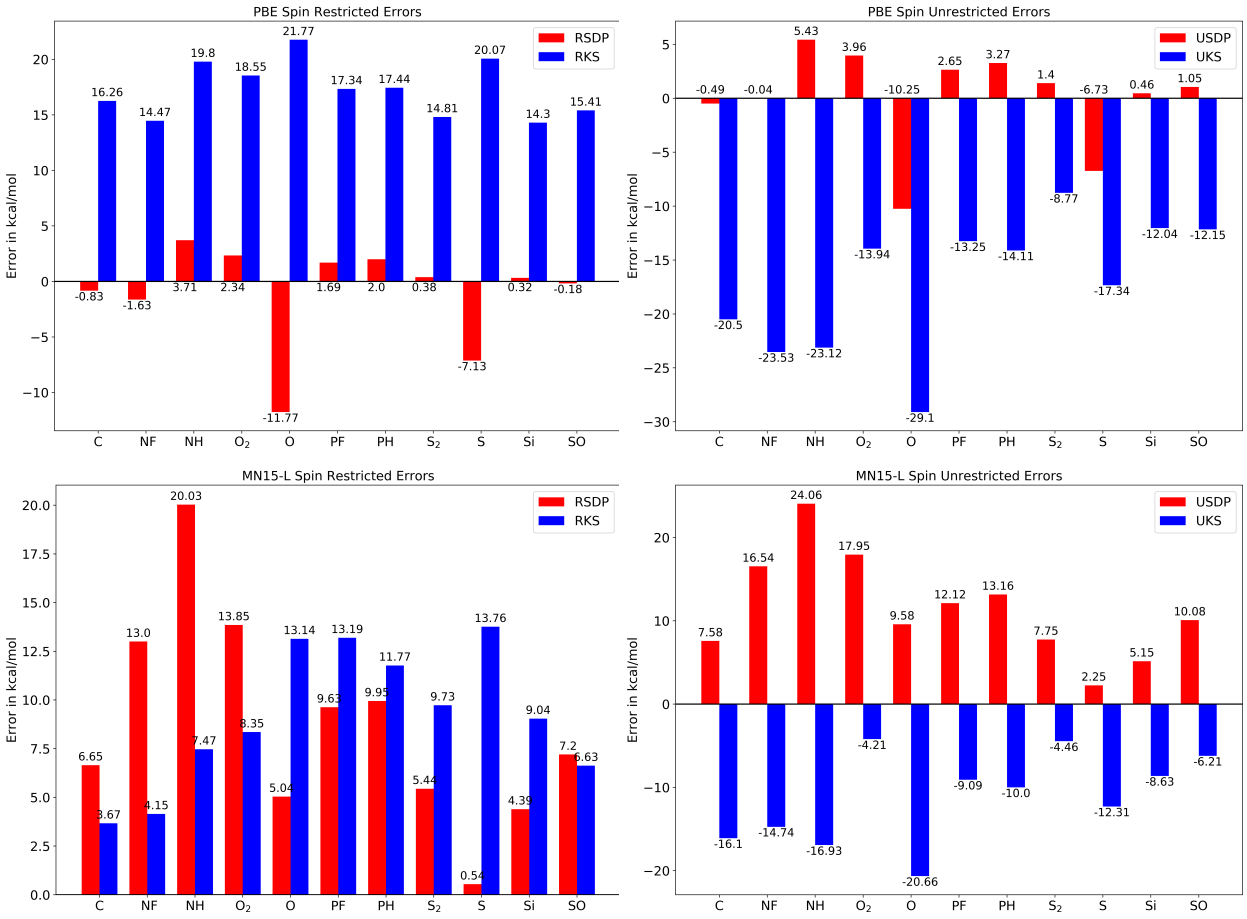

Figure 3.1: Errors in kcal/mol with respect to experimental values for each species in our test set with the PBE and MN15-L functionals in traditional KS and SDP DFT. Left column: spin restricted calculations; right column: spin unrestricted calculations.

major outliers. The O and S atoms again present negative deviations from the mean error; however, because of the large, general overestimation of the gap these species now profit from favorable error cancellations.

3.4 Conclusion

We present a new SCF minimization procedure for DFT functionals based on semidefinite programming that allows for inclusion of some strong correlation effects via a non-idempotent 1-electron density in systems exhibiting orbital degeneracies. The SDP-DFT method delivers significant improvements over traditional DFT and, unlike traditional KS-DFT, yields results that are consistent across both spin restricted and spin unrestricted implementations. However, improvements are strongly functional-dependent. LDA and GGA functionals show consistent refinements from the SDP procedure while improvements from newer, highly parametrized meta-GGA functionals are inconsistent and minor. In particular, the MN15-L functional performs worse in the SDP implementation.

The present results are comparable to those achieved by Head-Gordon and co-workers with the use of complex spin-restricted orbitals (presented in ref [36]). The only modifications in the present method from traditional DFT are based on its most fundamental quantity, the electron density, which through the use of SDP rather than KS-SCF minimization, is allowed to derive from nonidempotent and correlated 1-RDMs. The variation of the tested functional's response to this change in density reveals flaws in the path of modern functional development. Medvedev and co-workers found in their 2017 paper[29] that as functional development has progressed from LDA and GGA to modern, highly parametrized meta- and hyper-GGA functionals their predictions improve although DFT's fundamental quantity, the 1-electron density, has strayed further from the true solution. Our results lead to a complementary conclusion, namely that as we progress up "Jacob's Ladder" a functional's prediction of electronic properties, in our case the singlet-triplet gap of selected simple open

shell systems, exhibits less improvement from a refined electron density, pointing towards systematic overfitting in modern hybrid functionals. Nonetheless, the results show that this problem is not universal to DFT as promising improvements are possible with the simplest functionals. Developments focusing on improving implementations of DFT to yield more accurate electron densities may be a more viable path forward than functional development that is based on prediction-driven parametric fitting. This work presents important first steps toward the use of SDP to resolve strong correlation in a DFT framework through the use of improved densities which may improve the value of DFT as a tool in the resolution of properties affected by strong correlation such as bond dissociation energies and the electronic and magnetic properties of materials.

CHAPTER 4

DENSITY FUNCTIONAL THEORY TRANSFORMED INTO A ONE-ELECTRON REDUCED-DENSITY-MATRIX FUNCTIONAL THEORY FOR THE CAPTURE OF STATIC CORRELATION

4.1 Introduction

Since its formulation by Kohn and Sham [7] in the 1960s, Density Functional Theory (KS-DFT) has seen widespread adoption within the chemistry community for the prediction and modeling of various chemically relevant properties such as reaction barriers, vibrational modes, ionization potentials, and molecular geometries. [21, 96, 97, 98, 99, 100] This widespread adoption is owed to DFT's favorable computational scaling compared to wave function-based alternatives such as Coupled Cluster (CC) or Complete Active Space (CAS) theories as well as its ease of use as an effectively black-box method. [101, 102] The inexpensive computational scaling of DFT is a direct result of describing the complex exchange correlation interactions through the use of an efficient energy functional of the electronic density, referred to as the exchange correlation functional. However, while DFT is in principle exact, [6] the fact that the universal functional is unknown requires the use of approximations, giving us the so-called "functional zoo" of modern DFT functionals [103] and leading to the creation of a Jacob's Ladder classification scheme by Perdew.[8]

While functional developments have resulted in improvements to the description of many physical properties such as reaction barriers and ground-state geometries, [96, 100, 104]

DFT continues to be plagued by three notable failures: (1) the self-interaction error, (2) the charge transfer (or noncovalent interaction) error, and (3) the static correlation error arising from degenerate or near-degenerate states, [25, 24, 33] which is rooted in the fact that KS-DFT is inherently based on a single Slater determinant. [105] Additionally, it has recently been noted by Medvedev et al. that while the energies obtained with modern functionals have been systematically improving, the fundamental property of DFT, the ground-state electron density, has become less accurate in recent years. [29] This suggests that new improvements to DFT's functionals are the result of overfitting of the functional form to reproduce experimental results, and without the development of a multireference formalism, DFT with inherently continue to struggle with the description of strongly correlated systems. Recent attempts to rectify this behavior within DFT have involved utilizing the universal functional's known flat plane behavior [106, 107, 108, 109] as well as the expansion of KS-DFT into the complex plane to allow for solutions beyond what is possible with traditional idempotent DFT. [36]

One-electron reduced density matrix functional theory (1-RDMFT) provides a viable path to solve the static correlation problem in KS-DFT while retaining favorable computational scaling compared to wave function based alternatives. 1-RDMFT utilizes Gilbert's theorem [14] to express the energy of any chemical system as a functional of the 1-electron reduced density matrix (1-RDM). [110, 111, 112] By using the 1-RDM as the fundamental variable, 1-RDMFT is capable of capturing fractional occupation as required for the description of strongly correlated systems. [37, 113, 114] Within this area of work, promising approaches for creating 1-RDM functionals involve using the known functional for two-electron atoms and molecules as a starting point [110, 115, 37] as well as reconstructions of the connected (or cumulant) part of the 2-electron reduced density matrix in terms of the 1-RDM. [110, 116, 117, 49] These methodologies, while promising for capturing static correlation, are computationally more demanding than DFT.

In this work, we demonstrate that DFT can be formally and practically transformed into a 1-RDMFT to address DFT's limitations without sacrificing its computational efficiency. Unlike previously developed 1-RDMFT theories that dispense with DFT's exchange-correlation functional, we convert DFT into a 1-RDM functional theory by (1) relaxing the idempotency restriction on the 1-RDM to recover the full kinetic energy of the electronic system including the contribution from correlation and (2) adding a quadratic 1-RDM-based term to DFT's density-based exchange-correlation functional. The second modification is important because it allows us to capture static correlation including fractional orbital occupations in generic atoms and molecules. We implement the method by a quadratically constrained semidefinite programming algorithm [13, 62, 63, 64, 66, 65] at DFT's computational scaling of $O(r^3)$. We apply our 1-RDMFT algorithm to the dissociation of a set of 11 molecules into radicals as well as the Mott metal-to-insulator transition of H_4 where the computed 1-RDMs are comparable in accuracy to those from high-level multireference wave function-based methods.

The DFT and RDMFT functionals are defined in terms of the N-electron density matrix ${}^N D$ as follows: [14, 112, 17, 15]

$$F_{\mathrm{DFT}}[\rho] = \min_{{}^N D \to \rho} \mathrm{Tr}(\hat{T}\,{}^N D) + \mathrm{Tr}(\hat{U}\,{}^N D) \tag{4.1}$$

$$F_{\mathrm{RDMFT}}[{}^1 D] = \min_{{}^N D \to {}^1 D} \mathrm{Tr}(\hat{U}\,{}^N D) \tag{4.2}$$

Here $\hat{T}$ is the sum of the kinetic energy operator and the external potential, $\hat{U}$ is the pairwise electron repulsion, ρ is the one-electron density, and ${}^1 D$ is the 1-RDM. To transform DFT into 1-RDMFT, we connect them through a functional $C[{}^1 D]$ such that

$$F_{\mathrm{RDMFT}}[{}^1 D] = F_{DFT}[\rho] + C[{}^1 D] \tag{4.3}$$

Written in this way, the 1-RDMFT functional is a correction of the DFT functional. The

knowledge of this functional implies two significant advantages: first, from the perspective of 1-RDMFT, the large number of existing DFT functionals could be used in 1-RDM theories, hastening the development of functionals, and second, from the perspective of DFT, the potential ability of 1-RDMFT to treat static correlation could be used to address DFT's challenge in capturing static correlation. A potential drawback is that the functional $C[^1D]$ might be complicated.

To convert the DFT functional to the 1-RDMFT functional, the correction must accomplish two separate but related adjustments: (1) addition of the full kinetic energy correction to the explicit part of the functional (part of the functional that depends explicitly upon the 1-RDM) and (2) removal of the kinetic energy correction from the universal part of the functional. In recent work, we accomplished the first part by expressing the self-consistent-field Kohn-Sham equations as a special type of optimization known as a semi-definite program (SDP). [118] The SDP formulation, which differs from local or complex extensions of DFT, [36, 119] relaxes the usual criterion that the 1-RDM be strictly idempotent, allowing the eigenvalues (natural occupations numbers) of the 1-RDM to become fractional and thereby represent bi- or polyradical character when the molecular-orbital energies in the Kohn-Sham Hamiltonian are degenerate.

The caveat "when molecular orbitals in the Kohn-Sham Hamiltonian are degenerate" introduces a significant restriction that limits applicability of our recent SDP-DFT [118] to static (multireference) correlation arising from orbitals that are nearly but not exactly energetically degenerate. Here we remove this restriction by implementing the second point above: removing the kinetic energy from the universal part of the functional. The term converting DFT to 1-RDMFT must obey several fundamental conditions-it must: (1) vanish in the limit of no correlation, (2) obey particle-hole symmetry, and (3) reward the formation of fractional occupation numbers for molecular orbitals that are degenerate or nearly degenerate in energy. Taken together, these conditions suggest the following 1-RDMFT energy

functional:

$$E_{\mathrm{RDMFT}}[^1D] = E_{\mathrm{DFT}}[\rho] - \mathrm{Tr}[(^1W\,^1Q)\,^1D] \tag{4.4}$$

Here ^1Q is the 1-hole RDM($=^1I - {}^1D$), and ^1W is a general positive–semidefinite weight matrix. Importantly, the weight matrix introduces significant flexibility into the functional form that can be used to optimize the universal functional correction. The simplest possible weight matrix ^1W is a scalar multiple of the identity matrix, which we represent as $^1W_I = w\,^1I$. Upon substitution into Eq 4.4, we obtain

$$E_{\mathrm{RDMFT}}[^1D] = E_{\mathrm{DFT}}[\rho] - w(\mathrm{Tr}(^1D^2) - N) \tag{4.5}$$

Physically, the correction contributes a negative energy to the functional as the 1-RDM deviates from idempotency with the orbital occupations becoming fractional. The magnitude of the negative energy contribution depends on the selection of the weight matrix or, in this case, the parameter w.

Because this correction is quadratic in the 1-RDM, its addition to the Kohn–Sham energy generates a quadratic semidefinite program (QSDP):

$$E_{\mathrm{gs}} = \min_{^1D} E_{MKS}[^1D] \tag{4.6}$$

such that

$$^1D \succeq 0 \tag{4.7}$$

$$^1Q \succeq 0 \tag{4.8}$$

where the modifies Kohn-Sham energy (MKS) is

$$E_{MKS}[^1D] = \mathrm{Tr}[(H_{\mathrm{KS}} - {}^1W\,^1Q)\,^1D] \tag{4.9}$$

and H_{KS} is the conventional Kohn-Sham Hamiltonian. An SDP is a special type of optimization in which a linear objective functional of a matrix M is minimized with respect to both linear equalities and the constraint that M is positive semidefinite (nonnegative eigenvalues), $M \succeq 0$. [13, 62, 63, 120] A QSDP is a generalized SDP in which the linear objective is replaced with a quadratic objective.

While quadratic semidefinite programs can be solved directly, we relax it to a regular semidefinite program [13, 62, 63, 120] which can be solved with the scaling of conventional DFT $\mathcal{O}(r^3)$ by the boundary-point SDP algorithm that we developed for solving the optimization problem in the variational 2-RDM method. [62, 68] Minimization of the quadratic correction can be relaxed to minimization of the trace of a positive semidefinite slack-variable matrix M

$$M = \begin{pmatrix} {}^1F & {}^1D \\ {}^1D & {}^1I \end{pmatrix} \succeq 0. \tag{4.10}$$

By constructing M in this form, ${}^1F$ is bounded through the determinant as ${}^1F - {}^1D{}^1D \succeq 0$. Therefore, the solution of the Kohn–Sham equations can be replaced by a semidefinite program whose energy

$$E_{\mathrm{MKS}}[{}^1D, {}^1F] = \mathrm{Tr}({}^1H_{KS}{}^1D) + \mathrm{Tr}({}^1W({}^1F - {}^1D)) \tag{4.11}$$

is a function of the 1-RDM and the slack variable ${}^1F$.

By solving the semidefinite program iteratively until convergence of the energy and the 1-RDM, we obtain a general 1-RDM solution of the 1-RDMFT. Importantly, unlike DFT, the solution of the 1-RDMFT returns a general, nonidempotent 1-RDM whose fractional occupation numbers provide critical information about the degree of electron correlation in the chemical system. In contrast to other 1-RDMFTs, our theory is constructed as an inexpensive $\mathcal{O}(r^3)$ correction to existing density functional theories.

In our calculations, we consider only the simplest form of the weight matrix (${}^1W_I = w^1I$) in which it is equal to the one-electron identity matrix multiplied by the scalar w. The parameter w is "trained" to reproduce the dissociation curve of N_2 obtained from either a complete-active-space self-consistent-field (CASSCF) [121, 122] [6,6] or an anti-Hermitian contracted Schrödinger equation (ACSE) [123, 124, 78] calculation in the 6-31G [125] basis set. This allows us to evaluate the differences arising from optimizing w for primarily static correlation (CASSCF) or the total energy of the system near the full configuration interaction (FCI) limit (ACSE). In each case the training of the parameter w is accomplished by fitting the predicted dissociation curve to the target dissociation curve at a set of discrete points. Note that only a single value of w is trained for all points of a dissociation curve. The ACSE calculations were performed in Maple using the Quantum Chemistry Toolbox [126, 127] while the CASSCF results were obtained using PySCF. [128] B3LYP [129, 130] is utilized as the DFT exchange correlation functional for both DFT and 1-RDMFT in this work.

Following optimization of w with either CASSCF or ACSE data, we find that the resulting 1-RDMFT accurately reproduces the dissociation curve of N_2 with only minor deviations. The trained values of w are 0.150 and 0.143 from CASSCF and ACSE, respectively. The dissociation curve obtained from the 1-RDMFT trained on CASSCF is compared to CASSCF and B3LYP in Figure 4.1. Use of the 1-RDM correction yields major improvements over traditional B3LYP, closely mirroring the CASSCF curve and recovering the correct behavior in the dissociated regime. The CASSCF dissociation energy is recovered to within 5.53 kcal/mol. Minor deviations from CASSCF arise in the intermediate bonding region where dynamical correlation plays a major role. Training of the 1-RDMFT on the ACSE solution further improves the description of the bonding and intermediate bonding regions and the ACSE dissociation energy is again reproduced with high accuracy at a deviation of 1.69 kcal/mol. The two 1-RDMFTs trained on the ACSE and CASSCF are displayed with the ACSE curve in Figure 4.2.

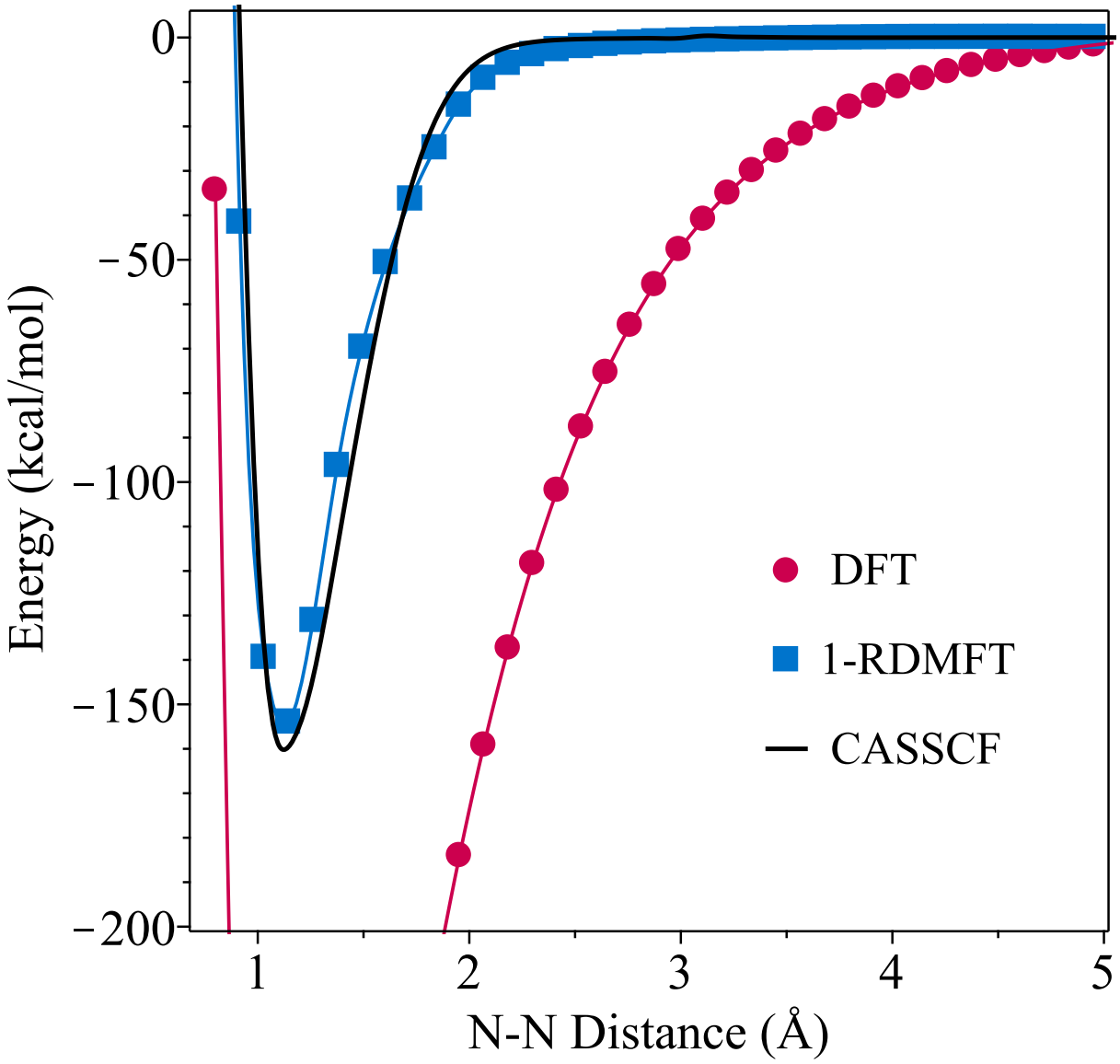

Figure 4.1: N_2 dissociation curves obtained from [6,6] CASSCF, our algorithm with a CASSCF optimized w parameter, and B3LYP.

Investigation of orbital occupations along the dissociation coordinate of N_2 (displayed in Figure 4.3) reveals that our algorithm, while optimized to reproduce the energy along the dissociation curve, also recovers orbital occupations in line with those of the CASSCF [6,6] calculation. In the bonding region of 1 Å, there are no deviations from integer occupa-

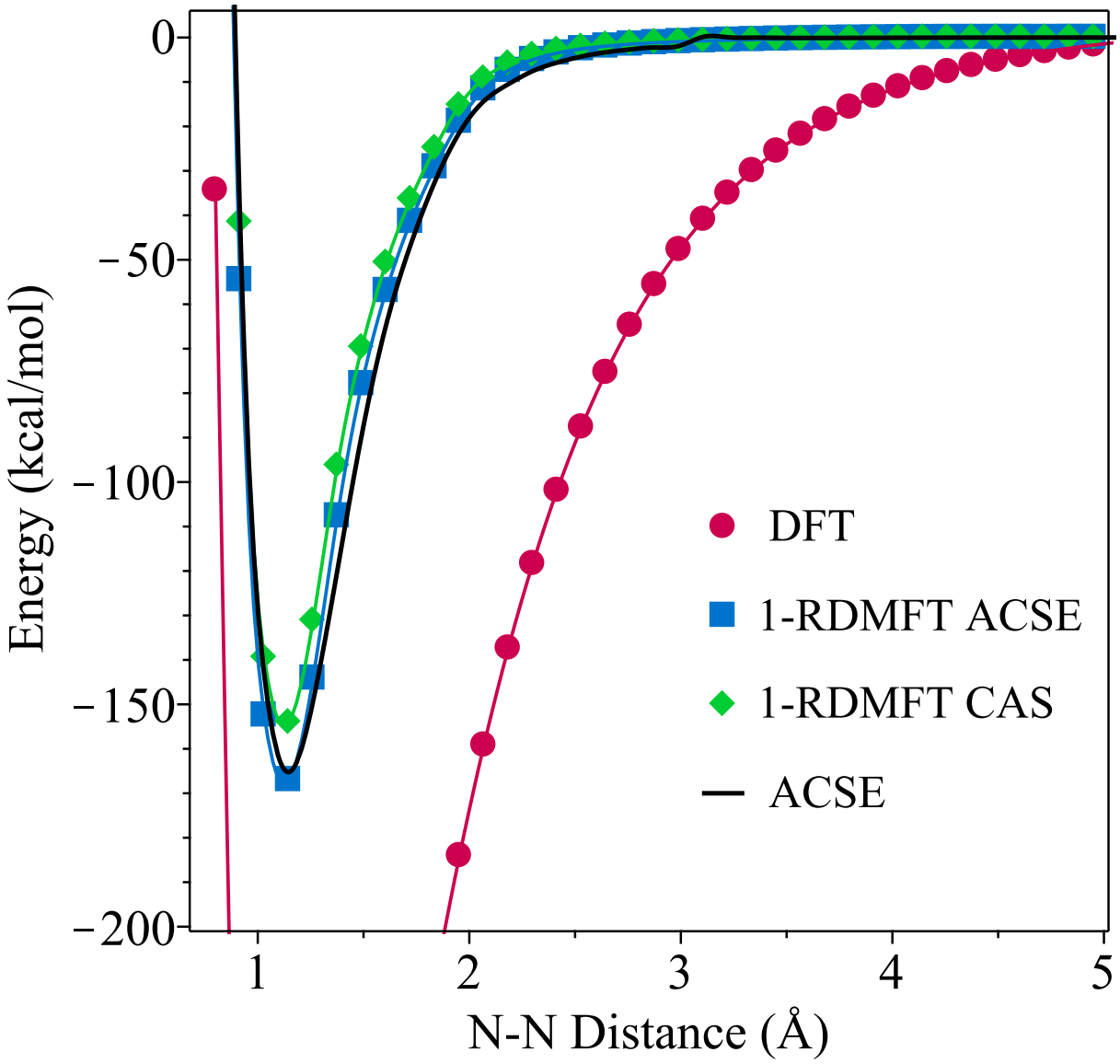

Figure 4.2: N_2 dissociation curves obtained from the ACSE, our algorithm with ACSE- and CASSCF-optimized w parameters, and B3LYP.

tions and single-reference behavior is recovered. However, as the bond is stretched, the six strongly correlated frontier orbitals deviate from their integer occupations with the deviations approaching half occupation at 4 Å, while the remaining orbitals display the correct integer occupations.

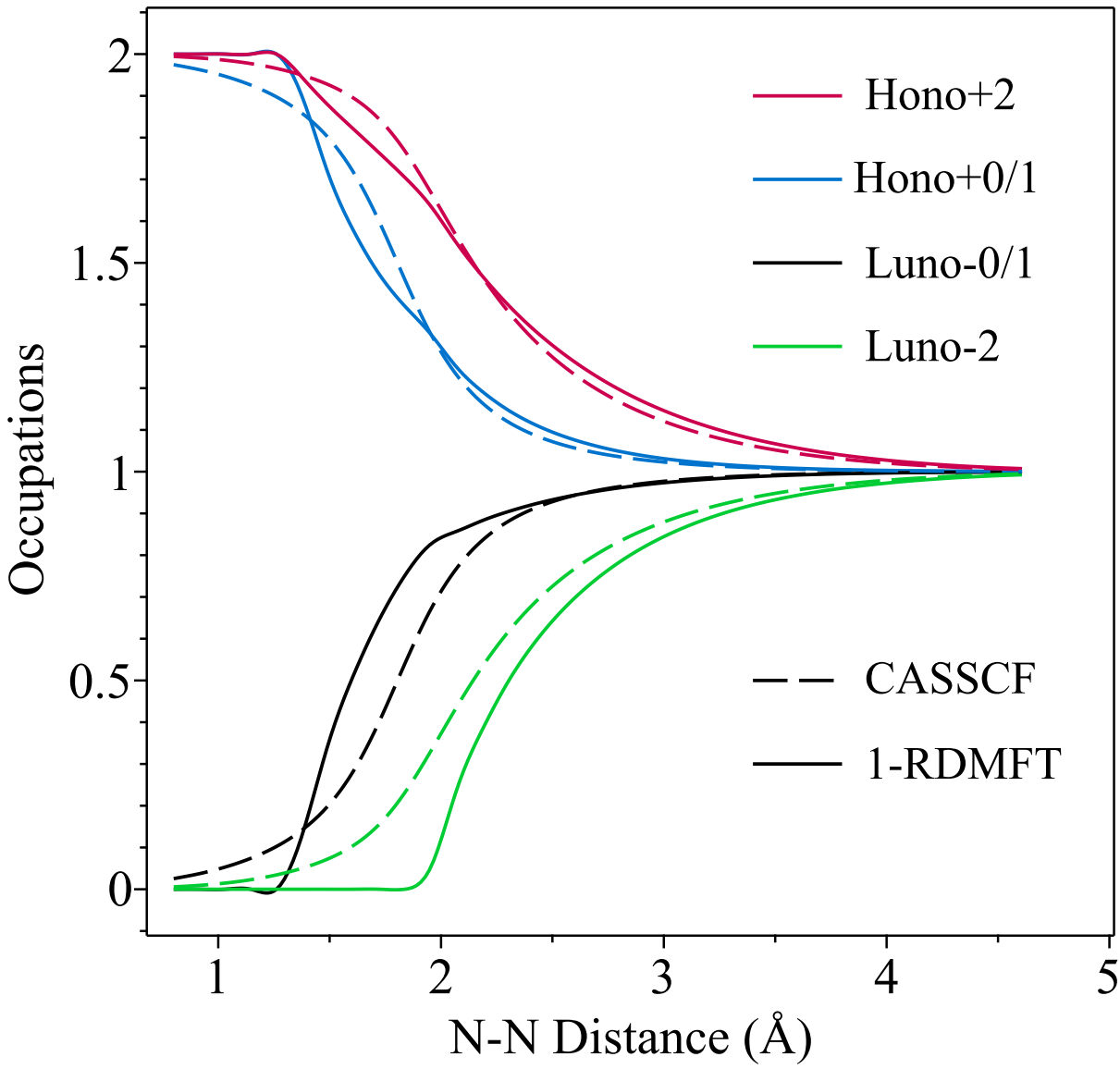

Figure 4.3: Occupations of the six frontier orbitals in the dissociation of N_2 from a 1-RDMFT with w optimized by CASSCF (solid lines) and [6,6] CASSCF (dashed lines).

Using the 1-RDMFT with the w parameter fitted to the N_2 dissociation, we apply our algorithm to a set of 11 molecules, B_2, C_2, CN, CO_2, CO, F_2, N_2, NF_3, NO, S_2, and SiO, selected from the MR-MGN-BE17 test set, [131] which is designed to benchmark a method's ability to describe multireference correlation in bond dissociation. Results obtained with

Table 4.1: Errors of the dissociation energies in kcal/mol obtained with DFT (B3LYP) and 1-RDMFT Relative to the [6,6] CASSCF and ACSE References

REF		B3LYP	1-RDMFT
CASSCF OPTIMIZED ($w = 0.150$)			
CASSCF	MSE	154.09	-17.68
	MUE	154.09	32.19
ACSE	MSE	137.03	-34.73
	MUE	137.03	39.83
ACSE OPTIMIZED ($w = 0.143$)			
ACSE	MSE	137.03	-27.76
	MUE	137.03	36.19

w fit to the CASSCF and ACSE dissociation curves of N_2 are compared to the respective CASSCF and ACSE reference data. In order to maintain consistency between the different molecular systems, the CASSCF active space was constructed to include those molecular orbitals that display a significant contribution from the valence atomic p-orbitals.

We first consider the dissociation energies from the 1-RDMFT with CASSCF-optimized w. Data are shown in the top rows of Table 4.1. It is evident that B3LYP substantially overestimates the dissociation energies as it fails to capture the static correlation of the dissociated systems, yielding a mean unsigned error (MUE) of 154.09 kcal/mol. In contrast, the 1-RDMFT displays a MUE of 32.19 kcal/mol, yielding a 5-fold reduction in error compared to traditional KS-DFT. Additionally, our algorithm results in a sign change of the mean signed error (MSE), that corresponds to an underestimating of the dissociation energy on average in contrast to KS-DFT which consistently overestimates it.

The calculations are repeated with the 1-RDMFT in which the w is based on the dissociation curve of N_2 from the ACSE. Recovery of additional dynamical correlation in the N_2 training data improves the results obtained with our 1-RDM functional corrections. The ACSE reference columns of Table 4.1 compare the CASSCF- and ACSE-trained functional forms. ACSE optimization reduces the 1-RDMFT's MUEs by approximately -3 kcal/mol. Errors for the individual molecular systems in the data set can be found in Tables A.5 and A.6

in the appendix. Overall the 1-RDMFT yields significantly lower errors in the dissociation energy of the small molecules in the set surveyed compared to traditional B3LYP.

Last, we investigate the Mott metal-to-insulator transition of linear H_4 using 1-RDMFT with $w = 0.143$, where w is trained on the dissociation curve of N_2 from the ACSE, and compare the results to those obtained from FCI [132, 133] and B3LYP using the 6-31G basis set. [125] Figure 4.4 displays the dissociation curves obtained from 1-RDMFT and KS-DFT with the B3LYP functional as well as FCI. The 1-RDMFT yields a dissociation error of just 5.9 kcal/mol when compared to FCI. Additionally, the 1-RDM functional is able to prevent the convergence failure seen in DFT at large interatomic distances, yielding smooth asymptotic behavior in the dissociation limit.

As the linear hydrogen chain dissociates, it should become an insulator with the between-atom elements of the 1-RDM in the local atomic-orbital basis set decaying to zero. The sum of these 1-RDM elements squared from 1-RDMFT, shown in Figure 5, correctly tends toward zero as the interatomic distance is increased, recovering FCI behavior, while in B3LYP it erroneously approaches 0.83, indicating that in DFT the hydrogen chain remains metallic. This failure in traditional KS-DFT arises because KS-DFT has an idempotent 1-RDM that makes it difficult to localize the density in the dissociation limit.

Density functional theory, we show, can be formally and practically transformed into a one-electron reduced-density-matrix functional theory, in which the exact correlated 1-RDM is used as the basic variable in the theory. Use of the exact 1-RDM allows us to address the limitations of DFT in its treatment of static correlation that often leads to inaccuracies in the prediction of molecular properties, especially at nonequilibrium geometries. In contrast to most 1-RDMFTs, we retain the use of DFT's exchange-correlation functional of the density. While recent work including our own has relaxed the idempotency restriction on the 1-RDM in the kinetic energy term, here we also add a quadratic 1-RDM-based term to DFT's density-based exchange-correlation functional. This additional term is especially

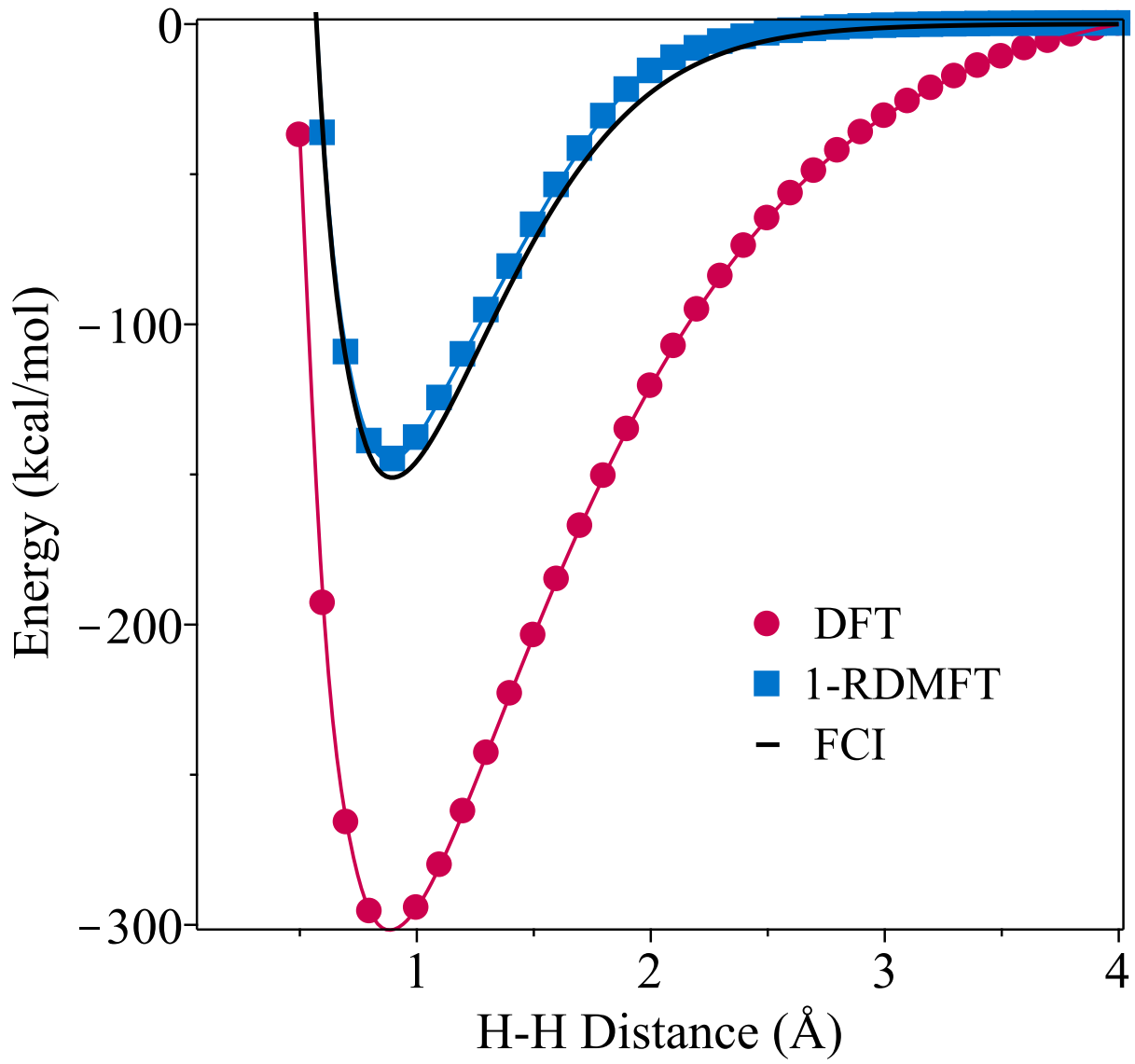

Figure 4.4: Symmetric dissociation of linear H_4 in the 6-31G basis from B3LYP, FCI, and 1-RDMFT with $w = 0.143$ from a fit to the ACSE N_2 dissociation curve.

important because it allows us to treat static correlation in molecular systems without energetically degenerate frontier orbitals. The retention of DFT's exchange-correlation functional allows us to implement the 1-RDMFT algorithm by quadratic semidefinite programming at DFT's computational scaling of $\mathcal{O}(r^3)$. The 1-RDMFT, as shown in the results, yields signif-

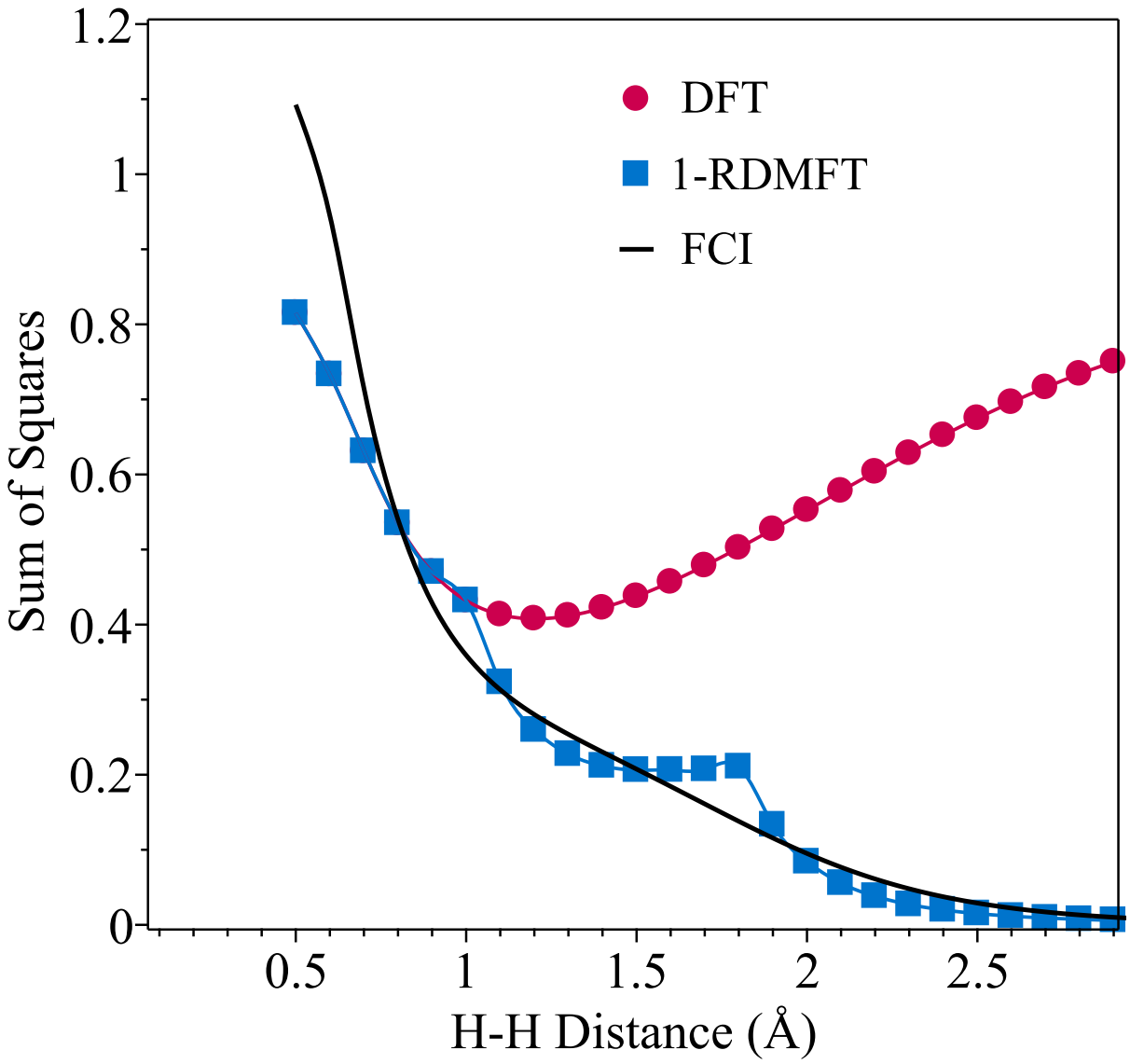

Figure 4.5: Sum of squares of the off diagonal elements of the 1-RDM obtained as a function of interatomic distance for linear H_4. The sum is defined as $\sum_{i \neq j} {D_j^i}^2$ where i and j are atomic centers.

icant improvements over traditional DFT in the description of static correlation in chemical structures and processes such as singlet biradicals and bond dissociations.

Accurate descriptions of molecular bond dissociations are achieved with a simple form of ${}^1W$ based solely on the identity matrix modified by a scalar term. Using only N_2 as the

training set, this functional form displays significant improvements over traditional KS-DFT in the capture of the dissociation energies of small molecules. Furthermore, while our parameter training focuses solely on the capture of static correlation within the π and π^* orbitals of N_2, the resulting 1-RDM functionals accurately describe the Mott insulator transition of H_4, a system lacking statically correlated π orbitals. Moreover, even though functional optimization for the capture of fractional natural occupation numbers is not performed, the 1-RDM correction in all systems studied yields natural occupations in line with those obtained from CASSCF. While we train the w parameter in the one-parameter weight matrix with standard optimization algorithms, the multiparameter flexibility of the weight matrix ${}^1W$ suggests a natural combination with machine learning, which has recently been applied to developing functionals of DFT [134, 135, 136, 137, 138] and, most recently, RDMFT. [134]

In summary, the present work provides a foundation for further research into the capture of multireference correlation through the inclusion of fractional 1-RDMs in a DFT framework. The functional developed in this work shows significant promise for the development of an efficient 1-RDM functional theory that uses existing DFT exchange-correlation functionals, or modifications thereof, for the evaluation of electronic energies of strongly correlated systems. In independent work, appearing after we completed our study, Wang and Baerends [139] developed a correction to the Hartree–Fock functional by adding a term based on the von Neumann entropy. Both this study and our study suggest new directions for progress in DFT and 1-RDMFT.

CHAPTER 5

COMPARISON OF DENSITY-MATRIX CORRECTIONS TO DENSITY FUNCTIONAL THEORY

5.1 Introduction

While density functional theory in the Kohn-Sham formulation (KS-DFT) has seen significant success throughout chemistry due to its computational affordability as well as its relative accuracy,[101, 102, 21, 96, 97, 98, 99, 100] it has been noted to struggle with three significant failures, namely: (i) the self-interaction error, (ii) the charge transfer error, and (iii) the static correlation error arising from near-degenerate electronic states.[33, 25, 24] While KS-DFT is, in theory, exact when using the unknown universal functional,[6] the aforementioned errors are rooted in the approximate nature of current density functionals. Furthermore, in contrast to wave function-based theories where there exists a clear path to improving the prediction of electronic properties via the inclusion of higher-order excitations from the Hartree-Fock (HF) reference, for example, using the configuration interaction (CI) or coupled cluster approaches, DFT does not offer such a clear systematic path of improvement.[132, 133, 140]

Modern functional developments have utilized a wide variety of different approximations with varying complexities to try to improve DFT, resulting in the so-called "functional zoo." A Jacob's ladder style scheme has been conceptualized to aid in functional classification,[8] with the idea being that ascending the ladder to more computationally complex functionals will yield improvements. While modern functionals have generally predicted chemical prop-

erties with increasing accuracy,[141] it has been argued by Medvedev et al.[29] and Brorsen et al.[142] that, while properties predicted by newer functionals are more accurate, their underlying electronic densities are increasingly deviating from the exact density. This disconnect has been attributed to newer density functional approximations relying on fitting to reproduce specific chemical properties of interest from reference calculations or experimental results instead of attempting to improve upon the fundamental quality of DFT, the electronic density.[143, 144] This is due, in part, to the difficulty in identifying and reproducing properties of the universal functional as compared to simply optimizing a set of parameters to reproduce reference data. Therefore, approaches outside of functional development may be necessary to further improve upon DFT.

Several methods have been developed aiming to enable DFT to describe static correlation. These approaches include the expansion of DFT into the complex plane to allow for static correlation to be captured using fractional orbital occupations, which requires transforming the real-valued functionals into the complex plane as well.[36] Complex orbital DFT has recently been expanded to utilize hypercomplex numbers for describing statically correlated systems beyond biradicals.[145] Another approach relies on enforcing the Perdew-Parr-Levy-Balduz flat-plane conditions through a scaling correction,[106, 107, 108, 109] aiming to recover the piece-wise linearity of density functionals between integer numbers of electrons. These methodologies both utilize fractional occupations as part of their improvement over KS-DFT.

Another area of research which focuses on fractional occupations for describing static correlation is presented by one-electron reduced density matrix functional theory (1-RDMFT).[14, 37, 113, 114, 49, 38] These approaches utilize Gilbert's theorem to express the ground-state energy as a functional of the one electron reduced density matrix (1-RDM) rather than the

wave function $\Psi(12...N)$[14] where

$$^1D(1;\bar{1}) = \int \Psi(12...N)\Psi^*(\bar{1}2...N)d2...dN \tag{5.1}$$

with each roman number representing the spatial and spin coordinates of an electron. Using the 1-RDM as the fundamental variable allows for the description of static correlation through fractional occupation numbers.[37, 113, 114] Natural orbital functional theory presents a related approach which uses the natural orbitals and their occupation numbers, which may be obtained from the 1-RDM, to reconstruct the 2-RDM subject to N-representability conditions.[49, 116, 117, 146, 40] Taking inspiration from these methods, we previously transformed KS-DFT into a 1-RDMFT to retain the favorable computational scaling of KS-DFT while enabling the description of static correlation.[118, 147]

In this article, we further expand upon the theory of translating DFT into a 1-RDMFT framework and compare how our current implementation of our 1-RDMFT method relates to the information density matrix functional theory (iDMFT) method developed by Wang and Baerends.[139, 148] To facilitate this comparison, we generalize iDMFT to use density functionals in addition to the Hartree-Fock functional. Since our 1-RDMFT approach as well as iDMFT rely on functional selection, we perform benchmarking calculations on a test set of small statically correlated molecules to elucidate the functional dependence of the two surveyed methods. Finally, the magnitude of the correction term required with a given functional for 1-RDMFT or iDMFT, obtained from our benchmark, provides insight into its inherent ability to describe multi-reference correlation.

5.2 Theory

We review and expand upon the conversion of DFT into 1-RDMFT in Section 5.2.1 and compare the resulting 1-RDMFT with iDMFT in Section 5.2.2.

5.2.1 Conversion of DFT into a 1-RDMFT.

Consider the energy functional for DFT

$$E_{\mathrm{DFT}}[\rho] = T_{\mathrm{s}}[\rho] + V[\rho] + F_{\mathrm{xc}}[\rho] \tag{5.2}$$

where ρ is the one-electron density, $T_{\mathrm{s}}[\rho]$ is the noninteracting kinetic energy functional - the kinetic energy from the single Slater determinant that yields the density ρ, $V[\rho]$ is the sum of the one-electron (external) potential and the Coulomb potential, and $F_{\mathrm{xc}}[\rho]$ is the exchange-correlation functional. As in ref [147], we convert DFT into a 1-RDMFT by replacing the non-interacting kinetic energy by the full kinetic energy and adding a 1-RDM-based correction functional $C[^1D]$

$$E_{\mathrm{RDMFT}}[^1D] = E_{\mathrm{DFT+T}}[^1D] + C[^1D] \tag{5.3}$$

where $E_{\mathrm{DFT+T}}[^1D]$ is defined as

$$E_{\mathrm{DFT+T}}[^1D] = E_{\mathrm{DFT}}[\rho] + (T[^1D] - T_s[\rho]) \tag{5.4}$$

Because the exchange-correlation functionals in traditional DFT are not exact, we can treat $C[^1D]$ as a general functional that, as part of its conversion of DFT into a 1-RDMFT, also accounts for the limitations of existing functionals to treat static electron correlation.

The correction has several advantages relative to traditional approaches in DFT and 1-RDMFT. From the perspective of 1-RDMFT, the correction allows us to build upon the wealth of functionals that have been developed for DFT as well as the low computational scaling afforded by DFT's exchange-correlation potential. From the perspective of DFT, the correction allows us to use explicit 1-RDM information for an improved treatment of static correlation.

As a practical correction to DFT, we focus on approximating the part of the correction $C[^1D]$ that lowers the energy from the presence of static electron correlation. We assume that this part of the correction functional: (i) obeys particle-hole symmetry, (ii) vanishes in the limit of no correlation, and (iii) rewards the formation of fractional occupation for orbitals as they near energetic degeneracy. Note that assumption (ii) is an approximation for the exact $C[^1D]$ functional. Using these assumptions, we previously obtained the following form in ref [147]

$$E_{\mathrm{RDMFT}}[^1D] = E_{\mathrm{DFT+T}}[^1D] - \mathrm{Tr}[^1W(^1D - {}^1D^2)] \tag{5.5}$$

where ^1W is an arbitrary positive semidefinite weight matrix. By taking ^1W to be a weighted identity matrix w^1I, we produce the final form of our correction[147]

$$E_{\mathrm{RDMFT}}[^1D] = E_{\mathrm{DFT+T}}[^1D] + w(\mathrm{Tr}[^1D^2 - {}^1D]) \tag{5.6}$$

If the 1-RDM is idempotent, we note that this correction vanishes, and if the 1-RDM is not idempotent, it is nonzero and serves to remove the double counting of the correlated kinetic energy and to account for static correlation that is missing from traditional DFT.

When $w = 0$, the energy functional is readily minimized by a conventional Kohn-Sham self-consistent-field (SCF) calculation; when $w \neq 0$, the functional can be minimized by a modified Kohn-Sham SCF calculation where the modified Kohn-Sham energy is given by

$$E_{\mathrm{MKS}} = \mathrm{Tr}[H_{KS}{}^1D] + w(\mathrm{Tr}[^1D^2 - {}^1D]) \tag{5.7}$$

where H_{KS} is the Kohn-Sham Hamiltonian. To express the minimization of E_{MKS} at each SCF iteration as a semidefinite program (SDP), we can relax the quadratic term by intro-

ducing an auxiliary matrix variable ${}^1F$

$$E_{\mathrm{MKS}} = \mathrm{Tr}[H_{KS}{}^1D] + w(\mathrm{Tr}[{}^1F - {}^1D]) \tag{5.8}$$

in which

$$\begin{pmatrix} {}^1I & {}^1D \\ {}^1D & {}^1F \end{pmatrix} \succeq 0 \tag{5.9}$$

The semidefinite constraint causes the trace of ${}^1F$ to be bounded by the trace of the 1-RDM squared,[147] and hence, the minimization of eq 5.8 as an SDP is equivalent to the minimization of eq 5.7. The overall algorithm for our 1-RDMFT procedure is shown in Figure 5.1. It should be noted that the modified Kohn-Sham energy, just like the Kohn-Sham energy in DFT, does not yield the energy of the system, which instead is obtained by evaluating eq 5.6 using the converged 1-RDM.

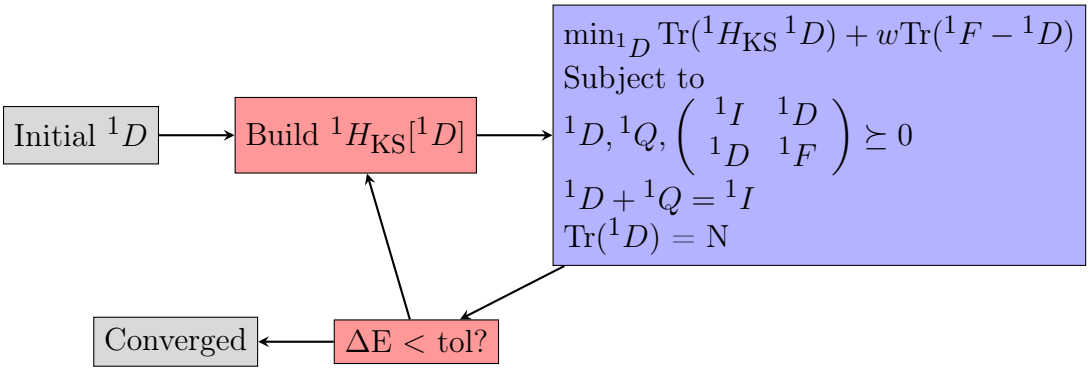

Figure 5.1: Schematic description of the 1-RDMFT algorithm. From an initial guess density, ${}^1D$, the Kohn-Sham 1-body Hamiltonian, $H_{\mathrm{KS}}[{}^1D]$, is generated using a traditional DFT exchange correlation functional. This Hamiltonian is then used in an SDP-based minimization to yield a new 1-RDM. Self-consistent-field iterations are continued until the energy is converged below a selected target threshold.

5.2.2 Comparison to iDMFT

We briefly review iDMFT [139] and then draw a comparison between iDMFT and our 1-RDMFT. The iDMFT postulates that the missing correlation energy from the Hartree–Fock method can be expressed as the fermionic entropy, defined as

$$S = -\theta \sum_i [n_i \ln(n_i) + (1 - n_i)\ln(1 - n_i)] \tag{5.10}$$

where n_i is the energy of the i^{th} orbital. Minimizing the Hartree–Fock energy plus this entropic term leads to orbital occupations defined by the Fermi–Dirac distribution

$$n_i = \frac{1}{1 + \exp\left[(\epsilon_i - \mu)/\theta\right]} \tag{5.11}$$

where ϵ_i is the energy of the i^{th} orbital and μ is the chemical potential which is constrained such that $\sum_i n_i = N$. This distribution naturally leads to non-idempotent 1-RDMs, with the degree of fractional occupation increasing as orbital energies become degenerate or the fictitious temperature θ increases. The fractional occupations are then used in the fermionic entropy correction to the energy, which is simply subtracted from the total electronic energy of the system. iDMFT uses the same principles as thermally assisted occupation DFT and the Fermi-smearing technique; however, it applies them to the Hartree-Fock theory instead of a density functional. [33, 149, 150] In this work, we have implemented iDMFT to utilize both the Hartree-Fock method (or functional) and available density functionals to facilitate a more thorough comparison with 1-RDMFT.

The energy correction of iDMFT is based on the information entropy of the 1-RDM, while the correction of the SDP-formulated 1-RDMFT is based on the idempotency relation of the 1-RDM. These two corrections, we can show, agree with each other through second order in a Taylor series expansion of the information entropy. We first recast eq 5.6 in terms

of particle and hole matrices

$$S = -\theta \mathrm{Tr}[{}^1D \ln({}^1D) + {}^1Q \ln({}^1Q)] \tag{5.12}$$

Second, we expand the natural logarithm of ${}^1D$ in powers of ${}^1Q$ through second order

$$\ln({}^1D) = \ln({}^1I - {}^1Q) \tag{5.13}$$

$$= -\sum_{n=1}^{\infty} \frac{{}^1Q^n}{n} \tag{5.14}$$

$$= -{}^1Q - \frac{{}^1Q^2}{2} - \mathcal{O}({}^1Q^3) \tag{5.15}$$

Similarly, by particle-hole symmetry

$$\ln({}^1D) = -{}^1Q - \frac{{}^1D^2}{2} - \mathcal{O}({}^1D^3) \tag{5.16}$$

Inserting eqs 5.15 and 5.16 into eq 5.12 yields

$$S \approx -\theta \mathrm{Tr}[{}^1D(-{}^1Q - \frac{{}^1Q^2}{2}) + {}^1Q(-{}^1D - \frac{{}^1D^2}{2})] \tag{5.17}$$

Upon substituting the identity ${}^1Q = {}^1I - {}^1D$ and simplifying without further approximation, we obtain

$$S \approx -\frac{5}{2}\theta \mathrm{Tr}[{}^1D^2 - {}^1D] \tag{5.18}$$

Comparing this form with eq 5.6 reveals that our energy correction and iDMFT's correction agree with each other through second order in the expansion of the natural logarithms of the 1-particle and 1-hole RDMs in the information entropy for $\theta = 2w/5$. Furthermore, it can also be seen from eq 5.17 that truncation of the logarithmic expansions to only first order also yields eq 5.18 with the scalar value of $5/2$ replaced by 2.

5.3 Results

In this work, we utilize our 1-RDMFT method with a simple weight matrix defined as $({}^1W = w{}^1I)$, where w is a system-specific constant and is optimized to reproduce either the dissociation energy or rotational barrier obtained from full CI (FCI) or anti-Hermitian contracted Schrödinger equation (ACSE) [132, 133, 123, 124, 78] calculations. Three different functionals of varying HF exchange are surveyed and reported in the text, namely, SCAN, [91] M06-2X, [151] and HF, with percent HF exchanges of 0, 54, and 100%, respectively. Additional data obtained with the functionals M06-L, [143] B3LYP, [130, 129] M06, [143] and M06-HF [152] are reported in Tables A.7 and A.8 in the appendix. All DFT, HF, and 1-RDMFT calculations were performed using PySCF [128] with the cc-pVDZ basis set, [94] while the ACSE calculations for CO, N_2, HF, and C_2H_4 were performed in Maple using the Quantum Chemistry Toolbox.[126, 127] All 1-RDMFT calculations were started with the converged 1-RDM from the respective DFT or HF results. The SDP was solved using a boundary-point SDP algorithm previously developed by one of the authors for solving the variational 2-RDM problem. [62, 68]

While both KS-DFT and HF struggle with the capture of static correlation due to their single-reference nature, KS-DFT's errors are generally smaller than those produced by HF. [153] This is attributable to KS-DFT's approximate exchange correlation functional that captures some correlation effects. To investigate, we apply conventional DFT and our 1-RDMFT with the SCAN and HF functionals to linear H_4 where all adjacent hydrogens are equally spaced, shown in Figure 5.2. The data reveal that in the KS-DFT formalism, the SCAN functional fails to describe the dissociation limit, yielding an error of 122.72 kcal/mol at 4 Å, while in the 1-RDMFT method, it accurately reproduces the dissociation curve including the dissociation limit. Plots of the errors in the potential energy curves (PECs) are shown in Figures A.2 and A.3 in the appendix. Furthermore, although the HF method yields an even greater error of 218.68 kcal/mol at 4 Å than the DFT functional SCAN, it

also yields an accurate PEC in the framework of the 1-RDMFT. Minor differences arise in the stretched bonding region of 1.8–2.2 Å where the HF-based 1-RDMFT overestimates the energy, which results in a faster approach to the dissociation energy limit relative to the FCI reference curve.

Next, we consider the C–C bond rotation in C_2H_4. Here, the SCAN functional in KS-DFT overestimates the barrier height by 31 kcal/mol, while in 1-RDMFT, the barrier height can be recovered within sub-milli-kcal/mol accuracy (Figure 5.3). Although the 1-RDMFT curve is unable to match the reference with the same level of accuracy as seen for H_4, it is able to remove the non-physical discontinuity observed from KS-DFT at the 90° dihedral angle. This discontinuity is attributable to the increasingly diradical nature of the molecule as the dihedral angle approaches 90° and the highest occupied natural orbital and lowest unoccupied natural orbital become degenerate, which may not be properly described using a single Slater determinant. Using HF in its traditional implementation also results in a non-physical discontinuity as well as a barrier height error of 41 kcal/mol, which is an increase relative to the barrier height error of 31 kcal/mol from SCAN. However, using HF within our 1-RDMFT framework, we once again reproduce the barrier height to within sub-milli-kcal/mol accuracy although the deviations from the reference curve are, as with H_4, larger than those seen using SCAN. Furthermore, while KS-DFT deviates from the 1-RDMFT curve when using SCAN at a dihedral angle of 57.5°, traditional HF deviates from the 1-RDMFT curve when using HF at a smaller angle of 50°. This points toward the 1-RDMFT correction resulting in non-idempotency earlier in the bond rotation for HF than SCAN as our 1-RDMFT method produces no energetic change until idempotency is broken. This is verified through investigations of the non-idempotent residual in Figures A.4 and A.5 in the appendix.

Expanding our test set to also include the statically correlated dissociations of H_2, N_2, HF and CO, as well H_4 and C_2H_4, we tabulate the maximal deviation and average signed

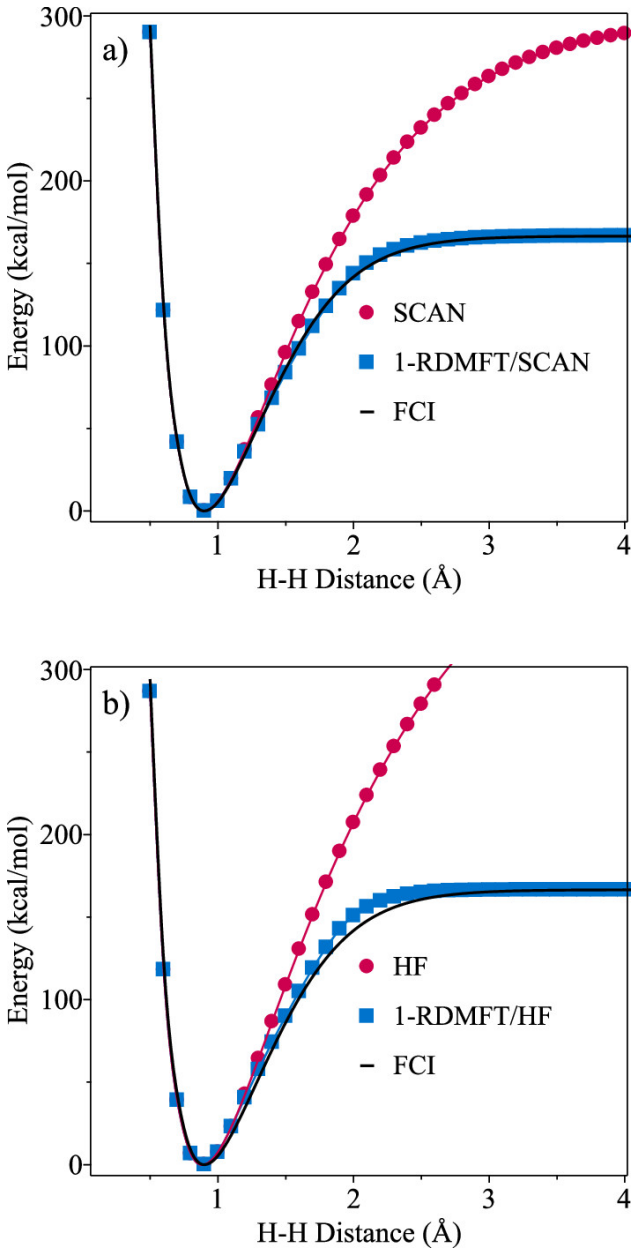

Figure 5.2: Plot of the linear dissociation of H_4 in the cc-pVDZ basis set with equal distances between all pairs of adjacent hydrogens. (a) Comparison of the SCAN functional in the traditional KS-DFT implementation and within our 1-RDMFT method using a w value of 0.104 to FCI. (b) Comparison of HF in its traditional formulation and within our 1-RDMFT method using a w value of 0.249 to FCI.

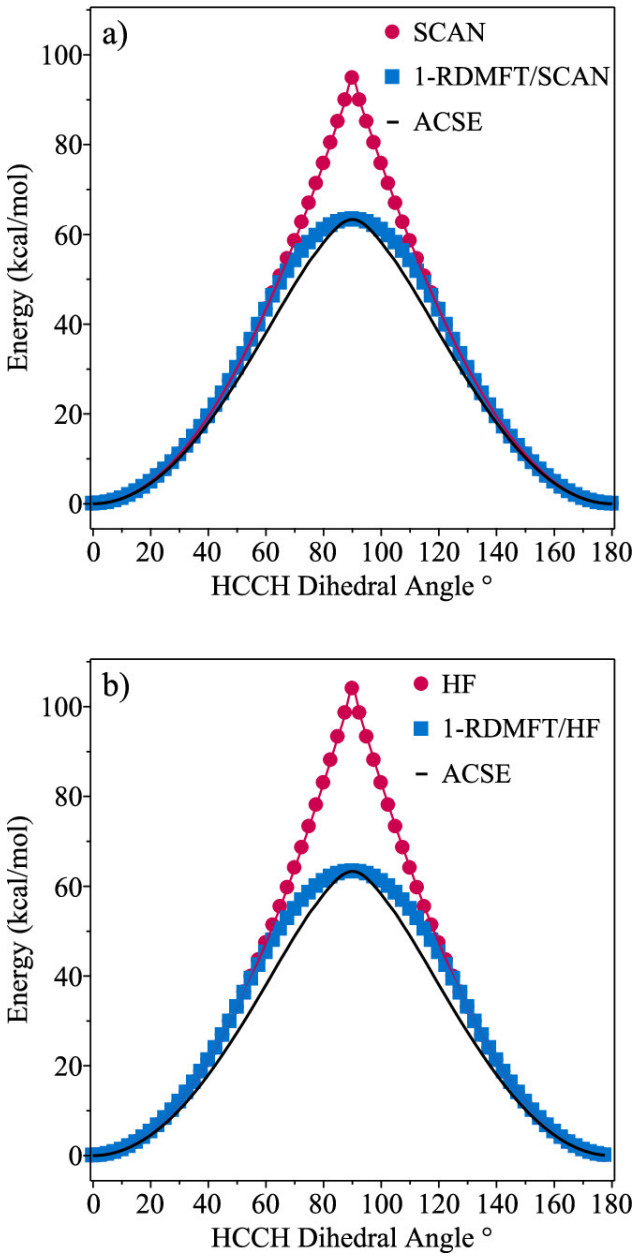

Figure 5.3: Plot of the rotation of C_2H_4 along its HCCH dihedral angle. The relative energies are zeroed to the planar geometry at 0°. (a) Comparison of the SCAN functional in the traditional KS-DFT implementation and within our 1-RDMFT method using a w value of 0.052 to the ACSE. (b) Comparison of HF in its traditional formulation and within our 1-RDMFT method using a w value of 0.215 to the ACSE.

and unsigned errors from the reference PEC in Table 5.1. The reference PEC is computed from FCI for H_2 and H_4 and from ACSE for the other molecules; the signed and unsigned errors for the dissociations are computed from the average errors in the reference curve between equilibrium and 4 Å in 0.1 Å step sizes, while for C_2H_4, the errors are calculated from finely spaced points over the entire dihedral angle. Comparing the surveyed density functionals in Table 5.1 reveals that using any of them within the 1-RDMFT framework reproduces the reference curve more accurately than when using HF in 1-RDMFT, which consistently gives the largest errors. Comparing the maximal errors of the two density functionals SCAN and M06-2X in Table 5.1 shows the SCAN functional obtaining a root mean squared error (RMSE) of 5.72 kcal/mol, approximately half that of M06-2X's 12.06 kcal/mol, with SCAN only having a slightly larger absolute error in two systems, H_4 and C_2H_4. Additionally, when including the functionals from Tables A.7 and A.8 in the appendix, which, in terms of increasing HF exchange, have RMSEs of the maximal errors of 6.43, 6.56, 9.46, and 23.48 kcal/mol for M06-L, B3LYP, M06, and M06-HF, respectively, it is observed that as the fraction of HF exchange in the DFT functional increases, the errors tend to increase as well. The RMSEs of the mean signed errors being 1.31, 2.97, and 6.58 kcal/mol for SCAN, M06-2X, and HF further clarifies that as the HF exchange increases, 1-RDMFT increasingly overestimates the energy of the system. The relative improvements of the density functionals over HF are attributable to their recovery of additional dynamical correlation as the 1-RDMFT method is intended to treat strongly correlated orbitals, neglecting those with only small fractional occupations. The maximal errors consistently occur in the stretched bond region with both the equilibrium region and the dissociation limit being well described. There was no noticeable trend between the fraction of HF exchange and the location of the maximal error along a curve.

In the present exploratory calculations, because w is optimized for collections of calculations such as a given molecule's bond dissociation curve, we can use it as a gauge for the

Table 5.1: 1-RDMFT and iDMFT error values used to quantify their reproduction of the dissociations of H_2, H_4, N_2, HF, and CO as well as the bond rotation of C_2H_4. The maximal errors are defined as $E_{\text{1-RDMFT/iDMFT}}$ - $E_{\text{FCI/ACSE}}$ with the largest absolute magnitude being selected. Reference energies are computed from FCI for H_2 and H_4 and from the ACSE for the other molecules. The signed and unsigned errors are obtained as the average deviation from the reference curve from equilibrium to 4 Å using 0.1 Å step sizes.

		Maximal Error kcal/mol			Signed Error over PES			Unsigned Error over PES		
Method		SCAN	M06-2X	HF	SCAN	M06-2X	HF	SCAN	M06-2X	HF
1-RDMFT	H_2	6.14	11.53	14.11	1.71	2.60	4.19	1.71	2.64	4.19
	H_4	-2.88	2.66	9.02	0.34	0.40	3.24	1.00	0.98	3.24
	N_2	9.99	19.01	34.88	0.87	4.22	11.20	1.65	4.24	11.20
	HF	-2.35	6.87	17.39	-1.29	0.30	-0.39	1.30	2.05	7.06
	CO	3.80	17.31	35.05	0.79	4.99	9.84	1.68	5.89	11.06
	C_2H_4	5.54	4.98	7.21	2.07	1.76	3.10	2.07	1.76	3.10
	RMSE	5.72	12.06	22.66	1.31	2.97	6.58	1.60	3.36	7.48
iDMFT	H_2	-0.44	-1.88	-1.22	-0.12	-0.64	-0.36	0.15	0.67	0.37
	H_4	-8.38	-12.01	-9.87	-2.80	-4.59	-3.56	2.81	4.59	3.57
	N_2	-13.90	-12.03	2.92	-4.33	-3.97	0.51	4.33	3.97	0.85
	HF	-4.79	-4.08	3.56	-2.07	-2.32	-0.91	2.11	2.40	2.23
	CO	-7.89	-5.78	-8.50	-2.62	-2.10	-0.40	2.77	2.30	3.05
	C_2H_4	2.28	-2.24	-2.40	0.97	-1.04	-1.03	0.97	1.04	1.05
	RMSE	7.68	7.61	5.75	2.54	2.83	1.59	2.57	2.87	2.20

strength of the correction required for a given functional to capture static correlation. Comparing the w values used for H_4 in Table 5.2, for example, gives 0.098, 0.171, and 0.256 for the SCAN, M06-2X, and HF functionals, respectively. The data highlight that increasing HF exchange yields less accurate descriptions of statically correlated systems and therefore requires a larger correction weight w. The trend, not limited to H_4 but observed in all systems investigated here, supports previous work, arguing that larger contributions of HF exchange in the exchange correlation functional increase static correlation errors within DFT.[154]

After investigating the use of different functionals within our 1-RDMFT framework, we compare it to the iDMFT method. For this comparison, we utilize the same set of functionals and chemical systems, optimizing the adjustable parameter θ in iDMFT to reproduce the reference data. Starting with the maximum error from the reference curves, given in Table 5.1, it is evident that iDMFT reverses the trends seen in 1-RDMFT. In iDMFT, instead of

Table 5.2: Optimized 1-RDMFT w and iDMFT θ values and their ratios are reported.

	SCAN			M06-2X			HF		
	w	θ	w/θ ratio	w	θ	w/θ ratio	w	θ	w/θ ratio
H_2	0.098	0.036	2.76	0.171	0.062	2.74	0.256	0.095	2.70
H_4	0.104	0.038	2.72	0.170	0.063	2.69	0.249	0.094	2.66
N_2	0.114	0.042	2.72	0.213	0.080	2.66	0.325	0.124	2.62
HF	0.073	0.024	3.11	0.189	0.061	3.08	0.318	0.105	3.04
CO	0.076	0.027	2.86	0.176	0.062	2.83	0.287	0.103	2.79
C_2H_4	0.052	0.019	2.75	0.127	0.048	2.67	0.215	0.083	2.58

the local functional SCAN having the lowest maximum errors and HF having the largest, HF consistently gives lower errors relative to the DFT functionals. This is attributable to the over-inclusion of dynamical correlation, which is treated in iDMFT through the density functional as well as the small non-zero orbital occupations in the entropic correction. While 1-RDMFT and iDMFT have different trends in their maximum errors, the RMSEs of the maximal errors of the best performing functionals, SCAN and HF, are 5.72 and 5.75 kcal/mol for 1-RDMFT and iDMFT, respectively, leading to results of comparable accuracy between the two methods. Further support for their comparable accuracy is found in the RMSE of their unsigned errors where SCAN in 1-RDMFT has an RMSE of 1.60 kcal/mol, while HF in iDMFT has an RMSE of 2.20 kcal/mol. Additionally, while H_4 displays the smallest deviations from the reference FCI curve using 1-RDMFT, H_2 is the system most accurately reproduced by iDMFT with a signed error of -0.12, -0.64, and -0.36 kcal/mol for SCAN, M06-2X, and HF, respectively. Finally, comparing the signs of the signed errors between the two methods, it is evident that while 1-RDMFT generally overestimates the energy along the curve, iDMFT typically underestimates it due to the over-inclusion of the dynamical correlation.

Because the adjustable parameter θ in iDMFT - like the w in 1-RDMFT - is optimized for collections of calculations such as a given molecule's bond dissociation curve, its magnitude can again be used to gauge the degree of correction required for the HF and DFT functionals. These θ values, given in Table 5.2, display the same trend observed in 1-RDMFT's w values:

as the fraction of HF exchange increases in the functional, the magnitude of θ, reflecting the size of the correlation correction, increases. While the optimized values of θ are lower than the w values, there is a consistent ratio between them, with w being $\sim$2.7 times larger than θ (shown in Table 5.2). Additionally, the ratio also appears to be affected by the amount of HF exchange in the functional, with it decreasing as the fraction of HF exchange increases. The computed ratios are in good agreement with the factor of 2.5 predicted from the Taylor series expansion in Section 5.2.2.

5.4 Conclusion

In this work, we have expanded on the theoretical underpinnings of our recently developed methodology, which formally transforms traditional KS-DFT into a 1-RDFT via the inclusion of a 1-RDM-based correction. A modified Kohn-Sham formalism, solvable by semidefinite programming, allows for the accurate capture of strong correlation at favorable computational scaling. Here, we extend our 1-RDMFT to utilize the Hartree-Fock functional and delineate and formally derive the relation of our approach to the recently developed iDMFT method, which introduces multi-reference correlation effects to HF via the use of an entropic correction, demonstrating that the two theories are in agreement through second order. We also extend iDMFT to use DFT functionals for better comparison to our 1-RDMFT.

To demonstrate the potentially broad applicability of our 1-RDMFT as well as to investigate its dependence on the chosen DFT functional, we have calculated the potential energy surfaces for several bond dissociations and the bond rotation of ethene, covering a range of different chemical bonding environments and functionals. For the purpose of comparing HF and the DFT functionals, we optimize the w parameter in 1-RDMFT (or θ parameter in iDMFT) for each functional for a collection of calculations such as a molecule's PEC. The results reveal that the 1-RDMFT can be effective at capturing multireference correlation across entire potential energy surfaces, smoothly interpolating between the single-reference

equilibrium regime and the strongly correlated dissociated regime. Furthermore, we analyze the differences in the results from 1-RDMFT and iDMFT, obtaining a ratio between the w and θ values of 1-RDMFT and iDMFT, respectively, of 2.7 that is in good agreement with the theoretically predicted value of 2.5.

While the general effectiveness of our weight-matrix correction, $w^1 I$, suggests that all functionals investigated in this work suffer from the same fundamental failings in describing static correlation - exemplified by the fact that only the adjustment of a scalar multiplier for each system and functional combination is required to obtain accurate surfaces -, the results also reveal fundamental differences in the various functionals' ability to capture strong correlation, quantified by the magnitude of the required 1-RDM correction. In particular, we observe that the magnitude of the scalar value w (or θ for iDMFT) depends on the amount of HF exchange included in a chosen density functional, with an increasing percentage of HF exchange requiring a larger w and, hence, a bigger correction. Interestingly, while a pure functional yields the best agreement with high-level reference data in our 1-RDMFT framework, the opposite is true in the case of iDMFT, which performs best with the HF method.

Future work will focus on the determination of the system specific weight matrix, w, with particular promise being held by the use of machine learning[134, 135, 136, 137, 138] for this purpose. More generally, the transformation of DFT into a 1-RDMFT presents a fresh paradigm for the prediction of both dynamic and static correlation at a mean-field-scaling computational cost. Unlike traditional 1-RDMFT approaches, the present theory allows us to achieve a lower computational scaling by exploiting DFT's existing functionals, and in contrast to DFT, it allows us to harness the additional information of the 1-RDM, especially its fractional eigenvalues (natural-orbital occupations), to realize a more accurate description of static correlation, which has important applications to many molecular structures and processes.

CHAPTER 6

UNIVERSAL GENERALIZATION OF DENSITY FUNCTIONAL THEORY FOR STATIC CORRELATION

6.1 Introduction

The success of density functional theory (DFT) [155, 156, 157] lies in its ability to improve upon the energies and properties of mean-field theories like Hartree-Fock while retaining the computational scaling of a one-electron theory. Nonetheless, the exact energy functional of DFT, originally postulated by Hohenberg and Kohn [6], is not known in a practical form, which leads to limitations in the prediction of charges [158, 159], Van der Waals forces [160], barrier heights [161], and bi- and multiradicals [23]. These limitations largely arise from the inability of DFT to provide a complete description of static (or multireference) electron correlation, which occurs when two or more Slater determinants contribute equally or nearly equally to the wave function. Recently, it has been shown that modern density functionals typically improve the energy over more established functionals at the expense of other properties including electron density [29, 142], implying that such improvements may be arising in part from an overfitting of the energy rather than a fundamental enhancement of the underlying functional.

In this Letter, we combine DFT [155, 156, 157] and its extensions [162, 33, 12, 108, 36, 118, 163, 164, 145, 165, 166] with 1-RDM [14, 15, 17, 167, 44, 112, 168, 169, 42, 40, 38, 37, 49, 111, 139, 165, 170, 171] and 2-RDM [172, 124, 173, 174, 175, 176, 177, 178, 123, 179, 180, 181, 182, 183, 184, 185, 43, 76, 74, 13, 72, 71, 62, 70, 186, 187, 188, 189] theories to obtain a universal $\mathcal{O}(N^3)$ generalization of DFT for static correlation. We consider the invariants of

the cumulant part of the 2-RDM [175, 176, 177, 178] with respect to one-body unitary transformations [190, 191]. Using the lowest order invariant, we derive a universal transformation of DFT into a 1-RDM functional theory (1-RDMFT) whose convexity naturally allows the orbital occupations to become fractional upon correlation. Critically, the correction, derived from the cumulant invariant, has an explicit dependence on the trace of the electron-repulsion matrix that correctly determines the magnitude of the correction, removing a significant limitation of previous work [165, 147], to realize a predictive theory. The quadratic dependence of the functional on the 1-RDM produces a quadratic semidefinite program that we solve using an efficient boundary-point algorithm for semidefinite programming [62] developed for variational 2-RDM theory [172, 192, 43, 76, 74, 13, 72, 71, 62, 70, 186, 187, 188, 189]. To demonstrate, we apply the functional theory to examining the barrier to rotation in ethylene [193], the relative energies of the benzynes [194], as well as a benchmark based on the dissociation energies of 11 molecules [195]. The cumulant-based generalization of DFT has the potential to extend the reach of DFT to treat a broader range of molecules and materials including those whose properties are significantly influenced by static correlation.

6.2 Theory

Consider the energy of any many-electron atom or molecule in a finite basis of r spin orbitals as a functional of the 1- and 2-RDMs[112]

$$E_{\mathrm{2RDM}}[{}^1D, {}^2D] = Tr({}^1H\,{}^1D) + Tr({}^2V\,{}^2D), \tag{6.1}$$

in which ${}^1H$ is the matrix representation of the one-electron kinetic energy and nuclear-electron Coulomb terms, ${}^2V$ is the matrix representation of the two-electron repulsion term, and ${}^1D$ and ${}^2D$ are the 1- and 2-RDMs, normalized to N and $N(N-1)/2$, respectively. We

can reexpress the 2-RDM in terms of its cumulant expansion [175, 176, 177, 178]

$$^2D = {}^1D \wedge {}^1D + {}^2\Delta \tag{6.2}$$

where $\wedge$ denotes the antisymmetric (or Grassmann) tensor product [175] and $^2\Delta$ is the cumulant (or connected) part of the 2-RDM. Hence, the energy can also be written as a functional of the 1-RDM and the cumulant 2-RDM

$$E_{\text{2RDM}}[^1D, {}^2\Delta] = E[^1D] + E^{\Delta}[^2\Delta], \tag{6.3}$$

in which

$$E[^1D] = \text{Tr}(^1H\,{}^1D) + \text{Tr}(^2V[^1D \wedge {}^1D]) \tag{6.4}$$

$$E^{\Delta}[^2\Delta] = Tr(^2V\,{}^2\Delta). \tag{6.5}$$

Because the cumulant 2-RDM can be decomposed into three orthogonal subspaces based on the unitary group [190], known as the unitary decomposition [191], we have

$$^2\Delta = {}^2\Delta_0 + {}^2\Delta_1 + {}^2\Delta_2 \tag{6.6}$$

or

$$E^{\Delta}[^2\Delta] = E_0^{\Delta}[^2\Delta_0] + E_1^{\Delta}[^2\Delta_1]E_2^{\Delta}[^2\Delta_2] \tag{6.7}$$

where

$$E_k^{\Delta}[^2\Delta_k] = \text{Tr}(^2\Delta)^2 I. \tag{6.8}$$

Because the zeroth component of the unitary decomposition of the cumulant 2-RDM is [190]

$$^2\Delta_0 = \frac{2}{r(r-1)}\text{Tr}(^2\Delta)^2 I, \tag{6.9}$$

in which ${}^2I$ is the two-electron identity matrix, we can express the zeroth component of the cumulant correction to the energy as follows

$$E_0^{\Delta}[{}^2\Delta_0] = \frac{2}{r(r-1)}\mathrm{Tr}({}^2V)\mathrm{Tr}({}^2\Delta). \tag{6.10}$$

However, the trace of the cumulant 2-RDM can be expressed in terms of the 1-RDM's idempotency [196, 197, 198, 199]

$$\mathrm{Tr}({}^2\Delta) = -\frac{1}{2}\mathrm{Tr}({}^1D - {}^1D^2), \tag{6.11}$$

in which ${}^1D^2$ denotes the square of the 1-RDM, and the trace of ${}^2V$ can be expressed in terms of the two-electron repulsion integrals in physics notation

$$\mathrm{Tr}({}^2V) = 2\sum_{\tilde{i},\tilde{j}}(2\langle\tilde{i}\tilde{j}||\tilde{i}\tilde{j}\rangle - \langle\tilde{i}\tilde{j}||\tilde{j}\tilde{i}\rangle), \tag{6.12}$$

where the tilde denotes the index of the spatial part of the spin orbital. Therefore, using Eqs. 6.11 and 6.12 in Eq. 6.10, we can express the zeroth component of the cumulant energy correction as a functional of the 1-RDM

$$E_0^{\Delta}[{}^2\Delta_0] = -\gamma\mathrm{Tr}({}^1D - {}^1D^2), \tag{6.13}$$

where

$$\gamma = \frac{2}{r(r-1)}\sum_{\tilde{i},\tilde{j}}(2\langle\tilde{i}\tilde{j}||\tilde{i}\tilde{j}\rangle - \langle\tilde{i}\tilde{j}||\tilde{j}\tilde{i}\rangle) \tag{6.14}$$

Approximating the cumulant energy with its zeroth-order component yields a 1-RDM functional theory that corrects the Hartree-Fock energy.

The correction mainly accounts for static correlation. To see this, we consider the contribution of energetically low-lying excitations to the electron correlation, known as dynamic

correlation. The largest contribution arises from the double excitations in which two electrons in occupied orbitals are promoted to two unoccupied orbitals. These excitations appear in off-diagonal terms of the cumulant 2-RDM in which both upper indices correspond to unoccupied orbitals and both lower indices correspond to occupied orbitals [184]. These elements, however, only contribute to the final energy term from the unitary decomposition. Consequently, the zeroth energy term, arising from the trace of the cumulant 2-RDM, primarily accounts for static correlation. We can alternately establish the relationship between this correction and static correlation from directly evaluating the trace of the cumulant 2-RDM. The cumulant's trace equals the trace of the idempotency relation for the 1-RDM [196, 197, 198, 199]. The 1-RDM only deviates significantly from idempotency when its occupation numbers are highly fractional-far from zero and one, which occurs primarily when an atom or molecule possesses significant static correlation.

Previous work showed that we can transform DFT into a 1-RDMFT by adding a correction functional [165, 147]

$$E_{\mathrm{RDMFT}}[{}^1D] = E_{\mathrm{DFT+T}}[{}^1D] + C[{}^1D] \tag{6.15}$$

in which

$$E_{\mathrm{DFT+T}}[{}^1D] = E_{\mathrm{DFT}}[\rho] + (T[{}^1D] - T_s[\rho]), \tag{6.16}$$

$$E_{\mathrm{DFT}} = T_{\mathrm{s}}[\rho] + V[\rho] + F_{\mathrm{xc}}[\rho], \tag{6.17}$$

where ρ is the one-electron density, T_{s} is the noninteracting kinetic energy functional, $T[{}^1D]$ is the interacting kinetic energy functional, $V[\rho]$ is the sum of the external and Hartree potentials, $F_{\mathrm{xc}}[\rho]$ is the exchange-correlation functional, and $C[{}^1D]$ is the correction functional. An approximate form for $C[{}^1D]$ we derived to be [147]

$$C[{}^1D] = -w\mathrm{Tr}({}^1D - {}^1D^2) \tag{6.18}$$

in which w was an unknown parameter whose value, we showed, depends on the molecular system. Comparing Eq. 6.13 and 6.14, however, we find that $w = \gamma$ or that w depends on a subset of the electron repulsion integrals. We introduce a damping factor $k \in [0, 1]$ such that $w = k\gamma$ to account for the fact that the density functional already includes some of the static correlation. Importantly, k, we observe, is largely independent of the molecular system because the system-dependent behavior is captured by the trace of the two-body interaction matrix, and hence, for a given approximate density functional a single value for the damping parameter can be used across molecules. While the damping parameter does vary with the choice of the density functional, its optimal magnitude increases linearly with the amount of Hartree-Fock exchange. Consequently, we find that a greater correction for electron correlation is required for DFT functionals with a greater degree of Hartree-Fock exchange. Using the correction with DFT rather than Hartree-Fock theory has the important advantage that DFT already has a good approximation to the dynamic correlation.

The cumulant-based correction can also be viewed as a correction to the convexity of the energy functional [200]. The Hartree-Fock energy is a concave functional of the 1-RDM [201, 53]. This concave property causes the solutions of Hartree-Fock theory to occur at extreme points along the boundary of the convex set of 1-RDMs that correspond to Slater determinant wave functions [53]. The correct 1-RDM energy functional is convex, which causes its solutions, when correlated, to lie inside the convex set of 1-RDMs [60]. Incorporation of the cumulant-based energy correction, which is a convex functional of the 1-RDM, increases the convexity of both the Hartree-Fock and DFT-based energy functionals. This enhancement of convexity generates a movement, described by Schilling and Schilling as a force [38], arising from correlation that drives the 1-RDM into the convex set and away from its boundary.

6.3 Results

We apply the 1-RDMFT to treat the barrier to rotation in ethylene [193], the relative energies of the three geometric isomers of benzyne [194], as well as a benchmark based on the atomization energies of 11 molecules [195]. We use the formula $w = k\gamma$ with γ in Eq. 6.14 and $k = 0.158$ for correcting both SCAN-DFT [91] and PBE-DFT [86], which we denote as SCAN-RDMFT and PBE-RDMFT, respectively. All w values calculated and used are given in 6.1. Previous work showed empirically that the ratio of the optimal weight for correcting the Hartree-Fock method to the optimal weight for correcting the SCAN-DFT functional is a constant [165], which determines the value of k. The fact that k is significantly less than unity indicates that the SCAN and PBE functionals already account for a significant percentage of $^2\Delta_0$; nonetheless, as shown below, the missing part is critical to both generating the fractional occupations and correcting the energy errors. Because the degree to which a functional accounts for this term should be independent of the molecule, we can understand why a single value of k for a given functional is likely to be accurate across a wide range of molecules. All calculations use the correlation-consistent polarized valence double zeta (cc-pVDZ) basis set [94]. We solve the 1-RDMFT by an $\mathcal{O}(N^3)$ self-consistent-field method, detailed in Refs. [165, 147], that solves a semidefinite program by the boundary-point algorithm developed in Ref. [62] for variational 2-RDM theory [43, 76, 74, 13, 72, 71, 62, 70, 186, 187, 188, 189]. In general, the 1-RDMFT can be readily implemented on top of existing self-consistent-field implementations of DFT. While DFT can, in principle, employ only the occupied molecular orbitals, the 1-RDMFT can also exploit just the nonnegligible fractionally occupied orbitals, which will be a small fraction of the total number of orbitals. Calculations with the complete-active-space self-consistent-field method (CASSCF) [121] and the anti-Hermitian contracted Schrödinger equation (ACSE) [123, 180] are performed with the Quantum Chemistry Package in Maple [126], and calculations with coupled cluster with single, double, and perturbative triple excitations [CCSD(T)] [202] and multiconfiguration pair density func-

	w values
B_2	0.051
C_2	0.064
CN	0.071
CO_2	0.066
F_2	0.092
NF_3	0.064
NO	0.082
S_2	0.069
SiO	0.068
CO	0.076
N_2	0.077
C_2H_4	0.052
Obenzyne	0.040
Mbenzyne	0.040
Pbenzyne	0.040

Table 6.1: The w values used throughout this work calculated using eq. 6.14 and $w = k\gamma$ where k is 0.158.

tional theory (MC-PDFT) [12] are performed with PySCF [128].

First, we calculate the potential energy surface for the C-C bond rotation in C_2H_4, which corresponds to a transition from a double bond well captured by a single reference approach at a 0^o dihedral angle to a strongly correlated biradical at a 90^o dihedral angle. The results, plotted in Fig. 6.1, reveal a general overestimation of the barrier height in single-reference methods, with errors of 26.21, 31.50, and 6.70 kcal/mol for PBE-DFT, SCANDFT, CCSD(T), respectively, as compared to a CASSCF (12,12)/ACSE reference [here we use the $(N, r/2)$ convention where N is the number of electrons and $r/2$ is the number of spatial orbitals in the active space]. 1-RDMFT yields significant improvements with errors of -6.51, and 0.33 kcal/mol for PBE-RDMFT and SCAN-RDMFT, respectively. These results compare favorably to tPBE MC-PDFT, which yields an error of 5.72 kcal/mol. (The "t" in the acronym tPBE denotes the translation of the conventional PBE exchange-correlation functional in DFT to an on-top functional for use in MC-PDFT [12].) The DFT and 1-RDMFT potential energy surfaces reveal identical relative energies along the HCCH dihedral angle

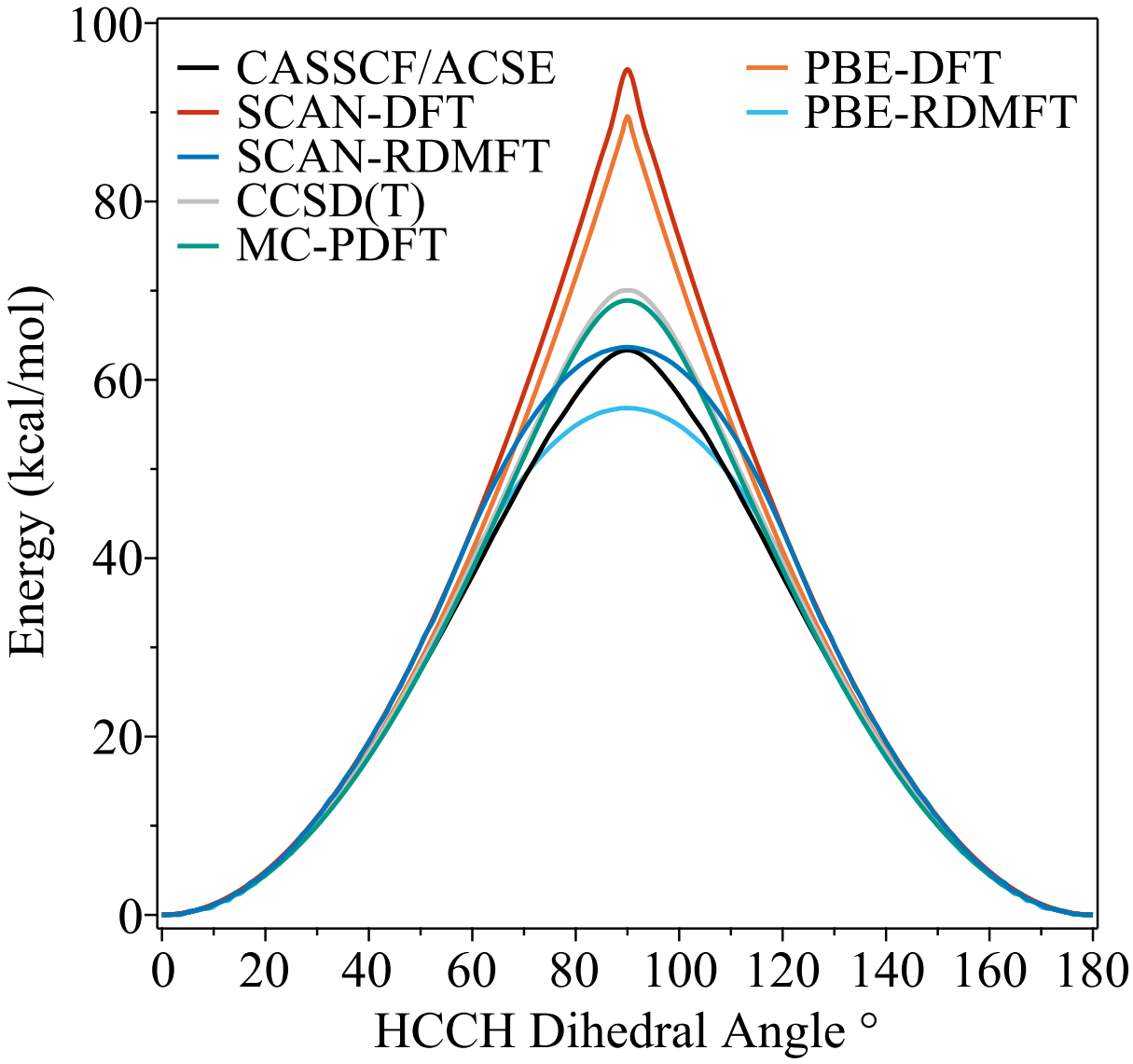

Figure 6.1: C_2H_4 rotational barrier potential energy surfaces obtained from CASSCF(12,12)/ ACSE, CCSD(T), PBE-RDMFT, SCAN-RDMFT, PBE-DFT, SCAN-DFT, and CASSCF(12,12)/ tPBE calculations with the cc-pVDZ basis set.

until the 1-RDMFTs yield fractionally occupied orbitals, starting at the 54^o and 57^o dihedral angles, for PBE and SCAN, respectively, owing to increasingly strong static correlation. A plot of the orbital occupations along the dihedral angle is available in Fig. A.6 of the appendix. Both PBE-RDMFT and SCAN-RDMFT are able to remove correctly the energetic discontinuity observed in DFT at the 90^o dihedral angle caused by the degeneracy of the highest occupied molecular orbital (HOMO) and lowest unoccupied molecular orbital (LUMO), resulting in a smooth potential energy surface. CCSD(T) and tPBE MC-PDFT, however, increasingly deviate from the reference CASSCF(12,12)/ACSE curve with a maximal error at the 90^o dihedral angle, where they both fail to fully resolve the multireference character, resulting in the overestimation of the barrier height compared to the ACSE and the 1-RDMFTs.

Next, we apply PBE-RDMFT and SCAN-RDMFT to a subset of the multireference main group non-metal bond energy molecular test set (MR-MGN-BE17) [195], previously developed as a set of systems for testing the accuracy of density functionals on bond dissociations. Equilibrium geometries and reference dissociation energies are obtained by scanning over the molecules' limited degrees of freedom using the ACSE seeded with a valence CASSCF calculation. The results, displayed in Table 6.2, yield mean unsigned errors (MUEs) of 29.50 and 36.91 kcal/mol for PBE-RDMFT and SCAN-RDMFT, respectively, compared to the reference CASSCF/ACSE energies. Here, CASSCF calculations utilize active spaces encompassing all valence electrons and orbitals. These results present significant improvements over traditional PBE-DFT and SCAN-DFT's MUEs of 114.46 and 127.85 kcal/mol with an approximate fourfold reduction in error. This is the result of 1-RDMFT fractionally occupying the valence orbitals as the molecules dissociate which corrects DFT's overestimation of the dissociated limit. The 1-RDMFT MUEs also compare favorably to the explicitly correlated tPBE MC-PDFT calculations' MUE of 22.15 kcal/mol. Finally, consideration of the mean signed error (MSE) for PBE-RDMFT of 7.06 kcal/mol, reveals a nearly equal over and

Table 6.2: Dissociation errors in kcal/mol for a subset of the MR-MGN-BE17 test set compared to the CASSCF(valence)/ACSE energies. Dissociation data taken at 5 Å internuclear distances.

	Dissociation errors				
	DFT		RDMFT		MC-PDFT
	PBE	SCAN	PBE	SCAN	tPBE
$B_2 \rightarrow 2B$	19.53	23.01	-2.12	-0.87	10.73
C_2 -> 2C	101.47	85.63	12.12	23.38	7.80
CN -> C + N	125.34	139.02	29.47	48.28	17.69
CO_2 -> C + 2O	172.11	205.46	8.17	46.22	35.37
F_2 -> 2F	73.84	84.91	-19.13	-17.53	22.51
NF_3 -> N + 3F	184.18	205.46	71.10	96.94	68.28
NO -> N + O	142.28	156.00	36.58	57.72	22.81
S_2 -> 2S	58.21	153.34	-40.02	-27.79	17.41
SiO -> Si + O	67.55	251.27	-36.07	-15.28	8.77
CO -> C + O	94.62	359.51	-26.09	-0.47	12.27
N_2 -> 2N	219.93	213.67	43.61	71.57	20.08
MSE	114.46	127.85	7.06	25.65	22.15
MUE	114.46	127.85	29.50	36.91	22.15

underestimation of the dissociation energies, while SCAN-RDMFT's MSE of 25.65 kcal/mol shows a stronger tendency to overestimate the dissociation energies. As PBE-DFT, SCAN-DFT, and tPBE never underestimate the dissociation energy, their MSEs match their MUEs with values of 114.46, 127.85, and 22.15 kcal/mol, respectively.

Finally, in Fig. 6.2 we investigate the relative energy differences between the three geometric isomers of benzyne with ground-state geometries obtained from Ref. [194], which become increasingly strongly correlated with increasing distance between the radical centers (ortho-benzyne < meta-benzyne < para-benzyne) [203]. As both meta- and ortho-benzyne have weak static correlation effects, the 1-RDMFTs are expected to remain idempotent, recovering traditional DFT's energies. This is, indeed, observed, with SCAN-RDMFT and SCAN-DFT both producing energy differences of 9.34 kcal/mol between the two isomers while PBE-RDMFT and PBE-DFT yield 8.4 kcal/mol. These results are both within 1.1 kcal/mol of CASSCF (4,4)/tPBE's predicted energy difference of 9.5 kcal/mol. CCSD(T) deviates more significantly from the previous results, yielding the largest energy difference

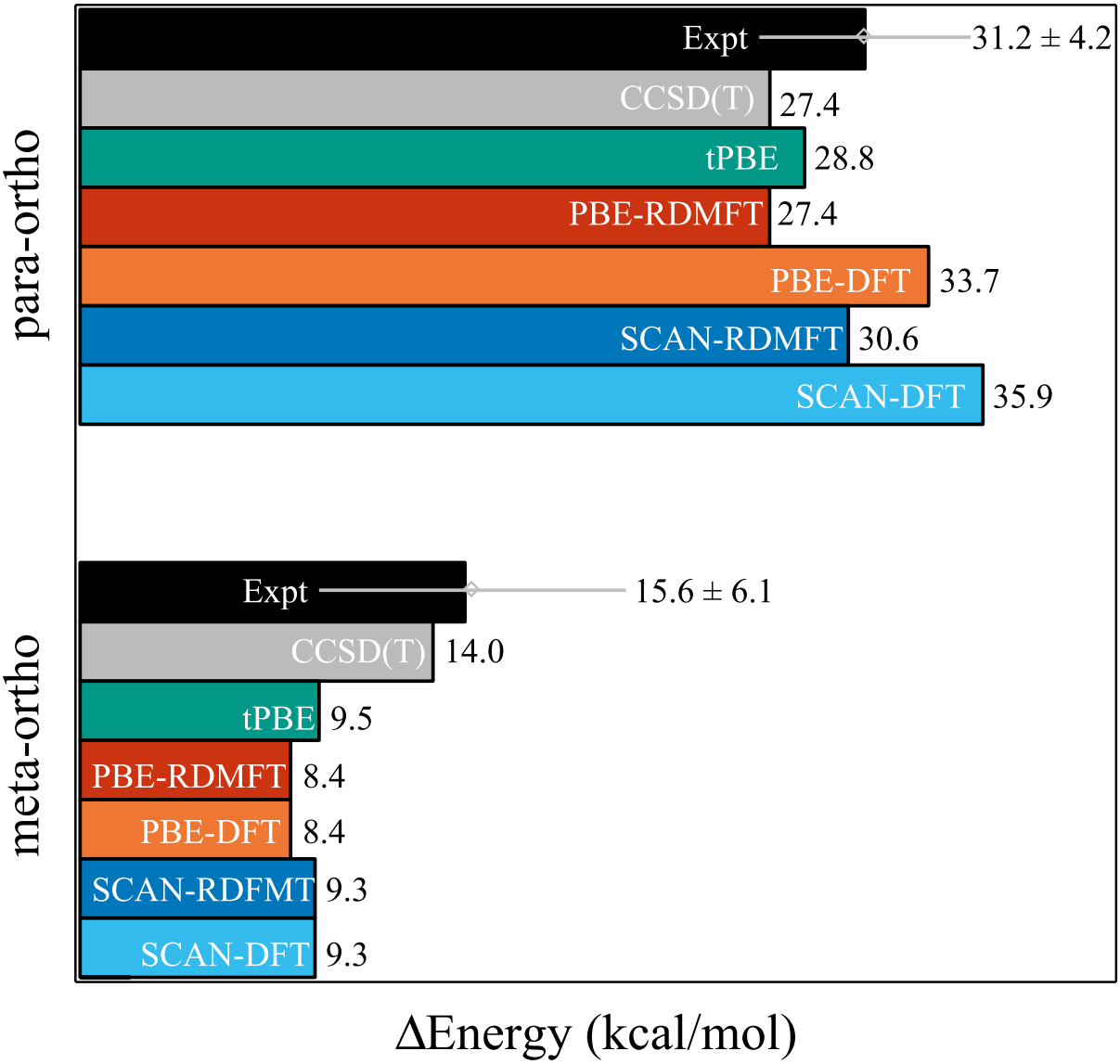

Figure 6.2: Relative energies of meta- and para-benzyne with respect to ortho-benzyne from RDMFT and DFT with the SCAN and PBE functionals, MC-PDFT using the tPBE functional, and CCSD(T).

at 14.03 kcal/mol, which is in good agreement with the experimentally predicted energy gap of 15.6 kcal/mol. Calculation of the more strongly correlated para-isomer yields deviations between 1-RDMFT and DFT, resulting in decreases in the para-ortho energy differences obtained from SCAN-DFT and PBE-DFT of 35.89 and 33.73 kcal/mol, respectively, to 30.62 and 27.4 kcal/mol from SCAN-RDMFT and PBE-RDMFT. These 1-RDMFT values are within the experimental error range and give significantly better agreement with CCSD(T) and tPBE's energy differences of 27.42 and 28.80 kcal/mol, respectively, compared to DFT.

6.4 conclusions

We present a universal 1-RDMFT functional for the treatment of strongly correlated systems, based on a transformation of traditional DFT. While the development of density-, 1-RDM-, and 2-RDM-based theories often occur separately, here we combine aspects of DFT and 2-RDM theory to develop a 1-RDMFT that retains DFT's $\mathcal{O}(N^3)$ efficiency while realizing the ability to capture static correlation. Importantly, by using the unitary invariants of the cumulant 2-RDM, we derive a general formula for the magnitude of the correction—the w parameter—in terms of the diagonal part of two-electron interaction matrix, which overcomes a limitation of earlier work, arising from the need to define a system specific w value [165, 147]. The derived formula for w can also be used to systematize related approaches, such as information density-matrix functional theory (iDMFT) [139] and thermally assisted-occupation DFT (TAO-DFT) [33, 166], which rely on unknown fictitious temperatures in Fermi-Dirac distributions. We can potentially improve the functional further by approximating the remaining terms of the unitary decomposition, which we will investigate in future work. We demonstrate the applicability of 1-RDMFT by investigating a set of small molecular dissociations in the MR-MGN-BE17 test set, as well as the rotational barrier height of ethylene and the relative energy differences of the benzyne isomers. Because of the 1-RDM correction in the energy functional, 1-RDMFT yields significant improvements over DFT in

the presence of strong correlation while recovering the DFT energy in the single-reference limit. The 1-RDMFT opens new possibilities for the treatment of static correlation in the accurate prediction of molecular structures and processes.

CHAPTER 7

ENHANCING DENSITY FUNCTIONAL THEORY FOR STATIC CORRELATION IN LARGE MOLECULES

Printed with permission from D.P. Gibney, J.-N. Boyn, and D.A. Mazziotti

7.1 Introduction

Despite its ability to treat the electron correlation of many molecular systems with mean-field computational cost, density functional theory (DFT) [155, 156, 157, 6] has limitations in its treatment of charges [158, 159], barrier heights [161], and bi- and multiradicals [23]. These limitations arise from the inability of the approximate functionals employed within DFT to provide a full description of static, or multireference, electron correlation. Static correlation occurs in molecular systems with energetically degenerate, or nearly degenerate, orbitals that lead to two or more Slater determinants contributing substantially to the wave function [65]. Recently, we combined DFT [155, 156, 157, 6] and its extensions [162, 33, 12, 108, 36, 118, 163, 164, 145, 165, 166] with 1-electron and 2-electron reduced density matrix (1-RDM [14, 15, 17, 167, 44, 112, 168, 169, 42, 40, 38, 37, 49, 111, 139, 147, 170, 171] and 2-RDM [172, 204, 173, 174, 175, 176, 177, 178, 123, 179, 180, 181, 182, 183, 184, 185, 43, 76, 74, 13, 72, 71, 62, 70, 186, 187, 188, 189]) theories to obtain a universal $O(N^3)$ generalization of DFT for static correlation [205]. This generalization transforms DFT into a 1-RDM functional theory (1-RDMFT) whose convexity allows the orbital occupations to become fractional.

In this Letter, we enhance the generalization of DFT for an improved treatment of static correlation in large molecules. The generalized DFT, or 1-RDMFT, that we previously derived [205], involves the trace of the two-electron identity matrix and the trace of the cumulant part of the 2-RDM [175, 176, 177, 178, 190, 191]. The former, however, scales

quadratically with system size r while the latter scales linearly with r. This scaling mismatch causes the correction to the DFT energy to become less effective for larger molecules. Here we renormalize the trace of the identity matrix by reweighting the two-electron space with the electron repulsion term $1/r_{12}$, reducing its scaling from quadratic to linear. The reweighting is performed with Cauchy-Schwarz inequalities [206] that relate the magnitudes of the diagonal and off-diagonal elements of the two-electron repulsion matrix. To demonstrate the effectiveness of this approach, we apply the corrected functional theory to linear hydrogen chains [207] as well as the prediction of the singlet-triplet gap and equilibrium geometries of acene chains [208, 209, 210]. The renormalization results in a 1-RDMFT, solvable by semidefinite programming [62], that accurately treats static correlation for a broad range of molecules and materials at the same $O(N^3)$ computational scaling as DFT.

7.2 Theory

Following a brief review of the correction in the generalized DFT, we derive the renormalization of the correction for large molecules. The energy of an N-electron atom or molecule in a finite basis of r spin orbitals can be written as a functional of the 1-RDM and the cumulant (or connected) part of the 2-RDM [112]

$$E_{\mathrm{RDMFT}}[{}^1D,{}^2\Delta] = E[{}^1D] + E^{\Delta}[{}^2\Delta] \tag{7.1}$$

in which

$$E[{}^1D] = \mathrm{Tr}({}^1H\,{}^1D) + \mathrm{Tr}({}^2V\,({}^1D \wedge {}^1D)) \tag{7.2}$$

$$E^{\Delta}[{}^2\Delta] = \mathrm{Tr}({}^2V\,{}^2\Delta) \tag{7.3}$$

and

$$^2\Delta = {}^2D - {}^1D \wedge {}^1D \tag{7.4}$$

where ^1H is the matrix representation of the one-electron kinetic energy and nuclear-electron Coulomb terms, ^2V is the matrix representation of the two-electron repulsion term, ^1D and ^2D are the 1- and 2-RDMs, normalized to N and $N(N-1)/2$, respectively, $\wedge$ denotes the antisymmetric (or Grassmann) tensor product [175] and $^2\Delta$ is the cumulant part of the 2-RDM [175, 176, 177, 178].

The cumulant 2-RDM can be decomposed into three orthogonal subspaces based on the unitary group [190], known as the unitary decomposition [191]

$$^2\Delta = {}^2\Delta_0 + {}^2\Delta_1 + {}^2\Delta_2. \tag{7.5}$$

By approximating the cumulant part of the energy in terms of just the zeroth component of the unitary decomposition, we have

$$E^{\Delta}[^2\Delta] \approx \mathrm{Tr}(^2V\, {}^2\Delta_0). \tag{7.6}$$

Further substituting the explicit unitary decomposition [190] in which ^2I is the two-electron identity matrix

$$^2\Delta_0 = \frac{1}{\mathrm{Tr}(^2I)}\mathrm{Tr}(^2\Delta)\, {}^2I, \tag{7.7}$$

yields

$$E^{\Delta}[^2\Delta] \approx \frac{1}{\mathrm{Tr}(^2I)}\mathrm{Tr}(^2V)\mathrm{Tr}(^2\Delta). \tag{7.8}$$

Finally, the trace of the cumulant 2-RDM can be expressed in terms of the 1-RDM's idempotency [196, 197, 198, 199] and the trace of ^2V can be expressed in terms of the two-electron

repulsion integrals in physicist's notation to obtain

$$E^{\Delta}[^2\Delta] \approx -\gamma \mathrm{Tr}(^1D - {}^1D^2) \tag{7.9}$$

where

$$\gamma = \frac{1}{\mathrm{Tr}(^2I)} \sum_{\tilde{i},\tilde{j}} \left(2\langle \tilde{i}\tilde{j}||\tilde{i}\tilde{j}\rangle - \langle \tilde{i}\tilde{j}||\tilde{j}\tilde{i}\rangle\right) \tag{7.10}$$

in which the tilde denotes the index of the spatial part of the spin orbital. Equation (7.9), derived in Ref. [205], provides a 1-RDM approximation for the cumulant energy that in combination with the effective one-electron energy $E[^1D]$ in Eq. (7.1) yields a 1-RDM functional theory that corrects the Hartree-Fock energy for static correlation.

As shown in previous work [205], we can apply this correction to transform DFT rather than Hartree-Fock into a 1-RDMFT. To treat DFT with Eq. 7.1, we first modify the one-body energy in Eq. (7.2) to include the exchange-correlation functional $F_{\mathrm{xc}}[\rho]$

$$E[^1D] = T[^1D] + V[\rho] + F_{\mathrm{xc}}[\rho] \tag{7.11}$$

where ρ is the one-electron density, $T[^1D]$ is the interacting kinetic energy functional, and $V[\rho]$ is the external potential including the electron-nuclei Coulomb potential and the Hartree-Fock Coulomb potential. Second, because an approximate exchange-correlation functional already includes some static correlation, we define the cumulant energy in Eq. (7.9) with the same functional form but a different weight parameter w

$$E^{\Delta}[^2\Delta] \approx -w\mathrm{Tr}(^1D - {}^1D^2) \tag{7.12}$$

where $w = \kappa\gamma$ in which γ is defined as before in Eq. (7.10) and κ is a damping factor such as $\kappa \in [0, 1]$. When $\kappa = 1$, the cumulant energy in Eq. (7.12) is identical to the cumulant energy in Eq. (7.9), but when $\kappa < 1$, the cumulant energy in Eq. (7.12) provides a

smaller correction than that in Eq. (7.9), reflecting that an approximate exchange-correlation functional contains some static correlation. Importantly, as observed previously in Ref. [205], the κ is largely independent of the molecular system because the system-dependent behavior is captured by γ, and thus, for a given approximate density functional a single value for κ can be used across molecules. We find that the optimal κ for a given functional increases linearly with the amount of Hartree-Fock exchange in the functional. The advantage of using the cumulant energy as a correction to DFT rather than Hartree-Fock theory is that DFT captures the dynamic correlation.

For large molecules, however, the cumulant energy in Eq. (7.9) generally does not recover enough of the static correlation. The problem arises because the trace of the two-electron identity matrix in γ,

$$\mathrm{Tr}({}^2I) = \frac{r(r-1)}{2}, \tag{7.13}$$

scales quadratically, rather than linearly, in r. Each of the diagonal elements of the identity matrix ${}^2I_{ij}^{ij}$ is equal to one even if the spin orbitals i and j correspond to spatial orbitals that are significantly separated in space. In taking the trace of the identity matrix, we need to reweight the two-electron space to account for the locality of the electron repulsion matrix due to the locality of the Coulomb repulsion.

To perform the reweighting, we consider the electron repulsion matrix in a local orbital basis, such as the atomic orbitals, with the indices arranged in chemist's notation, denoted by ${}^2\tilde{V}$

$${}^2\tilde{V}_{\tilde{j}\tilde{j}}^{\tilde{i}\tilde{i}} = \int \frac{|\chi_{\tilde{i}}(1)|^2 |\chi_{\tilde{j}}(2)|^2}{r_{12}} d1d2. \tag{7.14}$$

Because this matrix ${}^2\tilde{V}$ is positive semidefinite, that is ${}^2\tilde{V} \succeq 0$, its diagonal and off-diagonal elements must obey the Cauchy-Schwarz inequalities [206]

$$\left|{}^2\tilde{V}_{\tilde{j}\tilde{j}}^{\tilde{i}\tilde{i}}\right|^2 \leq {}^2\tilde{V}_{\tilde{i}\tilde{i}}^{\tilde{i}\tilde{i}} \, {}^2\tilde{V}_{\tilde{j}\tilde{j}}^{\tilde{j}\tilde{j}}. \tag{7.15}$$

Dividing the left-hand side by the right-hand side of the inequalities and taking the square root, we obtain weights $\tilde{W}_{\tilde{i}\tilde{j}}$ of the two-electron space

$$\tilde{W}_{\tilde{i}\tilde{j}} = \frac{{}^2\tilde{V}^{\tilde{i}\tilde{i}}_{\tilde{j}\tilde{j}}}{\sqrt{{}^2\tilde{V}^{\tilde{i}\tilde{i}}_{\tilde{i}\tilde{i}}\,{}^2\tilde{V}^{\tilde{j}\tilde{j}}_{\tilde{j}\tilde{j}}}} = \frac{\langle\tilde{i}\tilde{j}||\tilde{i}\tilde{j}\rangle}{\sqrt{\langle\tilde{i}\tilde{i}||\tilde{i}\tilde{i}\rangle\langle\tilde{j}\tilde{j}||\tilde{j}\tilde{j}\rangle}} \tag{7.16}$$

which lie between 0 and 1

$$0 \leq \tilde{W}_{\tilde{i}\tilde{j}} \leq 1. \tag{7.17}$$

When $\tilde{i} = \tilde{j}$, the weights equal one ($\tilde{W}_{\tilde{i}\tilde{i}} = 1$), but when the local spatial orbitals, $\tilde{i}$ and $\tilde{j}$, are far from each other, the weights are much less than one ($\tilde{W}_{\tilde{i}\tilde{j}} \ll 1$). The nonzero elements of the weight matrix in the local spin orbital basis set ${}^2W$ can be defined as

$${}^2W^{ij}_{ij} = \tilde{W}_{\tilde{i}\tilde{j}} \tag{7.18}$$

with $\tilde{i}$ denoting the spatial orbital associated with the spin orbital of i. Using these weights on the diagonal elements of the two-electron identity matrix renormalizes its trace to yield

$$\mathrm{Tr}({}^2W\,{}^2I) = 4\sum_{\tilde{i}<\tilde{j}} \tilde{W}_{\tilde{i}\tilde{j}} + \sum_{\tilde{i}} \tilde{W}_{\tilde{i}\tilde{i}}. \tag{7.19}$$

Asymptotically, the trace of the renormalized two-electron identity matrix scales linearly with system size, and therefore, substituting this identity matrix for the conventional identity matrix in Eq. (7.10) yields an approximation for the cumulant energy in Eq. (7.9) that scales linearly with system size. We denote the modified right-hand side of Eq. (7.10) as $\tilde{\gamma}$ which is related to the original γ by a ratio of the traces of the two identity matrices

$$\tilde{\gamma} = \frac{\mathrm{Tr}({}^2I)}{\mathrm{Tr}({}^2W\,{}^2I)}\gamma. \tag{7.20}$$

Similarly, we define the renormalized weight $\tilde{w}$ as $\tilde{w} = \tilde{\kappa}\tilde{\gamma}$ in which $\tilde{\kappa}$ is a modified damping parameter. Using these modified parameters, we can obtain accurate corrections for static correlation with either Hartree-Fock theory or DFT for both large and small molecules.

7.3 Results

We apply the 1-RDMFT (or RDMFT) with both the original w and renormalized $\tilde{w}$ weights to the stretching of linear hydrogen chains and the singlet-triplet gap as well as the carbon-carbon bond lengths of acene chains ranging in length from 5 to 12 units. We use $w = \kappa\gamma$ and $\tilde{w} = \tilde{\kappa}\tilde{\gamma}$ with γ and $\tilde{\gamma}$ being obtained from Eq. (7.10) and Eq. (7.20), respectively. All RDMFT calculations are performed with the correlation-consistent polarized valence double-zeta (cc-pVDZ) basis set [94] and the SCAN functional [91] with $\kappa = 0.158$, as employed in our previous work [205], and $\tilde{\kappa} = 0.112$. Analytical gradients [211] are implemented for geometry optimizations. The RDMFT calculations are solved using a self-consistent-field (SCF) procedure at $\mathcal{O}(N^3)$ scaling, described in Refs. [118, 165], in which the solution of the semidefinite program is computed at each SCF iteration with the splitting conic solver (SCS) [212, 213] in the CVXPY Python program [214]. The DFT calculations are performed in the Quantum Chemistry Package in Maple [215, 126] and PySCF [128] while the RDMFT calculations are performed with a customized Python program that works with the Quantum Chemistry Package in Maple [215, 126] and PySCF [128].

The energy per hydrogen atom as a function of the distance R between equally spaced hydrogen atoms is presented for linear H_{10} and H_{50} in Fig. 7.1, using DFT, w RDMFT, and $\tilde{w}$ RDMFT all with the SCAN functional. For H_{10}, while both w and $\tilde{w}$ RDMFTs improve upon the energy per hydrogen atom relative to DFT for $R > 2$ Å, only $\tilde{w}$ RDMFT exhibits the correct asymptotic behavior of a nearly flat potential energy curve for $R > 3$ Å. Moreover, for the larger H_{50}, because w is incorrectly decaying with system size, w RDMFT shows minimal improvement over DFT, but $\tilde{w}$ RDMFT produces a curve that agrees with

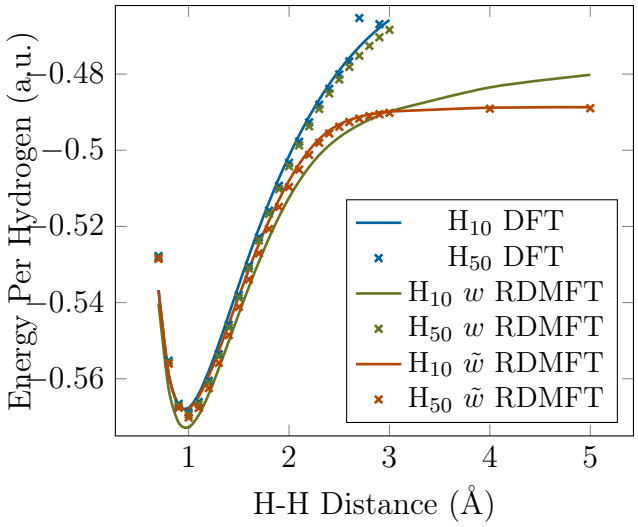

Figure 7.1: Energy per hydrogen atom as a function of the distance R between equally spaced hydrogen atoms is shown for linear H_{10} and H_{50}, using DFT, w RDMFT, and $\tilde{w}$ RDMFT all with the SCAN functional.

the one from H_{10}, exhibiting the expected convergence in the energy per hydrogen atom with respect to chain length in the dissociation limit.

Next, we consider the singlet-triplet gap—the energy difference between the lowest lying singlet and triplet states— for the n-acenes pentacene ($n = 5$) through dodecacene ($n = 12$), displayed in Figure 7.2. The n-acenes have been shown to develop bi- and multi-radical character with increasing chain length [208, 209, 210, 216]. Due to the conjugated π system increasing with the number of carbon atoms, acenes longer than tetracene are beyond the capabilities of traditional configuration-interaction-based based methodologies such as the complete-active-space self-consistent-field (CASSCF) wave function method. Therefore, we compare our results to those from the CASSCF variational 2-RDM (V2RDM) method [209, 70, 188], which replaces the calculation of the active-space wave function by configuration interaction by the calculation of the active-space 2-RDM by the V2RDM method with 2-positivity conditions [43, 76, 74, 13, 72, 71, 62, 70, 186, 187, 188, 189]. The CASSCF V2RDM method—denoted in the following as just V2RDM—can treat the (50,50) active space required for dodecacene. Relative to the results from V2RDM [217], DFT underpre-

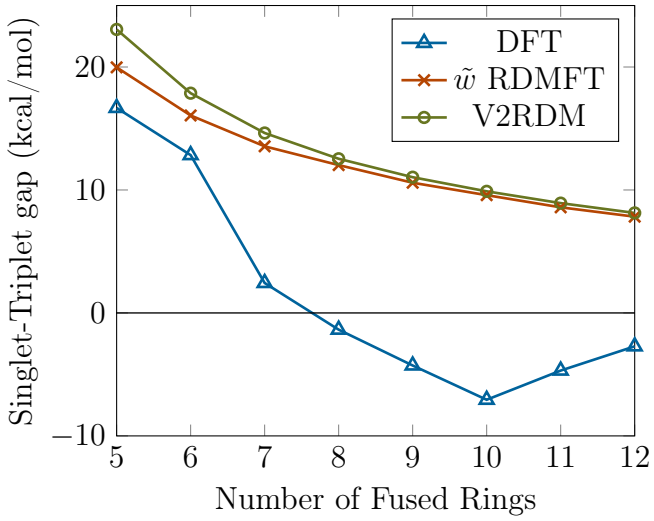

Figure 7.2: Adiabatic singlet-triplet gap—the energy difference between the lowest lying singlet and triplet states—for the n-acenes pentacene ($n = 5$) through dodecacene ($n = 12$), using $\tilde{w}$ RDMFT with comparisons to DFT and V2RDM. Both $\tilde{w}$ RDMFT and DFT use the SCAN functional.

dicts the gap for longer acenes with the triplet state becoming incorrectly lower in energy than the singlet state. In contrast, the $\tilde{w}$ 1-RDMFT closely matches the gap predicted by the V2RDM theory. Extrapolating to infinite chain length n using the function $a \exp(-n/b) + c$, we obtain singlet-triplet gaps of 7.23 and 7.77 kcal/mol from V2RDM theory and $\tilde{w}$ 1-RDMFT, respectively.

Finally, we compute the equilibrium geometry of dodecacene in its ground singlet state with $\tilde{w}$ RDMFT using analytical gradients. In Fig. 7.3 the edge carbon-carbon bond lengths are displayed in red with comparisons to those from DFT and V2RDM, shown in blue and green, respectively. The V2RDM method predicts edge carbon-carbon bond lengths that are fairly uniform in the interior of the acene; in contrast, DFT predicts an alternating bonding pattern with significant variations in the bond lengths. The $\tilde{w}$ RDMFT results, which exhibit fractional occupations, agree with those obtained from V2RDM in predicting equal bond lengths in the interior of the acene. All edge C-C bond lengths from napthalene to dodecance for both the singlet and triplet states are available in the appendix as Figs A.7 and A.8.

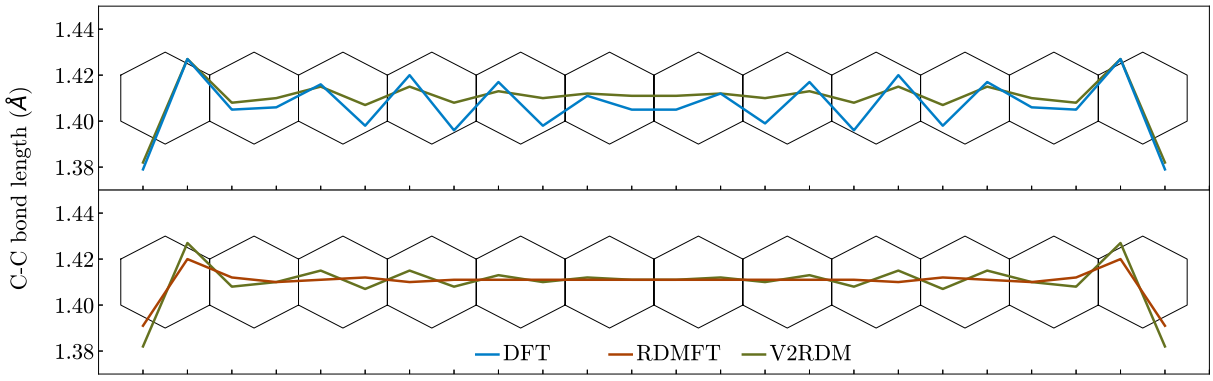

Figure 7.3: Edge carbon-carbon bond lengths from $\tilde{w}$ RDMFT are shown in red with comparisons to those from DFT and V2RDM in blue and green, respectively.

7.4 Conclusions

DFT provides an $O(N^3)$ electronic structure method that describes the electron correlation in many important molecules and materials, and yet it struggles to treat a specific type of correlation, known as static correlation, leading to errors in predicting charges, multi-radicals, and reaction barriers. Here we enhance a recent generalization of DFT for static correlation to improve its treatment of this correlation for large molecules. We renormalize a 1-RDM-based energy correction to DFT by using Cauchy-Schwarz inequalities of the electron-electron repulsion matrix to reweight the two-electron identity matrix, making the correction effective for large molecules. The resulting 1-RDMFT, while retaining the $O(N^3)$ scaling of DFT, significantly improves upon DFT within statically correlated systems while reproducing DFT in systems lacking static, or strong, correlation. We demonstrate its scalability with system size by considering a series of hydrogen and acene chains through H_{50} and dodecacene, respectively. The theory offers new possibilities for calculating a broad range of strongly correlated molecular systems beyond the reach of multi-reference methodologies.

CHAPTER 8

FUTURE DIRECTIONS

This work still has more directions to be explored. These include, but are not limited to, incorporating the ${}^2\Delta_1$ term in the RDMFT functional, finding a way to obtain excited states, creating a unique DFT like functional specifically for RDMFT, and exploring larger strongly correlated systems.

Starting with the next term in the unitary decomposition, ${}^2\Delta_1$, its final form should resemble $\mathrm{Tr}(A[{}^1D^2 - {}^1D])$ where A will be a matrix likely based upon the Hartree-Fock J and K matrices. This will expand upon the previous form of the RDMFT correction which is expressible as $\mathrm{Tr}(w{}^1I[{}^1D^2 - {}^1D])$ to add off diagonal elements to the minimization. For smaller systems with a well-defined Homo-Lumo gap this new term,${}^2\Delta_1$, is likely to be very similar to the original, ${}^2\Delta_0$. This is due to w being the trace of A. However, as ${}^2\Delta_1$ adds an energetic component to off diagonal elements to the residual of the 1-RDM, ${}^1D^2 - {}^1D$, it may result in orbital rotations that would not previously be possible. Unfortunately, this would be the last term that could be added to the unitary decomposition in RDMFT's current implementation. If the final term, ${}^2\Delta_2$, is included, RDMFT would effectively become V2RDM theory as it would require a matrix of the same size as the 2RDM.

Another direction that deserves exploration in is how to obtain excited states using this methodology. Excited states play an important role in many chemically relevant phenomenon as their higher energies allow for processes to occur that would be inaccessible via the ground state. This would include light-induced reactions[218, 219, 220], such as photosynthesis[221, 222], singlet-triplet fission[223], and conical intersections [224, 225]. Unfortunately, while DFT has a linear response theory known as TD-DFT [226, 227] for excited states and other RDMFTs have an ensemble approach to excited states[228], the RDMFT developed here is a functional of both the electronic density and 1RDM. Therefore, neither of the two approaches individually would work.

As this is a ground state method, it would be possible to target the ground states of different irreducible representations, which would allow for a limited exploration of excited states in symmetric molecules. Unfortunately, this would only apply to symmetric modules and the number of states accessible in this manner would depend on the degree of molecular symmetry, with more symmetric molecules - and thus more irreducible representations - allowing for more excited states. Even then, this would only allow for a limited exploration into the molecule's excited states.

Throughout this work, we found that the density functionals that were least parameterized and obtained no Hartree-Fock exchange tended to perform the best when used within RDMFT. Our hypothesis for this observation is that parameterized functionals, while designed to best reproduce properties of interest, are optimized with only idempotent 1-RDMs. This idea is supported by the primary implementation of DFT within electronic structure packages being idempotent. Therefore, unparameterized functionals would best respond to improvements in the underlying 1-RDM as they are developed independent of it.

Following through with this idea, it would be worthwhile to create a functional specifically designed with non-idempotent 1-RDMs in mind. Although most systems found in large functional test suites, such as the well known Minnesota databases [195, 229] which comprises over 400 test systems, will be idempotent, including strongly correlated systems and thus non-idempotent 1-RDMs should result in different optimized parameters for the resulting functional. It would be important that the training sets include a combination of systems that contain strong correlation and those without it. Over inclusion of strongly correlated systems in the test set may hamper the function's ability to respond appropriately to idempotent 1-RDMs.

This training could also have the benefit of enabling Hartree-Fock functionals to perform at a similar level as the completely unparameterized functionals. As Hartree-Fock exchange is often included to reduce electron self-interaction errors[230, 231], which is a common

issue in current density functionals, this would be an important development. Furthermore, Hartree-Fock exchange reduces the convexity of density functionals, further improving them towards known behavior of the exact universal functional.

APPENDIX A

ADDITIONAL FIGURES AND TABLES

A.1 Variation in the individual components to the total energy between SDP and KS implementations

		Restricted					Unrestricted				
	Functional	ΔE_{kin}	ΔE_{nuc}	ΔE_{C}	ΔE_{XC}	ΔE_{tot}	ΔE_{kin}	ΔE_{nuc}	ΔE_{C}	ΔE_{XC}	ΔE_{tot}
S	VWN	-81.19	197.62	34.16	-172.20	-21.60	-13.87	39.72	19.20	-33.79	11.26
	SPW92	-81.25	197.81	34.15	-172.34	-21.62	-14.92	42.11	19.16	-35.34	11.02
	PBE	-59.30	146.63	33.17	-137.80	-17.31	-22.99	62.51	30.20	-50.97	18.75
	BLYP	-36.78	98.54	31.24	-108.45	-15.45	-24.40	68.04	29.28	-55.12	17.80
	TPSS	-28.32	73.93	32.90	-89.48	-10.97	-31.87	81.96	39.60	-64.55	25.14
	SCAN	-26.08	60.62	31.97	-71.77	-5.26	-36.47	89.32	49.82	-69.32	33.34
	MN15-L	-0.46	8.47	38.71	-42.30	4.42	-35.68	109.94	45.52	-95.32	27.88
	B97M-V	-14.91	31.64	35.44	-53.26	-1.08	-34.85	98.73	39.13	-76.24	26.77
T	VWN	-4.27	10.13	5.01	-11.08	-0.21	-0.93	0.43	3.99	-3.29	0.20
	SPW92	-5.11	12.35	5.02	-12.39	-0.12	-0.95	0.49	3.98	-3.33	0.19
	PBE	-5.99	14.66	6.54	-14.22	0.99	-2.06	2.97	5.82	-5.12	1.60
	BLYP	-4.70	12.89	6.34	-13.53	1.00	-2.11	3.39	5.62	-5.47	1.42
	TPSS	-4.28	11.58	7.75	-12.37	2.69	-3.83	7.36	7.93	-8.36	3.10
	SCAN	-3.73	6.23	8.59	-7.04	4.05	-4.21	7.00	9.74	-7.89	4.65
	MN15-L	-5.22	15.79	10.19	-15.87	4.89	-6.91	20.27	11.26	-19.42	5.20
	B97M-V	-6.31	18.81	9.36	-17.87	3.99	-5.03	12.91	9.01	-12.70	4.18

Table A.1: Mean energy differences of the individual components of the total electronic energy between the SDP and KS solutions of singlet and triplet states in both spin restricted and unrestricted frameworks.

A.2 Idempotency

Calculations were performed to investigate the effect of idempotency breaking in the density matrix on the individual components of the total energy. The non-idempotent frontier orbital occupation numbers are shown in Table A.3. The total energies and their individual components were evaluated for the singlet states using the SDP-KS algorithm. The obtained 1-RDM was then projected back onto one of its degenerate idempotent solutions and the energies and their components were reevaluated. Table A.2 shows the differences between

the idempotent and non-idempotent solutions with $\Delta E = E_{non-idempotent} - E_{idempotent}$. Generally E_{kin} and E_{nuc} remain unchanged across all systems and functionals, demonstrating the absence of double counting in the kinetic energy functional. We observe decreases in E_{tot} across all systems in most functionals, as including multi-reference correlation lowers the energy of the system and we converge to a lower solution. However, in the modern meta-GGA functionals some non-physical E_{tot} increases are observed, pointing towards flaws in their construction. The changes in E_{tot} arise from a universal gain in E_C, which does not vary significantly between functionals, and the degree to which this is counteracted by an increase in E_{XC}. While simple LDA functionals like VWN and SPW92, show the smallest magnitude in ΔE_{XC} this increases as we go to GGA functionals like PBE, BLYP and finally becomes large enough to negate the decrease in E_C in meta-GGA functionals MN15-L and B97M-V, which yield non-physical increases in E_{tot} in many systems upon the inclusion of multi-reference correlation in the electron density matrix.

		C	NF	NH	O_2	O	PF	PH	S_2	S	Si	SO
VWN	ΔE_{tot}	-16.99	-15.34	-17.14	-14.68	-30.7	-12.55	-13.15	-10.36	-22.67	-13.05	-12.03
	ΔE_{kin}	-0.0	0.0	0.0	0.0	-0.0	-0.0	-0.0	0.0	0.0	0.0	-0.0
	ΔE_{nuc}	0.0	-0.01	-0.0	-0.01	0.0	0.01	0.0	0.0	0.0	0.0	0.01
	ΔE_C	-46.29	-33.53	-39.93	-28.8	-65.61	-25.82	-27.9	-18.71	-43.59	-32.43	-22.77
	ΔE_{XC}	29.29	18.19	22.8	14.13	34.9	13.27	14.75	8.34	20.92	19.38	10.73
SPW92	ΔE_{tot}	-17.0	-15.34	-17.15	-14.69	-30.71	-12.55	-13.16	-10.37	-22.68	-13.06	-12.04
	ΔE_{kin}	-0.0	-0.0	0.0	0.0	-0.0	-0.0	-0.0	0.0	0.0	0.0	0.0
	ΔE_{nuc}	0.0	0.01	-0.0	-0.01	0.0	0.01	0.0	0.0	0.0	0.0	-0.01
	ΔE_C	-46.27	-33.53	-39.93	-28.8	-65.59	-25.82	-27.89	-18.7	-43.58	-32.42	-22.75
	ΔE_{XC}	29.27	18.18	22.78	14.12	34.88	13.26	14.73	8.33	20.9	19.36	10.72
PBE	ΔE_{tot}	-12.88	-12.49	-13.36	-12.39	-24.56	-10.95	-11.23	-9.39	-19.98	-10.76	-10.63
	ΔE_{kin}	-0.0	0.0	0.0	0.0	-0.0	-0.0	-0.0	-0.0	0.0	0.0	0.0
	ΔE_{nuc}	0.0	-0.01	-0.0	-0.01	0.0	0.01	0.0	-0.0	0.0	0.0	-0.01
	ΔE_C	-46.27	-33.56	-39.98	-28.78	-65.67	-25.97	-28.05	-18.77	-43.8	-32.57	-22.81
	ΔE_{XC}	33.39	21.08	26.62	16.39	41.11	15.02	16.82	9.39	23.82	21.8	12.18
BLYP	ΔE_{tot}	-10.13	-10.47	-11.16	-10.86	-21.51	-10.38	-10.7	-8.82	-19.07	-10.19	-9.81
	ΔE_{kin}	-0.0	-0.0	0.0	0.0	0.0	-0.0	-0.0	-0.0	0.0	-0.0	0.0
	ΔE_{nuc}	0.0	0.01	-0.0	-0.01	-0.0	0.01	0.0	-0.0	0.0	-0.0	-0.01
	ΔE_C	-46.06	-33.59	-39.77	-28.73	-65.49	-25.83	-27.79	-18.63	-43.47	-32.14	-22.68
	ΔE_{XC}	35.93	23.11	28.61	17.87	43.99	15.45	17.08	9.82	24.4	21.95	12.87
TPSS	ΔE_{tot}	-2.63	-6.45	-6.63	-7.59	-14.46	-7.94	-8.0	-7.35	-15.29	-6.24	-7.7
	ΔE_{kin}	-0.0	0.0	-0.0	0.0	0.0	0.0	0.0	0.0	-0.0	0.0	0.0
	ΔE_{nuc}	0.0	-0.01	0.0	-0.01	-0.0	-0.01	-0.0	0.0	-0.0	0.0	-0.01
	ΔE_C	-46.22	-33.65	-40.01	-28.79	-65.79	-26.19	-28.28	-18.86	-44.01	-32.83	-22.88
	ΔE_{XC}	43.58	27.21	33.37	21.2	51.33	18.25	20.28	11.51	28.73	26.58	15.19
SCAN	ΔE_{tot}	-1.82	-4.17	-1.23	-5.92	-5.38	-7.73	-6.19	-7.59	-12.93	-5.6	-7.44
	ΔE_{kin}	0.0	-0.0	-0.0	0.0	0.0	-0.0	-0.0	0.0	-0.0	0.0	-0.0
	ΔE_{nuc}	-0.0	0.01	0.0	-0.01	-0.0	0.01	0.0	0.0	-0.0	0.0	0.01
	ΔE_C	-46.36	-33.99	-40.12	-28.96	-66.06	-26.41	-28.32	-18.97	-44.14	-32.92	-23.07
	ΔE_{XC}	44.54	29.82	38.89	23.05	60.69	18.67	22.13	11.37	31.21	27.32	15.62
MN15-L	ΔE_{tot}	13.42	7.11	11.59	3.98	16.51	-2.12	-0.88	-1.78	-1.62	0.25	-0.72
	ΔE_{kin}	0.0	0.0	0.0	0.0	0.0	-0.0	-0.0	-0.0	-0.0	0.0	0.0
	ΔE_{nuc}	-0.0	-0.01	-0.0	-0.01	-0.0	0.0	-0.0	-0.0	-0.0	0.0	-0.01
	ΔE_C	-44.35	-33.31	-38.92	-28.51	-65.27	-26.14	-27.64	-18.82	-43.8	-31.45	-22.85
	ΔE_{XC}	57.77	40.42	50.52	32.5	81.78	24.01	26.75	17.04	42.18	31.7	22.13
B97M-V	ΔE_{tot}	4.13	1.65	5.77	-0.17	7.13	-5.32	-2.83	-5.43	-6.72	-2.01	-4.47
	ΔE_{kin}	-0.0	0.0	-0.0	-0.0	0.0	0.0	-0.0	0.0	-0.0	0.0	0.0
	ΔE_{nuc}	0.0	-0.01	0.0	0.01	-0.0	-0.01	0.0	0.0	-0.0	0.0	-0.01
	ΔE_C	-45.38	-33.82	-39.57	-28.73	-65.7	-26.38	-27.99	-18.86	-44.02	-32.16	-22.91
	ΔE_{XC}	49.52	35.47	45.34	28.56	72.83	21.06	25.16	13.43	37.3	30.15	18.45

Table A.2: Changes in the total energy and its individual components, defined as $\Delta E = E_{non-idempotent}$ -$E_{idempotent}$. All calculations carried out with a aug-ccpvqz basis set.

A.3 Density

In accordance with Unsöld's theorem, the SDP-DFT algorithm overcomes the symmetry breaking issues for singlet states encountered in traditional KS-DFT. For validation, the electron densities of singlet states from KS-DFT and SDP-DFT are compared to those obtained via active-space 2-electron reduced density matrix (V2RDM) calculations performed in the Maple 2020 Quantum Chemistry Package [126, 232]. Depending on the number of energetically degenerate orbitals in the atom or molecule, we use either a [2,2] or a [2,3] active space. The V2RDM calculations are spin adapted, which enforces the correct expectation values of the $\hat{S}^2$ and $\hat{S}_z$ operators [78]. The electron densities for the carbon atom are shown in Figure A.1. While the PBE functional in KS-DFT leads to a symmetry-broken electron distribution around the nucleus, this is not observed in the SDP-DFT implementation of the PBE functional, where a spherically symmetrical electron density is recovered. The SDP-DFT density agrees with that obtained from the [2,3] active-space V2RDM calculation. We furthermore performed calculations in V2RDM for each atom and molecule in our test set and calculated the distance of the SDP-DFT electron density from the V2RDM electron density, given by the Frobenius norm of the difference between SDP-DFT and V2RDM 1-RDMs. The resulting norms are given in Table A.4. The largest distance between SDP and V2RDM densities is 3.3×10^{-4} and all distances remain in range of 10^{-5} to 10^{-4}, demonstrating that SDP-DFT recovers the V2RDM CASSCF density.

	Occupation		
C	0.333333	0.333333	0.333333
NF	0.5	0.5	
NH	0.5	0.5	
O_2	0.5	0.5	
O	0.666667	0.666667	0.666667
PF	0.5	0.5	
PH	0.5	0.5	
S_2	0.5	0.5	
S	0.666667	0.666667	0.666667
Si	0.333333	0.333333	0.333333
SO	0.5	0.5	

Table A.3: Frontier orbital occupations of each species with the LDA functional. Results are functional independent.

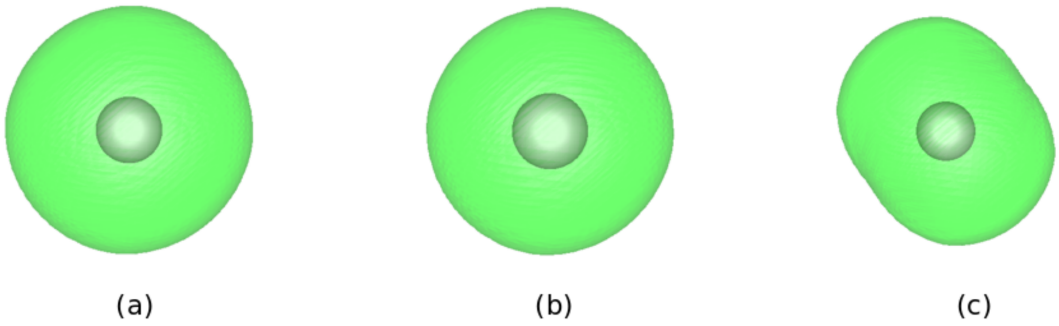

Figure A.1: Electron densities in the carbon atom for left: V2RDM, center: SDP-DFT, right: KS-DFT.

	C	NF	NH	O	O_2
B97MV	1.67E-04	6.93E-05	1.23E-04	1.57E-05	1.18E-04
BLYP	4.06E-05	7.16E-05	1.57E-04	2.47E-05	9.76E-05
VWN	1.42E-04	1.02E-04	5.29E-05	8.49E-05	1.01E-04
MN15L	4.90E-05	3.30E-04	3.94E-05	3.91E-04	2.05E-04
PBE	1.05E-04	1.11E-04	1.34E-04	3.21E-04	5.90E-04
SCAN	2.74E-04	9.60E-05	1.13E-04	4.42E-05	4.18E-04
SPW92	1.42E-04	1.02E-04	1.87E-04	1.51E-05	8.77E-05
TPSS	5.09E-05	1.21E-04	7.47E-05	2.55E-05	6.84E-05

Table A.4: Frobenius norm of the difference between the SDP-DFT and V2RDM 1-RDMs, defined as $||\Delta D^1|| = ||D^1(SDP-DFT) - D^1(V2RDM)||$.

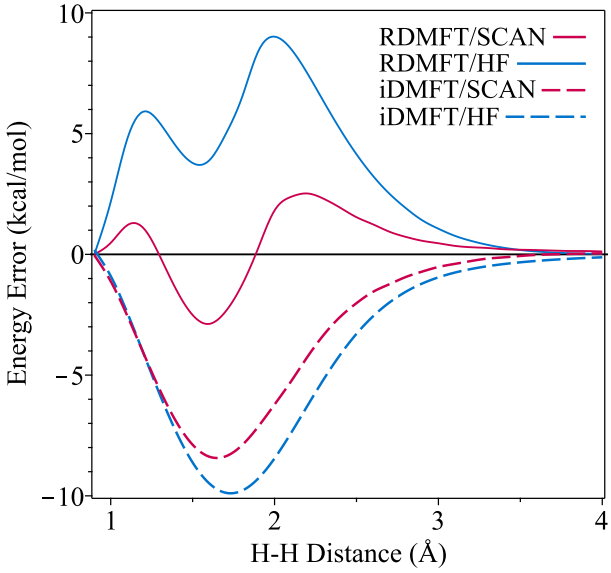

Figure A.2: Linear H_4 1RDMFT and iDMFT errors from FCI energy zeroed at 0.9 Å using the SCAN and HF functionals.

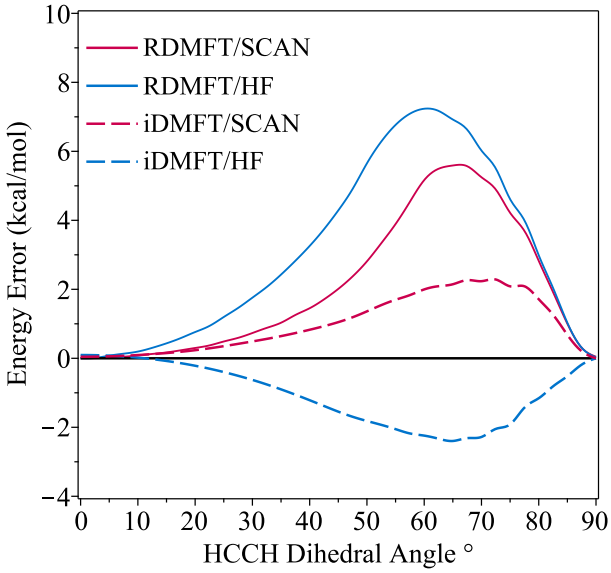

Figure A.3: Rotation of C_2H_4 1RDMFT and iDMFT errors from the ACSE energy zeroed at 0° HCCH Dihedral angle using the SCAN and HF functionals.

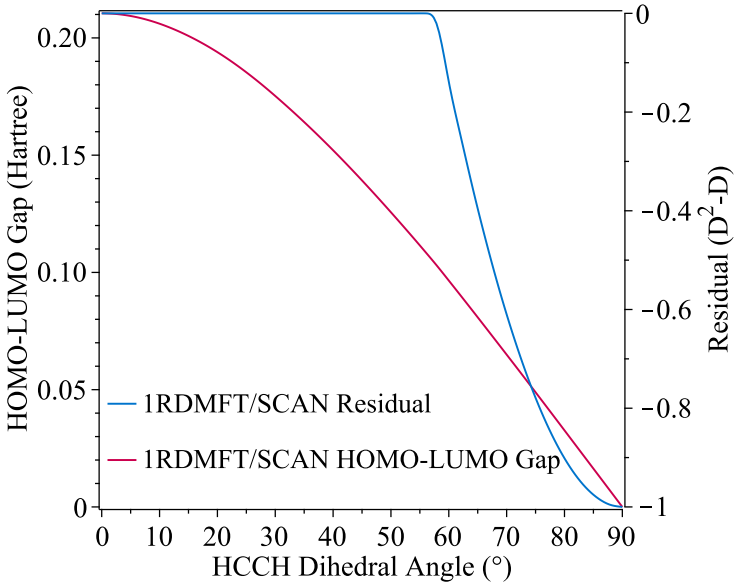

Figure A.4: The deviation from Non-Idempotency (Residual) and the HOMO-LUMO gap as a function of the rotation of C_2H_4 from 1-RDMFT/SCAN.

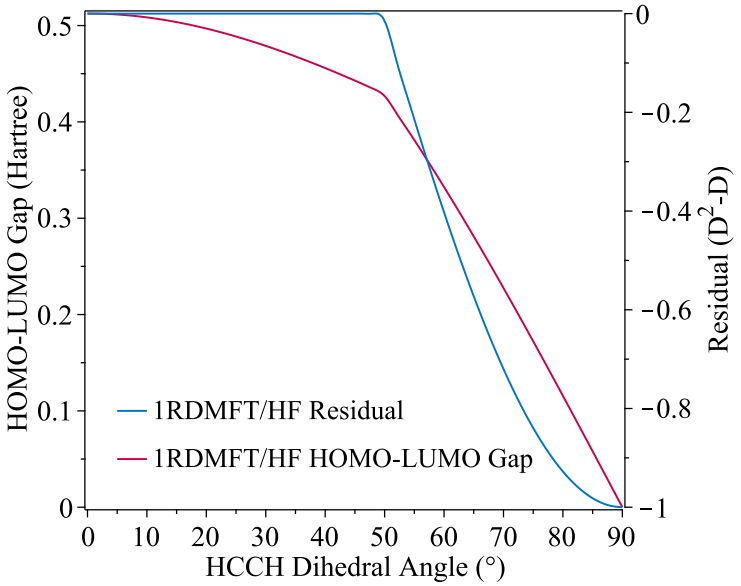

Figure A.5: The deviation from Non-Idempotency (Residual) and the HOMO-LUMO gap as a function of the rotation of C_2H_4 from 1-RDMFT/HF.

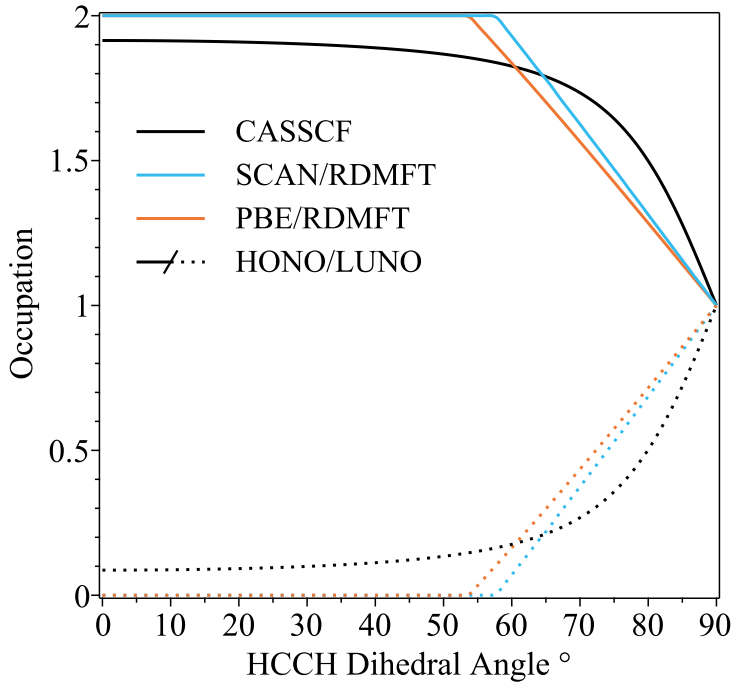

Figure A.6: HONO and LUNO occupations from CASSCF(Valence), PBE-RDMFT, and SCAN-RDMFT along the dihedral angle of C_2H_4

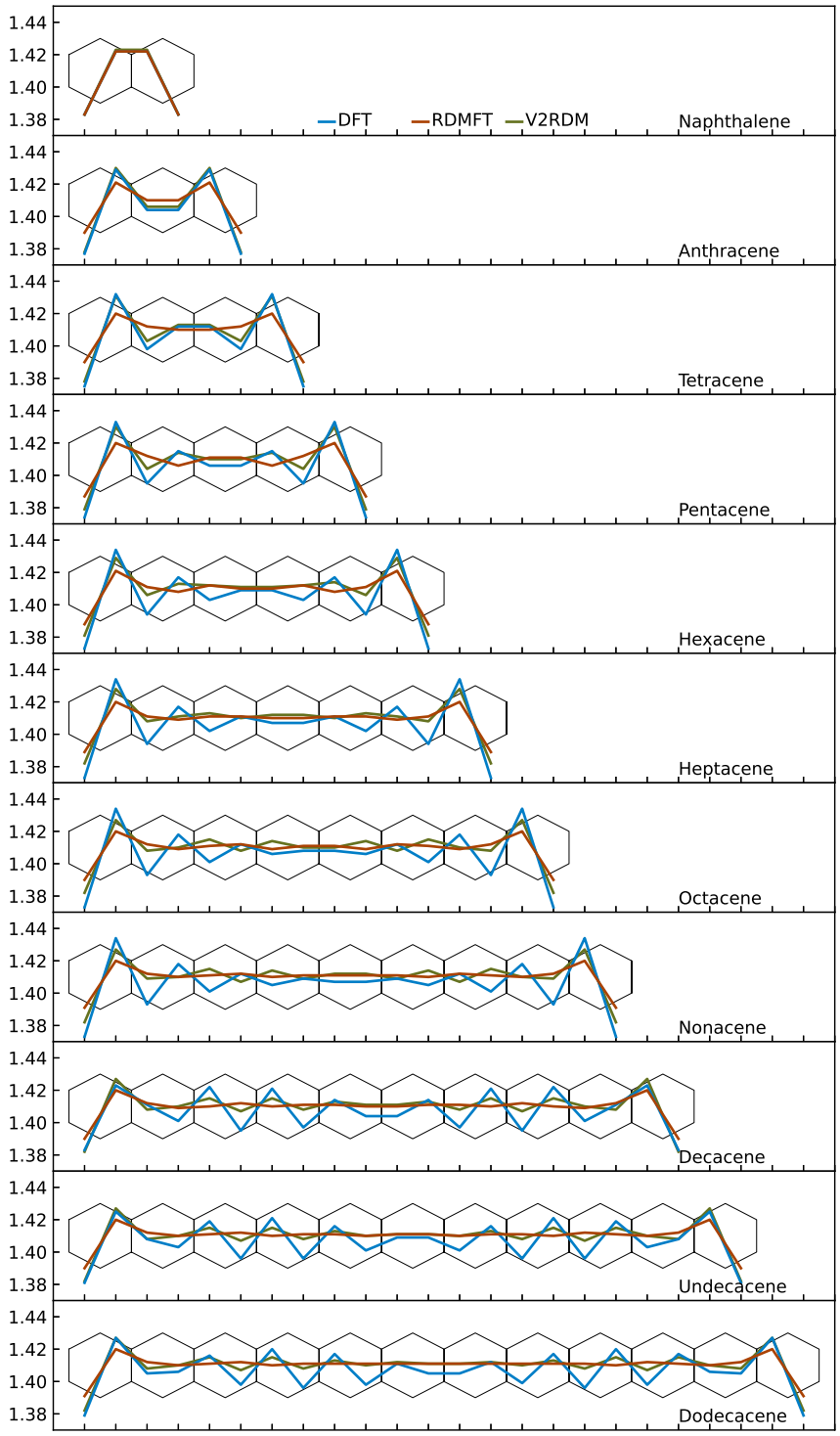

Figure A.7: Geometry optimized singlet C-C bond lengths for napthalene to dodecacene in angstroms.

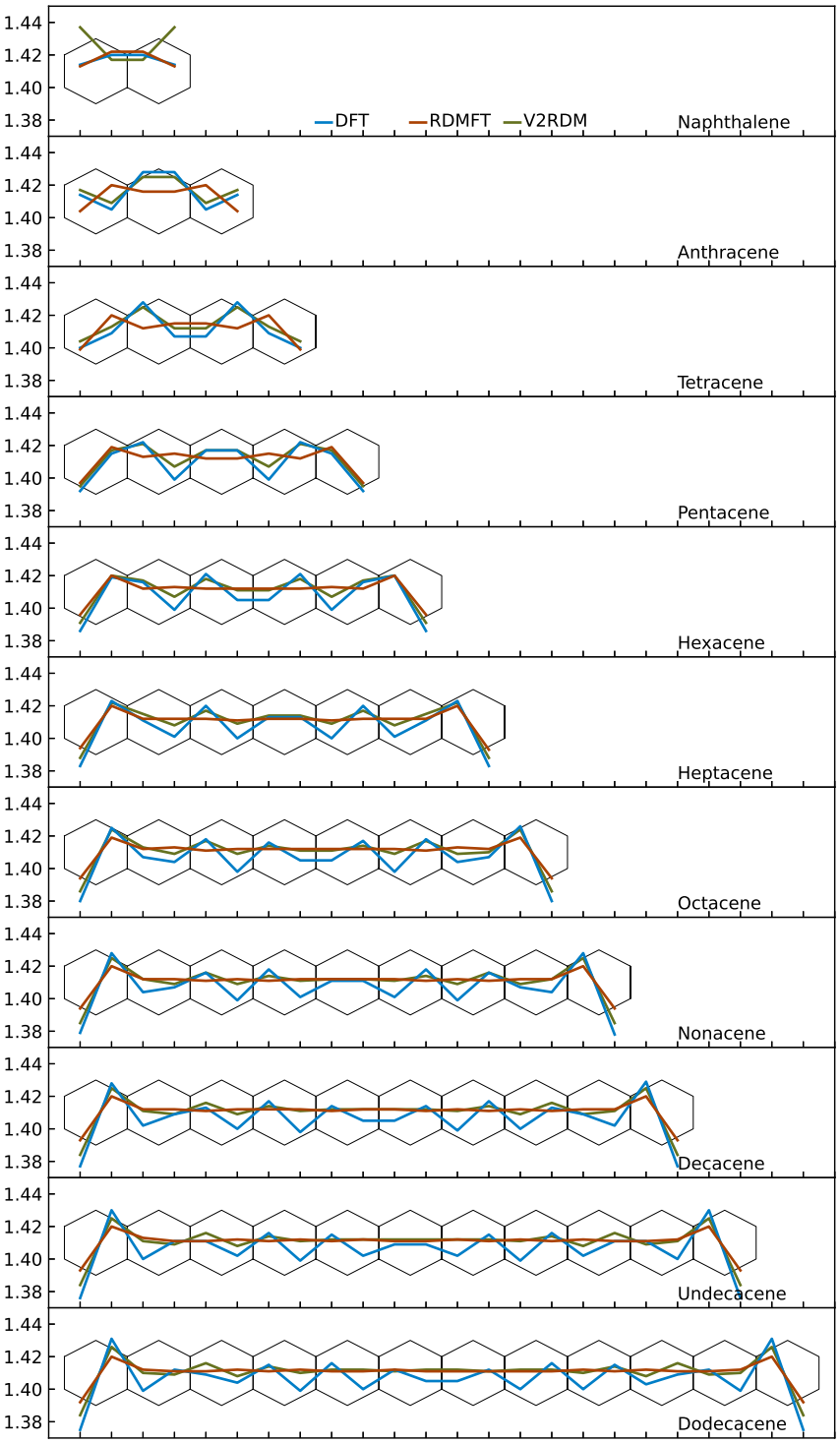

Figure A.8: Geometry optimized triplet C-C bond lengths for napthalene to dodecacene in angstroms.

Table A.5: Dissociation energies obtained from our algorithm with a CASSCF optimized w^1I in kcal/mol relative to CASSCF and the ACSE

	CASSCF		ACSE	
System	B3LYP	w^1I	B3LYP	w^1I
B_2	49.44	15.46	18.56	-15.41
C_2	133.11	-1.19	90.45	-43.87
CN	148.30	-5.33	127.05	-26.59
CO_2	238.70	-45.00	201.17	-82.54
CO	118.85	-72.08	121.79	-69.14
F_2	105.12	-8.07	95.27	-17.92
N_2	257.83	-5.25	252.10	-11.26
NF_3	291.60	45.97	266.67	21.04
NO	166.79	18.38	155.40	6.99
S_2	96.42	-40.05	83.23	-53.23
SiO	88.75	-97.05	95.62	-90.18
MSE	154.09	-17.68	137.03	-34.74
MUE	154.09	32.19	137.03	39.83

Table A.6: Dissociation energies obtained from our algorithm with an ACSE optimized w^1I in kcal/mol relative to the ACSE

System	B3LYP	w^1I
B_2	18.56	-15.08
C_2	90.45	-38.04
CN	127.05	-17.11
CO_2	201.17	-65.69
CO	121.79	-57.88
F_2	95.27	-15.79
N_2	252.10	1.69
NF_3	266.67	33.58
NO	155.40	16.63
S_2	83.23	-53.23
SiO	95.62	-83.42
MSE	137.03	-26.76
MUE	137.03	36.20

Table A.7: All 1-RDMFT obtained values. The maximal errors are defined as $E_{\text{1-RDMFT}}$ - E with the largest absolute magnitude being selected. The w values are optimized for each system and functional combination individually. Signed/Unsigned errors are defined as the average of $E_{\text{1-RDMFT}}$ - E from equilibrium to 4 Å in 0.1 Å steps.

	SCAN	M06-L	B3LYP	M06	M06-2X	M06-HF	HF
	Maximal Error kcal/mol						
H_2	6.14	7.09	6.17	8.03	11.53	17.35	14.11
H_4	-2.88	2.40	-3.03	-2.61	2.66	10.48	9.02
N_2	9.99	8.87	11.95	13.03	19.01	32.53	34.88
HF	-2.35	-1.57	-3.09	3.60	6.87	19.57	17.39
CO	3.80	9.20	5.90	16.24	17.31	37.44	35.05
C_2H_4	5.54	5.11	4.84	4.41	4.98	7.32	7.21
RMSE	5.72	6.43	6.56	9.46	12.06	23.48	22.66
	w Values						
H_2	0.098	0.098	0.116	0.128	0.171	0.284	0.256
H_4	0.104	0.105	0.121	0.131	0.170	0.281	0.249
N_2	0.114	0.112	0.143	0.157	0.213	0.348	0.325
HF	0.073	0.073	0.105	0.125	0.189	0.349	0.318
CO	0.076	0.074	0.105	0.120	0.175	0.314	0.287
C_2H_4	0.052	0.049	0.076	0.084	0.127	0.217	0.215
	Signed Error over PES kcal/mol						
H_2	1.71	1.68	1.58	1.94	2.60	4.93	4.19
H_4	0.34	0.52	0.17	-0.23	0.40	3.95	3.24
N_2	0.87	1.49	2.11	2.67	4.22	8.96	11.20
HF	-1.29	-0.94	-1.54	-0.55	0.30	2.80	-0.39
CO	0.76	1.80	1.64	3.59	4.99	9.80	9.84
C_2H_4	2.07	1.82	1.66	1.40	1.76	3.15	3.10
RMSE	1.31	1.46	1.57	2.09	2.97	6.24	6.58
	Unsigned Error over PES kcal/mol						
H_2	1.71	1.68	1.59	1.94	2.64	4.96	4.19
H_4	1.00	0.89	0.89	0.70	0.98	4.01	3.24
N_2	1.65	1.39	2.19	2.53	4.24	8.96	11.20
HF	1.30	1.01	1.54	1.58	2.05	5.08	7.06
CO	1.68	2.30	2.44	4.42	5.89	10.90	11.06
C_2H_4	2.07	1.82	1.66	1.40	1.76	3.15	3.10
RMSE	1.60	1.59	1.79	2.40	3.36	6.78	7.48

Table A.8: All iDMFT obtained values. The maximal errors are defined as E_{iDMFT} - E with the largest absolute magnitude being selected. The θ values are optimized for each system and functional combination individually. Signed/Unsigned errors are defined as the average of E_{iDMFT} - E from equilibrium to 4 Å in 0.1 Å steps.

	SCAN	M06-L	B3LYP	M06	M06-2X	M06-HF	HF
	Maximal Error kcal/mol						
H_2	-0.44	-0.65	-1.61	-1.42	-1.88	2.16	-1.22
H_4	-8.38	-7.53	-9.83	-9.81	-12.01	-7.98	-9.87
N_2	-13.90	-11.45	-12.76	-11.00	-12.03	-7.55	2.92
HF	-4.79	-4.08	-6.77	-4.52	-4.08	5.41	3.56
CO	-7.89	8.20	-7.91	15.24	-5.78	9.45	-8.50
C_2H_4	2.28	2.01	0.69	-0.84	-2.24	-2.24	-2.40
RMSE	7.68	6.78	7.86	8.88	7.61	6.44	5.75
	θ Values						
H_2	0.036	0.035	0.042	0.047	0.062	0.106	0.095
H_4	0.038	0.039	0.044	0.048	0.063	0.107	0.094
N_2	0.042	0.041	0.053	0.058	0.080	0.135	0.124
HF	0.023	0.023	0.034	0.040	0.061	0.116	0.105
CO	0.027	0.027	0.037	0.042	0.062	0.114	0.103
C_2H_4	0.019	0.018	0.028	0.031	0.048	0.084	0.083
	Signed Error over PES kcal/mol						
H_2	-0.12	-0.18	-0.64	-0.60	-0.64	0.32	-0.36
H_4	-2.80	-2.48	-3.54	-3.91	-4.59	-2.56	-3.56
N_2	-4.33	-3.79	-3.90	-3.80	-3.97	-1.03	0.51
HF	-2.07	-1.48	-3.39	-1.64	-2.32	-0.73	-0.91
CO	-2.62	-2.30	-2.85	-1.90	-2.10	-0.04	-0.40
C_2H_4	0.97	0.82	0.04	-0.22	-1.04	-0.97	-1.03
RMSE	2.54	2.19	2.82	2.46	2.83	1.24	1.59
	Unsigned Error over PES kcal/mol						
H_2	0.15	0.26	0.64	0.64	0.67	0.49	0.37
H_4	2.81	2.49	3.55	3.94	4.59	2.59	3.57
N_2	4.33	3.79	3.91	3.80	3.97	2.05	0.85
HF	2.11	1.65	3.41	2.07	2.40	2.85	2.23
CO	2.77	3.19	2.87	3.47	2.30	3.14	3.05
C_2H_4	0.97	0.82	0.17	0.37	1.04	0.98	1.05
RMSE	2.57	2.39	2.83	2.79	2.87	2.24	2.20

REFERENCES

[1] P. A. M. Dirac. A new notation for quantum mechanics. *Math. Proc. Cambridge Philos. Soc*, 35(3):416–418, 1939.

[2] M. Born and R. Oppenheimer. Zur quantentheorie der molekeln. *Ann. Phys.*, 389(20):457–484, 1927.

[3] W. Pauli. Über den zusammenhang des abschlusses der elektronengruppen im atom mit der komplexstruktur der spektren. *Zeitschrift für Physik*, 31(1):765–783, Feb 1925.

[4] D. R. Hartree. The wave mechanics of an atom with a non-coulomb central field. part ii. some results and discussion. *Math. Proc. Cambridge Philos. Soc*, 24(1):111–132, 1928.

[5] J. C. Slater. The self consistent field and the structure of atoms. *Phys. Rev.*, 32:339–348, Sep 1928.

[6] P. Hohenberg and W. Kohn. Inhomogeneous electron gas. *Phys. Rev.*, 136:B864–B871, Nov 1964.

[7] W. Kohn and L. J. Sham. Self-consistent equations including exchange and correlation effects. *Phys. Rev.*, 140:A1133–A1138, Nov 1965.

[8] John P. Perdew and Karla Schmidt. Jacob's ladder of density functional approximations for the exchange-correlation energy. *AIP Conf. Proc.*, 577(1):1–20, 2001.

[9] Konstantinos D. Vogiatzis, Dongxia Ma, Jeppe Olsen, Laura Gagliardi, and Wibe A. de Jong. Pushing configuration-interaction to the limit: Towards massively parallel MCSCF calculations. *J. Chem. Phys*, 147(18):184111, 11 2017.

[10] John Pople. Quantum chemical models.

[11] Isaiah Shavitt and Rodney J. Bartlett. *Foundations of coupled-cluster theory*, page 251–291. Cambridge Molecular Science. Cambridge University Press, 2009.

[12] Giovanni Li Manni, Rebecca K. Carlson, Sijie Luo, Dongxia Ma, Jeppe Olsen, Donald G. Truhlar, and Laura Gagliardi. Multiconfiguration pair-density functional theory. *J. Chem. Theory Comput*, 10(9):3669–3680, 2014. PMID: 26588512.

[13] David A Mazziotti. Realization of quantum chemistry without wave functions through first-order semidefinite programming. *Phys. Rev. Lett*, 93(21):213001, 2004.

[14] T. L. Gilbert. Hohenberg-kohn theorem for nonlocal external potentials. *Phys. Rev. B*, 12:2111–2120, Sep 1975.

[15] Mel Levy. Universal variational functionals of electron densities, first-order density matrices, and natural spin-orbitals and solution of the v-representability problem. *Proc. Natl. Acad. Sci. U.S.A*, 76(12):6062–6065, 1979.

[16] Mel Levy. Correlation energy functionals of one-matrices and hartree-fock densities. In Robert Erdahl and Vadene H. Smith, editors, *Density Matrices and Density Functionals*, pages 479–498, Dordrecht, 1987. Springer Netherlands.

[17] Steven M. Valone. Consequences of extending 1-matrix energy functionals from pure–state representable to all ensemble representable 1 matrices. *J. Chem. Phys*, 73(3):1344–1349, 08 1980.

[18] Steven M. Valone. A one-to-one mapping between one-particle densities and some n-particle ensembles. *J. Chem. Phys*, 73(9):4653–4655, 11 1980.

[19] A. J. Coleman. Structure of fermion density matrices. *Rev. Mod. Phys.*, 35:668–686, Jul 1963.

[20] Alexander A Klyachko. Quantum marginal problem and n-representability. *J. Phys. Conf. Ser*, 36(1):72, apr 2006.

[21] Kieron Burke. Perspective on density functional theory. *J. Chem. Phys*, 136(15):150901, 04 2012.

[22] Axel D. Becke. Perspective: Fifty years of density-functional theory in chemical physics. *J. Chem. Phys*, 140(18):18A301, 04 2014.

[23] Aron J. Cohen, Paula Mori-Sánchez, and Weitao Yang. Insights into current limitations of density functional theory. *Science*, 321(5890):792–794, 2008.

[24] Stefan Grimme. Density functional theory with london dispersion corrections. *Wiley Interdiscip. Rev. Comput. Mol. Sci.*, 1(2):211–228, 2011.

[25] Elfi Kraka Victor Polo and Dieter Cremer. Electron correlation and the self-interaction error of density functional theory. *Mol. Phys.*, 100(11):1771–1790, 2002.

[26] J. P. Perdew and Alex Zunger. Self-interaction correction to density-functional approximations for many-electron systems. *Phys. Rev. B*, 23:5048–5079, May 1981.

[27] Aron J. Cohen, Paula Mori-Sánchez, and Weitao Yang. Challenges for density functional theory. *Chem. Rev*, 112(1):289–320, 2012. PMID: 22191548.

[28] Aron J. Cohen, Paula Mori-Sánchez, and Weitao Yang. Fractional spins and static correlation error in density functional theory. *J. Chem. Phys*, 129(12):121104, 09 2008.

[29] Michael G. Medvedev, Ivan S. Bushmarinov, Jianwei Sun, John P. Perdew, and Konstantin A. Lyssenko. Density functional theory is straying from the path toward the exact functional. *Science*, 355(6320):49–52, 2017.

[30] John P. Perdew, Adrienn Ruzsinszky, Jianmin Tao, Viktor N. Staroverov, Gustavo E. Scuseria, and Gábor I. Csonka. Prescription for the design and selection of density functional approximations: More constraint satisfaction with fewer fits. *J. Chem. Phys*, 123(6):062201, 08 2005.

[31] Eric Cancès. Self-consistent field algorithms for Kohn–Sham models with fractional occupation numbers. *J. Chem. Phys*, 114(24):10616–10622, 06 2001.

[32] R. Takeda, S. Yamanaka, and K. Yamaguchi. Fractional occupation numbers and spin density functional calculations of degenerate systems. *Int. J. Quantum Chem*, 93(5):317–323, 2003.

[33] Jeng-Da Chai. Density functional theory with fractional orbital occupations. *J. Chem. Phys*, 136(15):154104, 04 2012.

[34] Nektarios N. Lathiotakis, Nicole Helbig, Angel Rubio, and Nikitas I. Gidopoulos. Local reduced-density-matrix-functional theory: Incorporating static correlation effects in kohn-sham equations. *Phys. Rev. A*, 90:032511, Sep 2014.

[35] Maria Hellgren and Tim Gould. Strong correlation and charge localization in kohn–sham theories with fractional orbital occupations. *J. Chem. Theory Comput*, 15(9):4907–4914, 2019. PMID: 31430145.

[36] Joonho Lee, Luke W. Bertels, David W. Small, and Martin Head-Gordon. Kohn-sham density functional theory with complex, spin-restricted orbitals: Accessing a new class of densities without the symmetry dilemma. *Phys. Rev. Lett.*, 123:113001, Sep 2019.

[37] Jonathan Schmidt, Carlos L. Benavides-Riveros, and Miguel A. L. Marques. Reduced density matrix functional theory for superconductors. *Phys. Rev. B*, 99:224502, Jun 2019.

[38] Christian Schilling and Rolf Schilling. Diverging exchange force and form of the exact density matrix functional. *Phys. Rev. Lett.*, 122:013001, Jan 2019.

[39] Mario Piris. Dynamic electron-correlation energy in the natural-orbital-functional second-order-møller-plesset method from the orbital-invariant perturbation theory. *Phys. Rev. A*, 98:022504, Aug 2018.

[40] Mario Piris. Global method for electron correlation. *Phys. Rev. Lett.*, 119:063002, Aug 2017.

[41] S. Sharma, J. K. Dewhurst, S. Shallcross, and E. K. U. Gross. Spectral density and metal-insulator phase transition in mott insulators within reduced density matrix functional theory. *Phys. Rev. Lett.*, 110:116403, Mar 2013.

[42] Daniel R. Rohr, Katarzyna Pernal, Oleg V. Gritsenko, and Evert Jan Baerends. A density matrix functional with occupation number driven treatment of dynamical and nondynamical correlation. *J. Chem. Phys*, 129(16):164105, 10 2008.

[43] David A Mazziotti. Energy functional of the one-particle reduced density matrix: a geminal approach. *Chem. Phys. Lett.*, 338(4):323–328, 2001.

[44] S. Goedecker and C. J. Umrigar. Natural orbital functional for the many-electron problem. *Phys. Rev. Lett.*, 81:866–869, Jul 1998.

[45] M. A. Buijse and E. J. Baerends. An approximate exchange-correlation hole density as a functional of the natural orbitals. *Mol. Phys.*, 100(4):401–421, 2002.

[46] Claude Garrod and Jerome K. Percus. Reduction of the N-Particle Variational Problem. *J. Math. Phys*, 5(12):1756–1776, 12 1964.

[47] A. J. Coleman. *Reduced-Density-Matrix Mechanics: With Application to Many-Electron Atoms and Molecules*. John Wiley & Sons, Inc., 2007.

[48] David A. Mazziotti. Structure of fermionic density matrices: Complete n-representability conditions. *Phys. Rev. Lett.*, 108:263002, Jun 2012.

[49] Mario Piris and Ion Mitxelena. Donof: An open-source implementation of natural-orbital-functional-based methods for quantum chemistry. *Comput. Phys. Commun*, 259:107651, 2021.

[50] Hermann Stoll Burkhard Miehlich and Andreas Savin. A correlation-energy density functional for multideterminantal wavefunctions. *Mol. Phys.*, 91(3):527–536, 1997.

[51] Keith V. Lawler Yair Kurzweil and Martin Head-Gordon. Analysis of multi-configuration density functional theory methods: theory and model application to bond-breaking. *Mol. Phys.*, 107(20):2103–2110, 2009.

[52] Junwei Lucas Bao, Andrew Sand, Laura Gagliardi, and Donald G. Truhlar. Correlated-participating-orbitals pair-density functional method and application to multiplet energy splittings of main-group divalent radicals. *J. Chem. Theory Comput*, 12(9):4274–4283, 2016. PMID: 27438755.

[53] Srikant Veeraraghavan and David A. Mazziotti. Global solutions of hartree-fock theory and their consequences for strongly correlated quantum systems. *Phys. Rev. A*, 89:010502, Jan 2014.

[54] Srikant Veeraraghavan and David A. Mazziotti. Global solutions of restricted open-shell Hartree-Fock theory from semidefinite programming with applications to strongly correlated quantum systems. *J. Chem. Phys*, 140(12):124106, 03 2014.

[55] Srikant Veeraraghavan and David A. Mazziotti. Semidefinite programming formulation of linear-scaling electronic structure theories. *Phys. Rev. A*, 92:022512, Aug 2015.

[56] Christian Schilling. Communication: Relating the pure and ensemble density matrix functional. *J. Chem. Phys*, 149(23):231102, 12 2018.

[57] Carlos L. Benavides-Riveros, Jakob Wolff, Miguel A. L. Marques, and Christian Schilling. Reduced density matrix functional theory for bosons. *Phys. Rev. Lett.*, 124:180603, May 2020.

[58] Christian Schilling, David Gross, and Matthias Christandl. Pinning of fermionic occupation numbers. *Phys. Rev. Lett.*, 110:040404, Jan 2013.

[59] Christian Schilling, Murat Altunbulak, Stefan Knecht, Alexandre Lopes, James D. Whitfield, Matthias Christandl, David Gross, and Markus Reiher. Generalized pauli constraints in small atoms. *Phys. Rev. A*, 97:052503, May 2018.

[60] Romit Chakraborty and David A. Mazziotti. Generalized pauli conditions on the spectra of one-electron reduced density matrices of atoms and molecules. *Phys. Rev. A*, 89:042505, Apr 2014.

[61] Scott E. Smart, David I. Schuster, and David A. Mazziotti. Experimental data from a quantum computer verifies the generalized pauli exclusion principle. *Comm. Phys.*, 2019.

[62] David A Mazziotti. Large-scale semidefinite programming for many-electron quantum mechanics. *Phys. Rev. Lett*, 106(8):083001, 2011.

[63] Lieven Vandenberghe and Stephen Boyd. Semidefinite programming. *SIAM review*, 38(1):49–95, 1996.

[64] RM Erdahl. Two algorithms for the lower bound method of reduced density matrix theory. *Rep. Math. Phys.*, 15(2):147–162, 1979.

[65] Jason M Montgomery and David A Mazziotti. Strong electron correlation in nitrogenase cofactor, femoco. *J. Phys. Chem. A*, 122(22):4988–4996, 2018.

[66] Jiaze Xie, Jan-Niklas Boyn, Alexander S Filatov, Andrew J McNeece, David A Mazziotti, and John S Anderson. Redox, transmetalation, and stacking properties of tetrathiafulvalene-2, 3, 6, 7-tetrathiolate bridged tin, nickel, and palladium compounds. *Chemical Science*, 11(4):1066–1078, 2020.

[67] David A Mazziotti. Dual-cone variational calculation of the two-electron reduced density matrix. *Phys. Rev. A*, 102(5):052819, 2020.

[68] Anthony W Schlimgen, Charles W Heaps, and David A Mazziotti. Entangled electrons foil synthesis of elusive low-valent vanadium oxo complex. *J. Phys. Chem. Lett*, 7(4):627–631, 2016.

[69] Jacob Fosso-Tande, Truong-Son Nguyen, Gergely Gidofalvi, and A Eugene DePrince III. Large-scale variational two-electron reduced-density-matrix-driven complete active space self-consistent field methods. *J. Chem. Theory Comput*, 12(5):2260–2271, 2016.

[70] David A Mazziotti. Enhanced constraints for accurate lower bounds on many-electron quantum energies from variational two-electron reduced density matrix theory. *Phys. Rev. Lett*, 117(15):153001, 2016.

[71] Brecht Verstichel, Helen van Aggelen, Ward Poelmans, and Dimitri Van Neck. Variational two-particle density matrix calculation for the hubbard model below half filling using spin-adapted lifting conditions. *Phys. Rev. Lett*, 108(21):213001, 2012.

[72] Neil Shenvi and Artur F Izmaylov. Active-space n-representability constraints for variational two-particle reduced density matrix calculations. *Phys. Rev. Lett*, 105(21):213003, 2010.

[73] Eric Cances, Gabriel Stoltz, and Mathieu Lewin. The electronic ground-state energy problem: A new reduced density matrix approach. *J. Chem. Phys*, 125(6), 2006.

[74] Zhengji Zhao, Bastiaan J Braams, Mituhiro Fukuda, Michael L Overton, and Jerome K Percus. The reduced density matrix method for electronic structure calculations and the role of three-index representability conditions. *J. Chem. Phys*, 120(5):2095–2104, 2004.

[75] David A Mazziotti. Variational minimization of atomic and molecular ground-state energies via the two-particle reduced density matrix. *Phys. Rev. A*, 65(6):062511, 2002.

[76] Maho Nakata, Hiroshi Nakatsuji, Masahiro Ehara, Mitsuhiro Fukuda, Kazuhide Nakata, and Katsuki Fujisawa. Variational calculations of fermion second-order reduced density matrices by semidefinite programming algorithm. *J. Chem. Phys*, 114(19):8282–8292, 2001.

[77] Daniel H Ess, Erin R Johnson, Xiangqian Hu, and Weitao Yang. Singlet- triplet energy gaps for diradicals from fractional-spin density-functional theory. *J. Phys. Chem. A*, 115(1):76–83, 2011.

[78] Gergely Gidofalvi and David A Mazziotti. Spin and symmetry adaptation of the variational two-electron reduced-density-matrix method. *Phys. Rev. A*, 72(5):052505, 2005.

[79] Albrecht Unsöld. Beiträge zur quantenmechanik der atome. *Ann. Phys.*, 387(3):355–393, 1927.

[80] Susi Lehtola. Fully numerical calculations on atoms with fractional occupations and range-separated exchange functionals. *Phys. Rev. A*, 101(1):012516, 2020.

[81] E.J. Baerends, V. Branchadell, and M. Sodupe. Atomic reference energies for density functional calculations. *Chem. Phys. Lett.*, 265(3):481–489, 1997.

[82] Lyudmila V. Slipchenko and Anna I. Krylov. Singlet-triplet gaps in diradicals by the spin-flip approach: A benchmark study. *J. Chem. Phys*, 117(10):4694–4708, 09 2002.

[83] John Clarke . Slater and James C. Phillips. Quantum theory of molecules and solids vol. 4: The self-consistent field for molecules and solids. *Physics Today*, 27:49–50, 1974.

[84] S. H. Vosko, L. Wilk, and M. Nusair. Accurate spin-dependent electron liquid correlation energies for local spin density calculations: a critical analysis. *Can. J. Phys.*, 58(8):1200–1211, 1980.

[85] John P. Perdew and Yue Wang. Accurate and simple analytic representation of the electron-gas correlation energy. *Phys. Rev. B*, 45:13244–13249, Jun 1992.

[86] John P. Perdew, Kieron Burke, and Matthias Ernzerhof. Generalized gradient approximation made simple. *Phys. Rev. Lett.*, 77:3865–3868, Oct 1996.

[87] John P. Perdew, Kieron Burke, and Matthias Ernzerhof. Generalized gradient approximation made simple [phys. rev. lett. 77, 3865 (1996)]. *Phys. Rev. Lett.*, 78:1396–1396, Feb 1997.

[88] A. D. Becke. Density-functional exchange-energy approximation with correct asymptotic behavior. *Phys. Rev. A*, 38:3098–3100, Sep 1988.

[89] Chengteh Lee, Weitao Yang, and Robert G. Parr. Development of the colle-salvetti correlation-energy formula into a functional of the electron density. *Phys. Rev. B*, 37:785–789, Jan 1988.

[90] Jianmin Tao, John P. Perdew, Viktor N. Staroverov, and Gustavo E. Scuseria. Climbing the density functional ladder: Nonempirical meta–generalized gradient approximation designed for molecules and solids. *Phys. Rev. Lett.*, 91:146401, Sep 2003.

[91] Jianwei Sun, Adrienn Ruzsinszky, and John P. Perdew. Strongly constrained and appropriately normed semilocal density functional. *Phys. Rev. Lett.*, 115:036402, Jul 2015.

[92] Haoyu S. Yu, Xiao He, and Donald G. Truhlar. Mn15-l: A new local exchange-correlation functional for kohn–sham density functional theory with broad accuracy for atoms, molecules, and solids. *J. Chem. Theory Comput*, 12(3):1280–1293, 2016. PMID: 26722866.

[93] Narbe Mardirossian and Martin Head-Gordon. Mapping the genome of meta-generalized gradient approximation density functionals: The search for B97M-V. *J. Chem. Phys*, 142(7):074111, 02 2015.

[94] Jr. Dunning, Thom H. Gaussian basis sets for use in correlated molecular calculations. I. The atoms boron through neon and hydrogen. *J. Chem. Phys*, 90(2):1007–1023, 01 1989.

[95] Rick A. Kendall, Jr. Dunning, Thom H., and Robert J. Harrison. Electron affinities of the first-row atoms revisited. Systematic basis sets and wave functions. *J. Chem. Phys*, 96(9):6796–6806, 05 1992.

[96] Serguei Patchkovskii and Tom Ziegler. Improving "difficult" reaction barriers with self-interaction corrected density functional theory. *J. Chem. Phys*, 116(18):7806–7813, 05 2002.

[97] Anthony P. Scott and Leo Radom. Harmonic vibrational frequencies: An evaluation of hartree-fock, møller-plesset, quadratic configuration interaction, density functional theory, and semiempirical scale factors. *J. Phys. Chem.*, 100(41):16502–16513, 1996.

[98] Adèle D. Laurent and Denis Jacquemin. Td-dft benchmarks: A review. *Int. J. Quantum Chem.*, 113(17):2019–2039, 2013.

[99] Chang-Guo Zhan, Jeffrey A. Nichols, and David A. Dixon. Ionization potential, electron affinity, electronegativity, hardness, and electron excitation energy: Molecular properties from density functional theory orbital energies. *J. Phys. Chem. A*, 107(20):4184–4195, 2003.

[100] Amir Karton and Peter R. Spackman. Evaluation of density functional theory for a large and diverse set of organic and inorganic equilibrium structures. *J. Comput. Chem.*, 42(22):1590–1601, 2021.

[101] Robert G. Parr. Density functional theory of atoms and molecules. In Kenichi Fukui and Bernard Pullman, editors, *Horizons of Quantum Chemistry*, pages 5–15, Dordrecht, 1980. Springer Netherlands.

[102] Jorge Kohanoff. *Electronic Structure Calculations for Solids and Molecules: Theory and Computational Methods*. Cambridge University Press, 2006.

[103] Lars Goerigk, Andreas Hansen, Christoph Bauer, Stephan Ehrlich, Asim Najibi, and Stefan Grimme. A look at the density functional theory zoo with the advanced gmtkn55 database for general main group thermochemistry, kinetics and noncovalent interactions. *Phys. Chem. Chem. Phys.*, 19:32184–32215, 2017.

[104] Tom. Ziegler. Approximate density functional theory as a practical tool in molecular energetics and dynamics. *Chem. Rev.*, 91(5):651–667, 1991.

[105] Robert C. Morrison and Libero J. Bartolotti. Exchange-correlation potentials for high-electron-density ions in the be isoelectronic series. *J. Chem. Phys.*, 121(24):12151–12157, 2004.

[106] John P. Perdew, Robert G. Parr, Mel Levy, and Jose L. Balduz. Density-functional theory for fractional particle number: Derivative discontinuities of the energy. *Phys. Rev. Lett.*, 49:1691–1694, Dec 1982.

[107] Xiao Zheng, Aron J. Cohen, Paula Mori-Sánchez, Xiangqian Hu, and Weitao Yang. Improving band gap prediction in density functional theory from molecules to solids. *Phys. Rev. Lett.*, 107:026403, Jul 2011.

[108] Chen Li, Xiao Zheng, Neil Qiang Su, and Weitao Yang. Localized orbital scaling correction for systematic elimination of delocalization error in density functional approximations. *Nat. Sci. Rev.*, 5(2):203–215, 09 2017.

[109] Yuncai Mei, Zehua Chen, and Weitao Yang. Self-consistent calculation of the localized orbital scaling correction for correct electron densities and energy-level alignments in density functional theory. *J. Phys. Chem. Lett.*, 11(23):10269–10277, 2020.

[110] S. Goedecker and C. J. Umrigar. *Natural Orbital Functional Theory*, pages 165–181. Springer US, Boston, MA, 2000.

[111] Christian Schilling and Stefano Pittalis. Ensemble reduced density matrix functional theory for excited states and hierarchical generalization of pauli's exclusion principle. *Phys. Rev. Lett.*, 127:023001, Jul 2021.

[112] David A. Mazziotti. Geminal functional theory: A synthesis of density and density matrix methods. *J. Chem. Phys*, 112(23):10125–10130, 06 2000.

[113] Florian Buchholz, Iris Theophilou, Soeren E. B. Nielsen, Michael Ruggenthaler, and Angel Rubio. Reduced density-matrix approach to strong matter-photon interaction. *ACS Photonics*, 6(11):2694–2711, 2019. PMID: 31788499.

[114] Katarzyna Pernal and Klaas J. H. Giesbertz. *Reduced Density Matrix Functional Theory (RDMFT) and Linear Response Time-Dependent RDMFT (TD-RDMFT)*, pages 125–183. Springer International Publishing, Cham, 2016.

[115] Harrison Shull and Per-Olov Löwdin. Correlation Splitting in Helium-Like Ions. *J. Chem. Phys*, 25(5):1035–1040, 11 1956.

[116] Mario Piris. A new approach for the two-electron cumulant in natural orbital functional theory. *Int. J. Quantum Chem*, 106(5):1093–1104, 2006.

[117] M. Piris. A natural orbital functional based on an explicit approach of the two-electron cumulant. *Int. J. Quantum Chem*, 113(5):620–630, 2013.

[118] Daniel Gibney, Jan-Niklas Boyn, and David A. Mazziotti. Toward a resolution of the static correlation problem in density functional theory from semidefinite programming. *J. Phys. Chem. Lett*, 12(1):385–391, 2021. PMID: 33356286.

[119] Neil Qiang Su, Chen Li, and Weitao Yang. Describing strong correlation with fractional-spin correction in density functional theory. *Proc. Natl. Acad. Sci. U.S.A*, 115(39):9678–9683, 2018.

[120] Mazziotti, David A. First-order semidefinite programming for the two-electron treatment of many-electron atoms and molecules. *ESAIM: M2AN*, 41(2):249–259, 2007.

[121] Björn O. Roos, Peter R. Taylor, and Per E.M. Sigbahn. A complete active space scf method (casscf) using a density matrix formulated super-ci approach. *Chem. Phys.*, 48(2):157–173, 1980.

[122] Per E. M. Siegbahn, Jan Almlöf, Anders Heiberg, and Björn O. Roos. The complete active space SCF (CASSCF) method in a Newton–Raphson formulation with application to the HNO molecule. *J. Chem. Phys*, 74(4):2384–2396, 02 1981.

[123] David A. Mazziotti. Anti-hermitian contracted schrödinger equation: Direct determination of the two-electron reduced density matrices of many-electron molecules. *Phys. Rev. Lett.*, 97:143002, Oct 2006.

[124] David A. Mazziotti. Anti-hermitian part of the contracted schrödinger equation for the direct calculation of two-electron reduced density matrices. *Phys. Rev. A*, 75:022505, Feb 2007.

[125] W. J. Hehre, R. Ditchfield, and J. A. Pople. Self—Consistent Molecular Orbital Methods. XII. Further Extensions of Gaussian—Type Basis Sets for Use in Molecular Orbital Studies of Organic Molecules. *J. Chem. Phys*, 56(5):2257–2261, 03 1972.

[126] Maplesoft, a division of Waterloo Maple Inc.. Maple.

[127] Illinois. RDMChem, Chicago. Quantum chemistry toolbox, 2021.

[128] Qiming Sun, Timothy C. Berkelbach, Nick S. Blunt, George H. Booth, Sheng Guo, Zhendong Li, Junzi Liu, James D. McClain, Elvira R. Sayfutyarova, Sandeep Sharma, Sebastian Wouters, and Garnet Kin-Lic Chan. Pyscf: the python-based simulations of chemistry framework. *Wiley Interdiscip. Rev. Comput. Mol. Sci.*, 8(1):e1340, 2018.

[129] P. J. Stephens, F. J. Devlin, C. F. Chabalowski, and M. J. Frisch. Ab initio calculation of vibrational absorption and circular dichroism spectra using density functional force fields. *J. Phys. Chem. A*, 98(45):11623–11627, 1994.

[130] Axel D. Becke. Density-functional thermochemistry. III. The role of exact exchange. *J. Chem. Phys*, 98(7):5648–5652, 04 1993.

[131] P. Verma and D. G Truhlar. Geometries for minnesota database 2019. *Retrieved from the Data Repository for the University of Minnesota*, Jul 2019.

[132] P.J. Knowles and N.C. Handy. A new determinant-based full configuration interaction method. *Chem. Phys. Lett.*, 111(4):315–321, 1984.

[133] Trygve Helgaker, Poul Jørgensen, and Jeppe Olsen. *Configuration-Interaction Theory*, chapter 11, pages 523–597. John Wiley & Sons, Ltd, 2000.

[134] Jonathan Schmidt, Carlos L. Benavides-Riveros, and Miguel A. L. Marques. Machine learning the physical nonlocal exchange–correlation functional of density-functional theory. *J. Phys. Chem. Lett*, 10(20):6425–6431, 2019. PMID: 31596092.

[135] Felix Brockherde, Leslie Vogt, Li Li, Mark E. Tuckerman, Kieron Burke, and Klaus-Robert Müller. Bypassing the kohn-sham equations with machine learning. *Nat. Commun*, 8(1):872, Oct 2017.

[136] Javier Robledo Moreno, Giuseppe Carleo, and Antoine Georges. Deep learning the hohenberg-kohn maps of density functional theory. *Phys. Rev. Lett.*, 125:076402, Aug 2020.

[137] Johannes T. Margraf and Karsten Reuter. Pure non-local machine-learned density functional theory for electron correlation. *Nat. Commun*, 12(1):344, Jan 2021.

[138] Bhupalee Kalita, Li Li, Ryan J. McCarty, and Kieron Burke. Learning to approximate density functionals. *Acc. Chem. Res*, 54(4):818–826, 2021. PMID: 33534553.

[139] Jian Wang and Evert Jan Baerends. Self-consistent-field method for correlated many-electron systems with an entropic cumulant energy. *Phys. Rev. Lett.*, 128:013001, Jan 2022.

[140] Jiří Čížek. On the Correlation Problem in Atomic and Molecular Systems. Calculation of Wavefunction Components in Ursell-Type Expansion Using Quantum-Field Theoretical Methods. *J. Chem. Phys*, 45(11):4256–4266, 12 1966.

[141] Diptarka Hait and Martin Head-Gordon. How accurate is density functional theory at predicting dipole moments? an assessment using a new database of 200 benchmark values. *J. Chem. Theory Comput*, 14(4):1969–1981, 2018. PMID: 29562129.

[142] Kurt R. Brorsen, Yang Yang, Michael V. Pak, and Sharon Hammes-Schiffer. Is the accuracy of density functional theory for atomization energies and densities in bonding regions correlated? *J. Phys. Chem. Lett*, 8(9):2076–2081, 2017. PMID: 28421759.

[143] Yan Zhao and Donald G. Truhlar. A new local density functional for main-group thermochemistry, transition metal bonding, thermochemical kinetics, and noncovalent interactions. *J. Chem. Phys*, 125(19):194101, 11 2006.

[144] Haoyu S. Yu, Xiao He, Shaohong L. Li, and Donald G. Truhlar. Mn15: A kohn–sham global-hybrid exchange–correlation density functional with broad accuracy for multi-reference and single-reference systems and noncovalent interactions. *Chem. Sci.*, 7:5032–5051, 2016.

[145] Neil Qiang Su. Unity of kohn-sham density-functional theory and reduced-density-matrix-functional theory. *Phys. Rev. A*, 104:052809, Nov 2021.

[146] Mario Piris and Jesus M. Ugalde. Perspective on natural orbital functional theory. *Int. J. Quantum Chem*, 114(18):1169–1175, 2014.

[147] Daniel Gibney, Jan-Niklas Boyn, and David A. Mazziotti. Density functional theory transformed into a one-electron reduced-density-matrix functional theory for the

capture of static correlation. *J. Phys. Chem. Lett*, 13(6):1382–1388, 2022. PMID: 35113577.

[148] Lexin Ding, Julia Liebert, and Christian Schilling. Comment on "self-consistent-field method for correlated many-electron systems with an entropic cumulant energy", 2022.

[149] Jeng-Da Chai. Thermally-assisted-occupation density functional theory with generalized-gradient approximations. *J. Chem. Phys*, 140(18):18A521, 03 2014.

[150] N. David Mermin. Thermal properties of the inhomogeneous electron gas. *Phys. Rev.*, 137:A1441–A1443, Mar 1965.

[151] Yan Zhao and Donald G. Truhlar. The m06 suite of density functionals for main group thermochemistry, thermochemical kinetics, noncovalent interactions, excited states, and transition elements: two new functionals and systematic testing of four m06 functionals and 12 other functionals. *Theor. Chem. Acc*, 119(5):525–525, Apr 2008.

[152] Yan Zhao and Donald G. Truhlar. Density functional for spectroscopy: No long-range self-interaction error, good performance for rydberg and charge-transfer states, and better performance on average than b3lyp for ground states. *J. Phys. Chem. A*, 110(49):13126–13130, 2006. PMID: 17149824.

[153] M. Grüning, O. V. Gritsenko, and E. J. Baerends. Exchange-correlation energy and potential as approximate functionals of occupied and virtual Kohn–Sham orbitals: Application to dissociating H2. *J. Chem. Phys*, 118(16):7183–7192, 04 2003.

[154] Dayou Zhang and Donald G. Truhlar. Unmasking static correlation error in hybrid kohn–sham density functional theory. *J. Chem. Theory Comput*, 16(9):5432–5440, 2020. PMID: 32693604.

[155] R. G Parr and W. Yang. *Density-Functional Theory of Atoms and Molecules*. Oxford University Press, 1994.

[156] R. M. Dreizler and E. K. U. Gross. *Density Funcitonal Theory*. Springer-Verlag, 1990.

[157] R. O. Jones. Density functional theory: Its origins, rise to prominence, and future. *Rev. Mod. Phys.*, 87:897–923, Aug 2015.

[158] Andreas Dreuw and Martin Head-Gordon. Failure of time-dependent density functional theory for long-range charge-transfer excited states: The zincbacteriochlorin-bacteriochlorin and bacteriochlorophyll-spheroidene complexes. *J. Am. Chem. Soc*, 126(12):4007–4016, 2004. PMID: 15038755.

[159] Stephan N. Steinmann, Cyril Piemontesi, Aurore Delachat, and Clemence Corminboeuf. Why are the interaction energies of charge-transfer complexes challenging for dft? *J. Chem. Theory Comput*, 8(5):1629–1640, 2012. PMID: 26593656.

[160] Jiří Klimeš and Angelos Michaelides. Perspective: Advances and challenges in treating van der Waals dispersion forces in density functional theory. *J. Chem. Phys*, 137(12):120901, 09 2012.

[161] Aaron D. Kaplan, Chandra Shahi, Pradeep Bhetwal, Raj K. Sah, and John P. Perdew. Understanding density-driven errors for reaction barrier heights. *J. Chem. Theory Comput*, 19(2):532–543, 2023. PMID: 36599075.

[162] Heather J. Kulik, Matteo Cococcioni, Damian A. Scherlis, and Nicola Marzari. Density functional theory in transition-metal chemistry: A self-consistent hubbard u approach. *Phys. Rev. Lett.*, 97:103001, Sep 2006.

[163] Akash Bajaj and Heather J. Kulik. Molecular dft+u: A transferable, low-cost approach to eliminate delocalization error. *J. Phys. Chem. Lett*, 12(14):3633–3640, 2021. PMID: 33826346.

[164] Yuncai Mei, Zehua Chen, and Weitao Yang. Exact second-order corrections and accurate quasiparticle energy calculations in density functional theory. *J. Phys. Chem. Lett*, 12(30):7236–7244, 2021. PMID: 34310157.

[165] Daniel Gibney, Jan-Niklas Boyn, and David A. Mazziotti. Comparison of density-matrix corrections to density functional theory. *J. Chem. Theory Comput*, 18(11):6600–6607, 2022. PMID: 36287002.

[166] Sonai Seenithurai and Jeng-Da Chai. Tao-dft with the polarizable continuum model. *Nanomaterials*, 13(10), 2023.

[167] A.M.K. Müller. Explicit approximate relation between reduced two- and one-particle density matrices. *Phys. Lett. A*, 105(9):446–452, 1984.

[168] Mario Piris. *Natural Orbital Functional Theory*, chapter 14, pages 385–427. John Wiley & Sons, Ltd, 2007.

[169] S. Sharma, J. K. Dewhurst, N. N. Lathiotakis, and E. K. U. Gross. Reduced density matrix functional for many-electron systems. *Phys. Rev. B*, 78:201103, Nov 2008.

[170] Y. Lemke, J. Kussmann, and C. Ochsenfeld. Efficient integral-direct methods for self-consistent reduced density matrix functional theory calculations on central and graphics processing units. *J. Chem. Theory Comput*, 18(7):4229–4244, 2022. PMID: 35818791.

[171] Julia Liebert, Adam Yanis Chaou, and Christian Schilling. Refining and relating fundamentals of functional theory. *J. Chem. Phys*, 158(21):214108, 06 2023.

[172] A. J. Coleman and V. I. Yukalov. *Reduced Density Matrices: Coulson's Challenge*. Springer, Berlin, 2000.

[173] F. Colmenero and C. Valdemoro. Approximating q-order reduced density matrices in terms of the lower-order ones. ii. applications. *Phys. Rev. A*, 47:979–985, Feb 1993.

[174] Hiroshi Nakatsuji and Koji Yasuda. Direct determination of the quantum-mechanical density matrix using the density equation. *Phys. Rev. Lett.*, 76:1039–1042, Feb 1996.

[175] David A. Mazziotti. Contracted schrödinger equation: Determining quantum energies and two-particle density matrices without wave functions. *Phys. Rev. A*, 57:4219–4234, Jun 1998.

[176] David A Mazziotti. Approximate solution for electron correlation through the use of schwinger probes. *Chem. Phys. Lett.*, 289(5):419–427, 1998.

[177] David A. Mazziotti. 3,5-contracted schrödinger equation: Determining quantum energies and reduced density matrices without wave functions. *Int. J. Quantum Chem*, 70(4-5):557–570, 1998.

[178] Debashis Mukherjee and Werner Kutzelnigg. Irreducible Brillouin conditions and contracted Schrödinger equations for n-electron systems. I. The equations satisfied by the density cumulants. *J. Chem. Phys*, 114(5):2047–2061, 02 2001.

[179] Diego R. Alcoba, Carmela Valdemoro, Luis M. Tel, Encarnación Pérez-Romero, and Ofelia B. Oña. Optimized solution procedure of the g-particle-hole hypervirial equation for multiplets: Application to doublet and triplet states. *J. Phys. Chem. A*, 115(12):2599–2606, 2011. PMID: 21388112.

[180] Jan-Niklas Boyn and David A. Mazziotti. Accurate singlet–triplet gaps in biradicals via the spin averaged anti-Hermitian contracted Schrödinger equation. *J. Chem. Phys*, 154(13):134103, 04 2021.

[181] Scott E. Smart and David A. Mazziotti. Quantum solver of contracted eigenvalue equations for scalable molecular simulations on quantum computing devices. *Phys. Rev. Lett.*, 126:070504, Feb 2021.

[182] Werner Kutzelnigg. Density-cumulant functional theory. *J. Chem. Phys*, 125(17):171101, 11 2006.

[183] Alexander Yu. Sokolov and III Schaefer, Henry F. Orbital-optimized density cumulant functional theory. *J. Chem. Phys*, 139(20):204110, 11 2013.

[184] David A. Mazziotti. Parametrization of the two-electron reduced density matrix for its direct calculation without the many-electron wave function. *Phys. Rev. Lett.*, 101:253002, Dec 2008.

[185] Andrew M. Sand, Christine A. Schwerdtfeger, and David A. Mazziotti. Strongly correlated barriers to rotation from parametric two-electron reduced-density-matrix methods in application to the isomerization of diazene. *J. Chem. Phys*, 136(3):034112, 01 2012.

[186] Run R. Li, Marcus D. Liebenthal, and III DePrince, A. Eugene. Challenges for variational reduced-density-matrix theory with three-particle N-representability conditions. *J. Chem. Phys*, 155(17):174110, 11 2021.

[187] Mitchell J Knight, Harry M Quiney, and Andy M Martin. Reduced density matrix approach to ultracold few-fermion systems in one dimension. *New J. Phys.*, 24(5):053004, may 2022.

[188] Jiaze Xie, Simon Ewing, Jan-Niklas Boyn, Alexander S. Filatov, Baorui Cheng, Tengzhou Ma, Garrett L. Grocke, Norman Zhao, Ram Itani, Xiaotong Sun, Himchan Cho, Zhihengyu Chen, Karena W. Chapman, Shrayesh N. Patel, Dmitri V. Talapin, Jiwoong Park, David A. Mazziotti, and John S. Anderson. Intrinsic glassy-metallic transport in an amorphous coordination polymer. *Nature*, 611(7936):479–484, Nov 2022.

[189] David A. Mazziotti. Quantum many-body theory from a solution of the n-representability problem. *Phys. Rev. Lett.*, 130:153001, Apr 2023.

[190] David A. Mazziotti. Purification of correlated reduced density matrices. *Phys. Rev. E*, 65:026704, Jan 2002.

[191] A. J. Coleman and I. Absar. Reduced hamiltonian orbitals. iii. unitarily invariant decomposition of hermitian operators. *Int. J. Quantum Chem*, 18(5):1279–1307, 1980.

[192] D. A. Mazziotti. *Reduced Density Matrix Mechanics: With Application to Many Electron Atoms and Molecules*. John Wiley & Sones, 2007.

[193] Douglas Henrique Pereira, Lucas Colucci Ducati, Roberto Rittner, and Rogério Custodio. A study of the rotational barriers for some organic compounds using the g3 and g3cep theories. *J. Mol. Model.*, 20(4):2199, Mar 2014.

[194] Yang Yang, Degao Peng, Ernest R. Davidson, and Weitao Yang. Singlet–triplet energy gaps for diradicals from particle–particle random phase approximation. *J. Phys. Chem. A*, 119(20):4923–4932, 2015. PMID: 25891638.

[195] Roberto Peverati and Donald G. Truhlar. Quest for a universal density functional: the accuracy of density functionals across a broad spectrum of databases in chemistry and physics. *Philos. Trans. R. Soc. A*, 372(2011):20120476, 2014.

[196] Manas Sajjan, Kade Head-Marsden, and David A. Mazziotti. Entangling and disentangling many-electron quantum systems with an electric field. *Phys. Rev. A*, 97:062502, Jun 2018.

[197] Alexandra Raeber and David A. Mazziotti. Large eigenvalue of the cumulant part of the two-electron reduced density matrix as a measure of off-diagonal long-range order. *Phys. Rev. A*, 92:052502, Nov 2015.

[198] David A. Mazziotti. Complete reconstruction of reduced density matrices. *Chem. Phys. Lett.*, 326(3):212–218, 2000.

[199] C. Valdemoro. Approximating the second-order reduced density matrix in terms of the first-order one. *Phys. Rev. A*, 45:4462–4467, Apr 1992.

[200] Stephen Boyd and Lieven Vandenberghe. *Convex Optimization*. Cambridge University Press, Cambridge, 2004.

[201] Elliot H. Lieb. Variational principle for many-fermion systems. *Phys. Rev. Lett.*, 46:457–459, Feb 1981.

[202] Krishnan Raghavachari, Gary W. Trucks, John A. Pople, and Martin Head-Gordon. A fifth-order perturbation comparison of electron correlation theories. *Chem. Phys. Lett.*, 157(6):479–483, 1989.

[203] Jan-Niklas Boyn, Aleksandr O. Lykhin, Scott E. Smart, Laura Gagliardi, and David A. Mazziotti. Quantum-classical hybrid algorithm for the simulation of all-electron correlation. *J. Chem. Phys*, 155(24):244106, 12 2021.

[204] David A. Mazziotti, editor. *Reduced-Density-Matrix Mechanics: With Application to Many-Electron Atoms and Molecules*, volume 135 of *Advances in Chemical Physics*. John Wiley & Sons, New York, 2007.

[205] Daniel Gibney, Jan-Niklas Boyn, and David A. Mazziotti. Universal Generalization of Density Functional Theory for Static Correlation. *Phys. Rev. Lett.*, 131(24):243003, 2023.

[206] E. T. Whittaker and G. N. Watson. *A Course of Modern Analysis*. Cambridge Mathematical Library. Cambridge University Press, 4 edition, 1996.

[207] Anton V. Sinitskiy, Loren Greenman, and David A. Mazziotti. Strong correlation in hydrogen chains and lattices using the variational two-electron reduced density matrix method. *J. Chem. Phys.*, 133(1):014104, 2010.

[208] Johannes Hachmann, Jonathan J. Dorando, Michael Avilés, and Garnet Kin-Lic Chan. The radical character of the acenes: A density matrix renormalization group study. *J. Chem. Phys.*, 127(13):134309, 2007.

[209] Gergely Gidofalvi and David A. Mazziotti. Active-space two-electron reduced-density-matrix method: Complete active-space calculations without diagonalization of the N-electron Hamiltonian. *J. Chem. Phys.*, 129(13):134108, 2008.

[210] Shayan Hemmatiyan and David A. Mazziotti. Unraveling the Band Gap Trend in the Narrowest Graphene Nanoribbons from the Spin-Adapted Excited-Spectra Reduced Density Matrix Method. *J. Phys. Chem. C*, 123(23):14619–14624, 2019.

[211] M. Weinert and J. W. Davenport. Fractional occupations and density-functional energies and forces. *Phys. Rev. B*, 45:13709–13712, Jun 1992.

[212] Brendan O'Donoghue, Eric Chu, Neal Parikh, and Stephen Boyd. Conic optimization via operator splitting and homogeneous self-dual embedding. *J. Optim. Theory Appl.*, 169(3):1042–1068, June 2016.

[213] Brendan O'Donoghue, Eric Chu, Neal Parikh, and Stephen Boyd. SCS: Splitting conic solver, version 3.2.4. `https://github.com/cvxgrp/scs`, November 2023.

[214] Steven Diamond and Stephen Boyd. CVXPY: A Python-embedded modeling language for convex optimization. *J. Mach. Learn. Res.*, 17(83):1–5, 2016.

[215] RDMChem. Quantum Chemistry Toolbox in Maple (RDMChem, Chicago, 2024).

[216] Jeffrey B. Schriber, Kevin P. Hannon, Chenyang Li, and Francesco A. Evangelista. A combined selected configuration interaction and many-body treatment of static and dynamical correlation in oligoacenes. *J. Chem. Theory Comp.*, 14(12):6295–6305, 2018.

[217] J. Wayne Mullinax, Evgeny Epifanovsky, Gergely Gidofalvi, and A. Eugene III DePrince. Analytic energy gradients for variational two-electron reduced-density matrix methods within the density fitting approximation. *J. Chem. Theory Comp.*, 15(1):276–289, 2019.

[218] Thomas Schultz, Elena Samoylova, Wolfgang Radloff, Ingolf V. Hertel, Andrzej L. Sobolewski, and Wolfgang Domcke. Efficient deactivation of a model base pair via excited-state hydrogen transfer. *Science*, 306(5702):1765–1768, 2004.

[219] Wolfgang J. Schreier, Tobias E. Schrader, Florian O. Koller, Peter Gilch, Carlos E. Crespo-Hernández, Vijay N. Swaminathan, Thomas Carell, Wolfgang Zinth, and Bern Kohler. Thymine dimerization in dna is an ultrafast photoreaction. *Science*, 315(5812):625–629, 2007.

[220] Clemens Rauer, Juan J. Nogueira, Philipp Marquetand, and Leticia González. Cyclobutane thymine photodimerization mechanism revealed by nonadiabatic molecular dynamics. *J. Am. Chem. Soc*, 138(49):15911–15916, 2016. PMID: 27682199.

[221] Yuan-Chung Cheng and Graham R. Fleming. Dynamics of light harvesting in photosynthesis. *Annu. Rev. Phys. Chem*, 60(Volume 60, 2009):241–262, 2009.

[222] G. Cerullo, D. Polli, G. Lanzani, S. De Silvestri, H. Hashimoto, and R. J. Cogdell. Photosynthetic light harvesting by carotenoids: Detection of an intermediate excited state. *Science*, 298(5602):2395–2398, 2002.

[223] Kiyoshi Miyata, Felisa S. Conrad-Burton, Florian L. Geyer, and X.-Y. Zhu. Triplet pair states in singlet fission. *Chem. Rev*, 119(6):4261–4292, 2019. PMID: 30721032.

[224] Frank Neese. Efficient and accurate approximations to the molecular spin-orbit coupling operator and their use in molecular g-tensor calculations. *J. Chem. Phys*, 122(3):034107, 01 2005.

[225] Martin Richter, Philipp Marquetand, Jesús González-Vázquez, Ignacio Sola, and Leticia González. Sharc: ab initio molecular dynamics with surface hopping in the adiabatic representation including arbitrary couplings. *J. Chem. Theory Comput*, 7(5):1253–1258, 2011. PMID: 26610121.

[226] Erich Runge and E. K. U. Gross. Density-functional theory for time-dependent systems. *Phys. Rev. Lett.*, 52:997–1000, Mar 1984.

[227] M. Petersilka, U. J. Gossmann, and E. K. U. Gross. Excitation energies from time-dependent density-functional theory. *Phys. Rev. Lett.*, 76:1212–1215, Feb 1996.

[228] Julia Liebert and Christian Schilling. Deriving density-matrix functionals for excited states. *SciPost Phys.*, 14:120, 2023.

[229] Haoyu S. Yu, Wenjing Zhang, Pragya Verma, Xiao He, and Donald G. Truhlar. Nonseparable exchange–correlation functional for molecules, including homogeneous catalysis involving transition metals. *Phys. Chem. Chem. Phys.*, 17:12146–12160, 2015.

[230] Jürgen Gräfenstein and Dieter Cremer. The self-interaction error and the description of non-dynamic electron correlation in density functional theory. *Theor. Chem. Acc*, 123(3):171–182, Jun 2009.

[231] Takao Tsuneda and Kimihiko Hirao. Self-interaction corrections in density functional theory. *J. Chem. Phys*, 140(18):18A513, 03 2014.

[232] David A. Mazziotti. Two-electron reduced density matrix as the basic variable in many-electron quantum chemistry and physics. *Chem. Rev*, 112(1):244–262, 2012. PMID: 21863900.

[233] Daniel Gibney, Jan-Niklas Boyn, and David A. Mazziotti. Toward a resolution of the static correlation problem in density functional theory from semidefinite programming. *J. Phys. Chem. Lett*, 12(1):385–391, 2021. PMID: 33356286.